UNIVERSITY OF PORTO - FACULTY OF ENGINEERING

GEOMETRICALLY NON-LINEAR OSCILLATIONS OF COMPOSITE LAMINATED PLATES BY THE HIERARCHICAL FINITE ELEMENT METHOD

by

Rui Pedro Monteiro Amaro Duarte, with a degree in Apllied Mathematics,

University of Coimbra, Faculty of Sciences

Thesis submitted in fulfilment of the degree of

Master

In Computational Methods in Sciences and Engineering

Thesis under the supervision of Dr. Pedro Leal Ribeiro,
From the Department of Mechanical Engineering and Industrial Management, Section of Applied Mechanics from the Faculty of Engineering of University of Porto

Porto, October 2004

SUMMARY

The geometrically non-linear forced vibration of fully clamped composite laminated plates is studied by the hierarchical finite element method (HFEM). Using the first order shear deformation theory (FSDT), Kirchhoff's hypothesis is relaxed by removing the third part, i.e., the transverse normals do not remain perpendicular to the midsurface after deformation. Von Kármán's non-linear strain-displacement relationships are employed and the middle plane in-plane displacements are included in the model, as well as the rotations about the in-plane axis *x* and *y*. The equations of motion are developed in the time domain by applying the principle of virtual work. The high order polynomials that emerge in the HFEM are integrated by symbolic manipulation. These equations are solved in the time domain using Newmark direct integration scheme. The time domain response is studied using the phase plane, Poincaré maps, Fourier spectra and Lyapunov exponents; periodic, quasi-periodic and chaotic motions are obtained. Two different types of forces are considered, the results for linear and non-linear analysis are compared with published ones and good agreement is found. It is demonstrated that the HFEM requires fewer degrees of freedom (DOF) than the more common *h*-version of the FEM. This is a very important advantage in non-linear analysis because the time required to solve the non-linear equations of motion increases significantly with the number of DOF.

SOMMAIRE

On s'intéresse ici à l'étude, à l'aide de la Méthode des Eléments Finis Hiérarchiques (MEFH), des vibrations forcées, en non-linéaire géométrique, de plaques composites encastrées. La modélisation utilisée repose sur la théorie de Reissner-Mindlin (déformation au première ordre), avec l'hypothèse de Kirchhoff où le troisième terme a été négligé (les normales au feuillet moyen ne sont plus nécessairement perpendiculaires à ce feuillet après déformation) et en considérant la relation non-linéaire tension-déplacement de Von Kármán. Les déplacements du feuillet moyen ainsi que les rotations suivant les axes *x* et *y* sont introduits dans le modèle. Les équations du mouvement sont obtenues par application du principe des travaux virtuels. Les polynômes d'ordres élevés qui interviennent dans la méthode des éléments finis hiérarchiques sont pris en compte par manipulation symbolique. Les équations du mouvement sont résolues numériquement dans le domaine temporel par la méthode de Newmark. Les réponses dans le domaine temporel sont analysées en étudiant le comportement des trajectoires dans le plan de phase, des sections de Poincaré, des spectres de Fourier et par calcul des exponents de Lyapunov. Deux types sollicitations externes sont considérés. Les réponses périodiques, quasi-périodiques et chaotiques sont mises en évidence. Les résultats pour l'analyse linéaire et non-linéaire sont comparés avec ceux publiés et un bon accord est trouvé. Le coût numérique pour résoudre les équations non-linéaires du mouvement augmente considérablement avec le nombre de degrés de liberté. Ceci est un inconvénient pour mener l'analyse de systèmes faiblement amortis où des simulations sur un temps long sont exigées. La méthode des MEFH nécessitant moins de degrés de liberté que la classique MEF version-*h*, elle est fortement indiquée pour l'analyse numérique dans le domaine temporel des oscillations non-linéaires des plaques composites laminées.

SUMÁRIO

A vibração forçada em regime não linear geométrico de placas assimétricas encastradas em materiais compósitos é estudada pelo método dos elementos finitos hierárquico (MEFH). A origem do sistema de eixos encontra-se no plano médio, sendo o eixo dos *zz* normal a este. Usando a teoria de Mindlin para placas (*first order shear deformation theory*), a hipótese de Kirchhoff é relaxada removendo a terceira parte, i.e, os deslocamentos transversos não se mantêm perpendiculares à superfície média, após deformação. As relações não lineares de von Kármán entre as deformações e os deslocamentos são aplicadas e os deslocamentos ao longo do plano médio são incluídos no modelo, bem como as rotações dos deslocamentos transversos ao longo do eixo dos *xx* e dos *yy*. As equações de movimento no domínio do tempo são determinadas aplicando os princípios dos trabalhos virtuais. Os polinómios de ordem superior que aparecem no MEFH são integrados usando manipulação simbólica. Estas equações são resolvidas no domínio do tempo usando o método de Newmark. A estabilidade da solução obtida, no domínio do tempo, é estudada, usando planos de fase, mapas de Poincaré, espectro de Fourier e expoentes de Lyapunov. Soluções periódicas, quase-periódicas e caóticas são obtidas. Dois tipos de forças são consideradas, os resultados obtidos em análise linear e não linear são comparados com outros publicados e boa concordância é encontrada. É demonstrado que o MEFH requer menos graus de liberdade (GL) que a versão-*h* do método. Esta é uma grande vantagem em análise não linear porque o tempo necessário para resolver as equações não lineares de movimento aumenta significativamente com o número de graus de liberdade.

TABLE OF CONTENTS

LIST OF FIGURES

CHAPTER 2

CHAPTER 4

CHAPTER 5

LIST OF TABLES

CHAPTER 4

ACKNOWLEDGEMENTS

I wish to thank:

My supervisor in this thesis, Professor Pedro Leal Ribeiro, for the time spent helping me to enter in the field on non-linear dynamics. His help and encouragement kept me going up to this day.

My mother Clídia Duarte and my father José Duarte and my sister Patrícia Duarte, who gave me love, affection, education and "*the tools to build a life*".

My lovely wife Alexandra, for the love and encouragement she always gave me. Her patience and devotion are something I shall never forget.

The support of Superior School of Engineering of Viseu and the Portuguese Science and Technology Foundation is gratefully acknowledge.

I dedicate this thesis to:

The memory of my grandmothers Júlia Amaro and Isaura Duarte, grandfathers José Amaro and Joaquim Duarte.

My son, Miguel Tomás Duarte, who will become the most important person in my life.

Chapter 1

INTRODUCTION

1. *GENERAL INTRODUCTION*

Composite laminated structures are used in many areas of engineering such as aeronautics, space engineering and naval industry [1.1, 1.2, 1.3]. Those structures are submitted to vibrations with large amplitude, therefore in the geometrically non-linear regime. Nowadays, typical examples of composite plates are the panels used in spaceships, aircrafts and automobiles which are submitted to large acoustic, aerodynamic and inertia excitation [1.4]. Vibrations with large amplitude cause large tensions and the diminution of life due to fatigue. Quasi periodic and chaotic behaviours are other consequences of non-linearity, completely ignored by linear models which are normally used [1.5, 1.6]. Therefore the study of geometrically non-linear vibration in laminated plates made of composite and hybrid materials becomes important.

A hierarchical finite element method developed recently [1.7 - 1.9], in which the model is improved by increasing the number of shape functions in each element, needs a small number of degrees of freedom. This is a big advantage, because the non-linear equations of motion are solved using iterative methods.

2. *REVIEW OF RESEARCH CARRIED OUT ON PLATE VIBRATIONS*

The combination of two or more materials in order to form a new material with better properties is something that can be understood as a simple definition of composite materials. There are various types of composite materials: fibre, particulate, laminar, flake and filled [1.10]. Laminated composite materials are made of layers with different materials, which include fibrous composites and

particulate materials. In this case, composites can be either metallic or non-metallic. Thus there are four possible combinations: metallic in non-metallic, non-metallic in metallic, non-metallic in non-metallic and metallic in metallic.

A lamina is a sheet of composite material. A fibre reinforced lamina consists of many fibres embedded in a matrix material like aluminium, or non-metal like a thermoset or thermoplastic polymer. The fibres can be continuous or discontinuous, wover, unidirectional, bidirectional or randomly distributed. Unidirectional fibre reinforced lamina exhibit the highest strength and stiffness in the direction of the fibres, but in the transverse direction of the fibres they have very low strength and stiffness. Poor bonding between a fibre and matrix results in poor transverse properties and failures in the form of a fibre pull out, fibre breakage and fibre buckling. Discontinuous fibre reinforced composites have lower strength and stiffness than continuous fibre reinforced composites.

A laminate is a set of laminae stacked to achieve the desired stiffness and thickness. As an example, unidirectional fibre reinforced laminae can be stacked so that the fibres in each lamina are oriented in the same or different directions. The layers are bonded together with the same matrix material. Because of the mismatch of material properties between layers, the shear stresses produced between the layers, especially at the edges of a laminate, may cause delamination [1.11].

3. *REVIEW OF PLATE VIBRATIONS*

The interest of investigators in large vibration amplitudes of plates has been constant since the first revelation of the classical elliptic function solution for simply supported plates by Chu and Herrmann [1.12]. Linear free vibration of composite plates has been studied in the past. The studies of Bert have largely contributed to the development of analytical methods for solution of plate problems [1.13, 1.14]. Reddy [1.15 - 1.18] has reviewed the literature extensively and focused the attention on the application of the finite element method to linear

and non-linear plate problems. For composite plates, non-linear strain displacements relationships are most commonly used in the literature for the development of non-linear theories.

Chia[1.19, 1.20] considered the non-linear response of various types of plates. Transverse shear deformation, rotatory inertia, anisotropy, initial imperfections, and variable rigidity have been discussed and reviewed. Developments in free-vibration of analysis of symmetric and unsymmetric laminates, non-linear vibrations of perfect and geometrically imperfect plates have been carried out by Kapania et al. [1.21].

To determine the solutions of the general problem of geometrically non-linear vibrations numerical, analytical or combined analytical numerical methods can be found. The finite element method has been applied to solve non-linear static and dynamic problems of plates. Mei is considered as one of the first researchers to apply the finite element method to large vibrations amplitudes of plates, namely in a work published in 1973 [1.22]. Using the finite element method, Mei et al. [1.23] studied the large amplitude steady state forced vibration response of symmetrically laminated composite thin rectangular plates, including both in-plane deformation and inertia in the formulation.

Most of the research has been carried out in symmetrical composite plates. Asymmetrical laminates are harder to analyse, since they exhibit bending-stretching coupling.

Recent investigations in the geometrically non-linear dynamic behaviour of symmetric laminated plates using the hierarchical finite element method have been developed by W. Han, M. Petyt and P. Ribeiro [1.7-1.9; 1.24-1.28].

In 2002, B. Harras studied the response of rectangular Carbon Fiber Reinforced Plastic (CFRP) and Glare 3 hybrid symmetrically laminated plates in order to investigate the non-linear mode shapes and associated bending stress patterns at large vibration amplitudes of various types of fully clamped rectangular plates. This material offers more resistance to impact than CFRP [1.29].

As referred so far, geometrically non-linear behaviour of asymmetrical laminated plates in composite materials by the hierarchical finite element method is a study

that has not been carried out. Based on the model derived in this work, the numerical results obtained will be compared to others in geometrically non-linear behaviour of symmetrical laminated plates in composite materials. Some important conclusions can be found. The first order shear deformation theory is used and compared with results obtained using Kirchooff's hypothesis.

4. *THE HIERARCHICAL FINITE ELEMENT METHOD*

Through the years, structures tended to become more complex. Thus the need to develop new methods to analyse them and the evolution of computers led to the finite element method, used to build non linear models of structures like plates.
Finite Element Analysis (FEA) is a computer-based numerical technique. It can be used to calculate deflection, stress, vibration, buckling behaviour and many other phenomena. It can be used to analyze either small or large-scale deflection under loading or applied displacement. It can analyze elastic deformation, or "permanently bent out of shape" plastic deformation. The computer is required because of the large number of calculations needed to analyze a large structure.
In the finite element method, a structure is broken down into many small simple blocks or elements. The behaviour of an individual element can be described with a relatively simple set of equations. Just as the set of elements would be joined together to build the whole structure, the equations describing the behaviours of the individual elements are joined into a large set of equations (which depends of the structure) that describe the behaviour of the whole structure. The computer can solve this large set of simultaneous equations. From the solution, the computer extracts the behaviour of the individual elements. From this, it can get the stress and deflection of all the parts of the structure. The stresses will be compared to allowed values of stress for the materials to be used, to see if the structure is strong enough [1.30].
The term "finite element" distinguishes the technique from the use of infinitesimal "differential elements" used in calculus, differential equations, and

partial differential equations. The method is also distinguished from finite difference equations, for which although the steps into which space is divided are finite in size, there is little freedom in the shapes that the discreet steps can take. Finite element analysis is a way to deal with structures that are more complex than can be dealt with analytically using partial differential equations. FEA deals with complex boundaries better than finite difference equations would, and gives answers to "real world" structural problems. It has been substantially extended in scope during the roughly 40 years of its use.

Finite Element Analysis makes it possible to evaluate a detailed and complex structure, in a computer, during the planning of the structure. The demonstration in the computer of the adequate strength of the structure and the possibility of improving the design during planning can justify the cost of this analysis work. FEA has also been known to increase the rating of structures that were significantly over designed and built many decades ago.

In the absence of Finite Element Analysis (or other numerical analysis), development of structures must be based on experience and hand calculations only. For complex structures, the simplifying assumptions required to make any calculations possible can lead to a conservative and heavy design. A considerable factor of ignorance can remain as to whether the structure will be adequate for all design loads. Significant changes in designs involve risk. Designs will require prototypes to be built and field tested. The field tests may involve expensive strain gauging to evaluate strength and deformation.

In the most used version of the FEM, the shape functions are polynomials with a small degree *p,* and the accuracy of the model is improved by increasing the number of elements in the structure. As a result, the number of the finite elements increases and their width *h* decreases, giving to this approach the designation "*h*-version of the FEM".

Another way of improving the accuracy of the finite element approximation is to keep the mesh constant and to increase the number of shape functions over the elements. When polynomials are used as shape functions, this approach implies an increase in their degree *p*; thus, it was designated as the "*p*-version of the finite

element method". If the set of functions corresponding to an approximation of lower order *p*, constitutes a subset of the set of functions corresponding to the approximation of order *p*+1, then the *p*-version of the FEM is called "hierarchical finite element method" (HFEM).

The use of the *p*-version of the finite element method has more advantages than the use of the *h*-version:

i) To achieve more accurate solutions, a change in the mesh is not required;

ii) The linear element matrices for a certain number of shape functions $p=p_1$ are always submatrices for $p=p_2$, $p_2 \geq p_1$[1.31, 1.32].

iii) If orthogonal polynomials are employed, the linear matrices obtained in the hierarchical finite element method are diagonal, thus they are better conditioned than the finite element method matrices [1.30].

iv) the Inclusion Principle, which states that the eigenvalues of the (n+1) order approximation bracket the eigenvalues of the nth order approximation, is valid for linear discretized systems modelled by the HFEM. Consequently, the HFEM linear solutions converge from above. In general, the Inclusion Principle is not valid for systems modelled by the *h*-version of the FEM [1.32, 1.33].

v) Joining elements of different polynomial degree is not difficult; therefore it is possible to include at low cost additional degrees of freedom where needed [1.31].

vi) Simple structures can be modelled using just one element, or "super-element". This avoids any problems in the satisfaction of inter-element continuity and avoids the assemblage of the elements.

vii) The possibility of choosing the number and type of displacement shape functions facilitates the study of the influence of each displacement component. For example, the influence of the middle plane in-plane displacement components in the dynamic behaviour of a plate can be easily studied.

viii) The HFEM tends to give accurate results with far fewer DOF than the *h*-version of the FEM, because of the flexibility of choosing the shape functions

employed according to the problem under study and because of the high order shape functions used. This is particularly true for smooth solutions, since strong mesh generation may be advantageous in the vicinity of singular points [1.34].

As a consequence of these properties, the HFEM model requires less time than the FEM, which is a major advantage in non-linear analysis, where the iterative methods of solution of the equations of motion involve a reformulation of the non-linear matrices in each iteration.

The quick convergence of the HFEM applied in the study of composite laminated plates has been proved [1.7-1.9; 1.24-1.28]. When compared with the *h*-version of the FEM, the HFEM consistently demanded fewer degrees of freedom to accurately calculate stresses, displacements and resonance frequencies.
The large disadvantage of the HFEM is the need to perform integration of high order polynomials which costs many operations in numerical integration. Thus the use of symbolic computation is required. A detailed introduction to the finite element method can be found in references [1.3, 1.32].

5. *OBJECTIVES OF THE PRESENT WORK*

The main objectives of the dissertation that follows this work are:

1. Development of hierarchic finite elements for asymmetrical laminated plates in composite materials. Only symmetric laminates are analysed in this thesis. However, a general model valid for symmetric and asymmetric laminates was derived for wider future use, and this is the model presented in the following text.

2. Analyse the vibration of plates in geometrically non-linear vibrations. To do that, Newmark method will be applied (like finite differences or Wilson-θ, the equations of motion are integrated numerically in time). The analysis will imply the study of the time response, the phase portraits and Fourier spectra. Particular attention will be given to:

- Transitions to chaos (implies the determination of Lyapunov exponents);
- influence of fibre variation.

Both of these objectives will be achieved and are presented in the following chapters.

6. *GENERAL ARRANGEMENT OF CHAPTERS IN THIS THESIS*

This thesis consists of 6 chapters. The first chapter, as has been seen above, is an introduction. The last one contains conclusions which summarize the whole work and suggests future investigations. The mathematical model for the non-linear vibration of composite laminated plates which is based on the Hierarchical Finite Element Method is derived in Chapter 2. In Chapter 3, different tools that can be used to characterize the responses of non-linear systems are presented, namely, Fourier analysis, Poincaré Analysis and Lyapunov exponents. The rest of the chapters are about the applications of the *p*-version finite element model to different cases. By applying the Newmark method to solve the equations of motion the forced vibrations of composite laminated plates due to transverse forces are analysed in Chapter 4. In Chapter 5, in-plane forces are added to the external excitation, and the ensuing motions are discussed.

Chapter 2

MATHEMATICAL MODEL

1. *INTRODUCTION*

In this chapter, a hierarchical finite element model for geometrically non-linear vibration in unsymmetrical laminated plates made of composite materials is developed. The model will be presented in the time domain.

2. *MATHEMATICAL MODEL*

2.1 - *Field Equations*

In this section, a hierarchical finite element method for asymmetric composite plates is presented. The plate with constant thickness h, width a and length b, is composed of orthotropic layers oriented at different angles θ.

The origin of the co-ordinate system is located at the middle plane with the z-axis being normal to the mid-plane. Using the first order shear deformation theory (FSDT), Kirchhoff's hypothesis is relaxed by removing the third part, i.e., the transverse normals do not remain perpendicular to the midsurface after deformation. The inextensibility of transverse normals requires that w is not a function of the thickness coordinate, z. The displacement field (Figure 1) of the first-order theory is of the form [2.1]

$$u(x, y, z, t) = u^0(x, y, t) + z\Phi_y(x, y, t) \quad (2.1)$$

$$v(x, y, z, t) = v^0(x, y, t) - z\Phi_x(x, y, t) \quad (2.2)$$

$$w(x, y, z, t) = w^0(x, y, t) \quad (2.3)$$

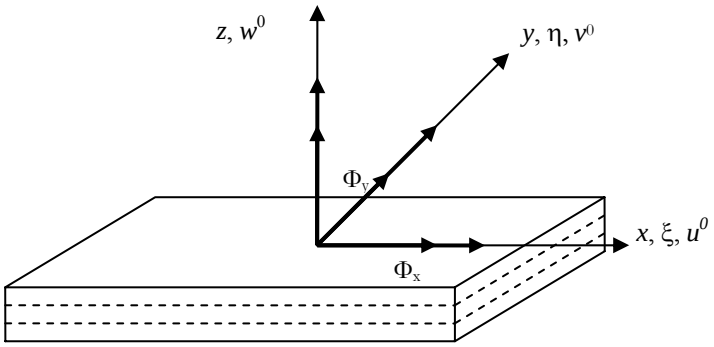

Figure 1 - Plate Element, coordinates, mid-plane displacements and rotations

where (u^0, v^0, w^0) are the displacements along the coordinate lines of a material point on the *xy* plane, therefore in the mid-plane (z=0), and where Φ_x and Φ_y are

$$\frac{\partial u}{\partial z} = \Phi_y \,,\ \frac{\partial v}{\partial z} = -\Phi_x$$

the rotations of a transverse normal about the x-axis and the y-axis, respectively. The functions (u^0, v^0, w^0, Φ_x, Φ_y) are unknown and are to be determined. For thin plates, i.e., when the plate in-plane characteristic dimension to thickness ratio is on the order 50 or higher ($a/h \geq 50$) [2.2], the rotation functions Φ_x and Φ_y should approach the respective slopes of the transverse deflection:

$$\Phi_x = \frac{\partial w_0}{\partial y} \,,\ \Phi_y = -\frac{\partial w_0}{\partial x}$$

In this case, the first order shear deformation theory becomes identical to the classical plate theory where Kirchhoff's hypothesis is followed [2.5].

The non-linear strains associated with the displacement field in Figure 1 are

$$\begin{Bmatrix} \varepsilon_x \\ \varepsilon_y \\ \gamma_{xy} \\ \gamma_{zx} \\ \gamma_{yz} \end{Bmatrix} = \begin{Bmatrix} \varepsilon_x^{\,0} \\ \varepsilon_y^{\,0} \\ \gamma_{xy}^{\,0} \\ \gamma_{zx}^{\,0} \\ \gamma_{yz}^{\,0} \end{Bmatrix} - \begin{Bmatrix} z\kappa_x \\ z\kappa_y \\ z\kappa_{xy} \\ 0 \\ 0 \end{Bmatrix} \qquad (2.4)$$

where $\varepsilon_x^{\,0}$, $\varepsilon_y^{\,0}$ and $\gamma_{xy}^{\,0}$ are the in-plane strain components at $z = 0$ defined by the von Kármán non-linear strain-displacement relationships[2.3]:

$$\varepsilon_x^{\,0} = u_{,x}^0 + \frac{1}{2}(w_{,x}^0)^2, \varepsilon_y^{\,0} = v_{,y}^0 + \frac{1}{2}(w_{,y}^0)^2, \ \gamma_{xy}^{\,0} = u_{,y}^0 + v_{,x}^0 + w_{,x}^0 w_{,y}^0 \qquad (2.5)$$

where $u_{,x}^0$ represents the partial derivate $\frac{\partial u_0}{\partial x}$.

Figure 2 shows these displacements.

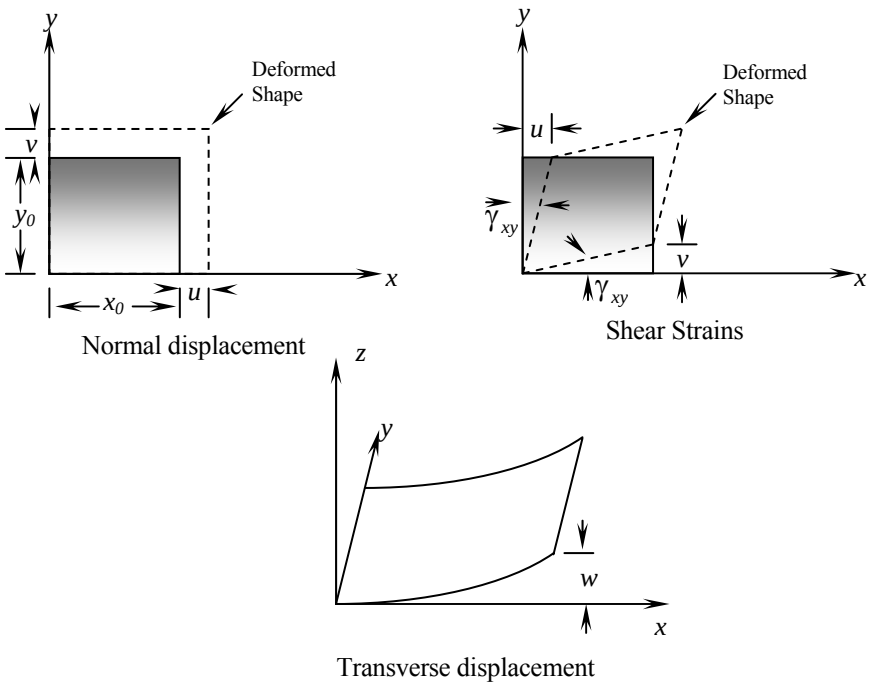

Figure 2 – Displacements of a plate

The terms κ_x, κ_y and κ_{xy} in equation (2. 4) are the curvatures or bending strains, which are given by:

$$\kappa_x = -\frac{\partial \Phi_y^0}{\partial x}, \kappa_y = \frac{\partial \Phi_x^0}{\partial y} \text{ and } \kappa_{xy} = -\frac{\partial \Phi_y^0}{\partial y} + \frac{\partial \Phi_x^0}{\partial x} \qquad (2.6)$$

The transverse shear strains are

$$\gamma_{zx}^0 = w_{,x}^0 + \Phi_y^0, \ \gamma_{yz}^0 = w_{,y}^0 - \Phi_x^0 \qquad (2.7)$$

For each element, the middle plane in-plane displacements and the rotations are expressed in the form:

$$\begin{Bmatrix} u^0 \\ v^0 \\ w^0 \\ \Phi_y^0 \\ \Phi_x^0 \end{Bmatrix} = [N] \begin{Bmatrix} q_u \\ q_v \\ q_w \\ q_{\Phi_y} \\ q_{\Phi x} \end{Bmatrix} \tag{2. 8}$$

where $\{q_u\}$, $\{q_v\}$ and $\{q_w\}$ are the vectors of generalised in and out-of-plane displacements, and $\{q_{\Phi_y}\}$ and $\{q_{\Phi_x}\}$ are the vectors of generalised rotations. The complete matrix of shape functions

$$[N] = \begin{bmatrix} \{N^u\}^T & 0 & 0 & 0 & 0 \\ 0 & \{N^u\}^T & 0 & 0 & 0 \\ 0 & 0 & \{N^w\}^T & 0 & 0 \\ 0 & 0 & 0 & \{N^{\Phi_y}\}^T & 0 \\ 0 & 0 & 0 & 0 & \{N^{\Phi_x}\}^T \end{bmatrix} \tag{2. 9}$$

is constituted by the row vectors of bi-dimensional in-plane, out-of-plane and rotational shape functions, which are, respectively,

$$\{N^u\}^T = \{g_1(\xi) g_1(\eta), g_1(\xi) g_2(\eta), ..., g_{p_i}(\xi) g_{p_i}(\eta)\} \tag{2. 10}$$

$$\{N^w\}^T = \{f_1(\xi) f_1(\eta), f_1(\xi) f_2(\eta), ..., f_{p_o}(\xi) f_{p_o}(\eta)\} \tag{2. 11}$$

$$\{N^{\Phi_y}\}^T = \{\Phi_{y_1}(\xi)\Phi_{y_1}(\eta), \Phi_{y_1}(\xi)\Phi_{y_2}(\eta), \cdots, \Phi_{y_{p_{\Phi y}}}(\xi)\Phi_{y_{p_{\Phi y}}}(\eta)\} \tag{2. 12}$$

$$\{N^{\Phi_x}\}^T = \{\Phi_{x_1}(\xi)\Phi_{x_1}(\eta), \Phi_{x_1}(\xi)\Phi_{x_2}(\eta), ..., \Phi_{x_{p_{\Phi x}}}(\xi)\Phi_{x_{p_{\Phi x}}}(\eta)\} \tag{2. 13}$$

The vectors $\{g\}$, $\{f\}$, $\{\Phi_y\}$ and $\{\Phi_x\}$ are the vectors of in-plane, transverse, and rotational one dimensional displacement shape functions; p_o, p_i, p_{Φ_y} and p_{Φ_x} are the

numbers of respective transverse, middle plane, rotation about *y* and rotation about *x*, displacement shape functions employed; ξ and η are the local coordinates, which are given by:

$$\xi = 2x/a, \quad \eta = 2y/b \tag{2. 14}$$

In the hierarchical finite element method, one is free to choose the number and set of displacement shape functions to be applied in the definition of the element. Increasing the order of the shape functions that represent the displacements within the element increases the accuracy of the element. In a plate element, there is a set of shape functions for the transverse displacements, a set of shape functions for the in-plane displacements and one set of shape functions for each rotation.

An element of a layer is now considered and the plate geometric axes are *x* and *y*, as in Figure 3. The principal material axes are labelled 1 and 2, that is, the 1 direction is parallel to the fibbers and the 2 direction is normal to them.

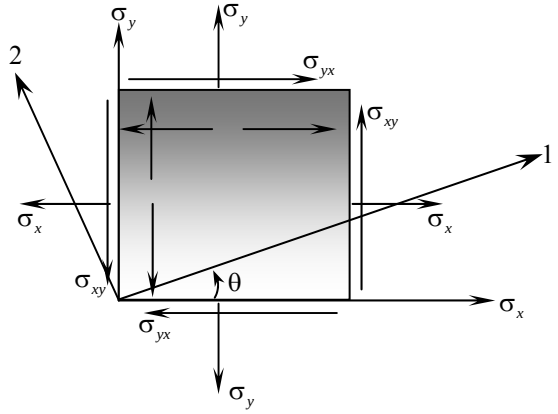

Figure 3 – Laminae Coordinate System

Mohr's circle analysis in basic strength of materials can be applied to establish that

$$\begin{Bmatrix} \sigma_1 \\ \sigma_2 \\ \sigma_6 \end{Bmatrix} = [T]_{CL} \begin{Bmatrix} \sigma_x \\ \sigma_y \\ \sigma_{xy} \end{Bmatrix} \tag{2. 15}$$

Analogously, the strain relationship is given by

$$\begin{Bmatrix} \varepsilon_1 \\ \varepsilon_2 \\ \varepsilon_{12} \end{Bmatrix} = [T]_{CL} \begin{Bmatrix} \varepsilon_x \\ \varepsilon_y \\ \varepsilon_{xy} \end{Bmatrix}, \tag{2. 16}$$

where

$$[T]_{CL} = \begin{bmatrix} m^2 & n^2 & +2mn \\ n^2 & m^2 & -2mn \\ -mn & mn & (m^2 - n^2) \end{bmatrix} \tag{2. 17}$$

where $m = \cos(\theta)$, $n = \sin(\theta)$, and θ is the positive angle defined, and CL refer to the 1-2 plane only. The effects of transverse shear deformation are shown in the inclusion of the relations $\sigma_4 - \varepsilon_4$ and $\sigma_5 - \varepsilon_5$ in composite materials [2.4], therefore the equations (2. 15)-(2. 17) are modified to:

$$\begin{Bmatrix} \sigma_1 \\ \sigma_2 \\ \sigma_4 \\ \sigma_5 \\ \sigma_6 \end{Bmatrix} = [T] \begin{Bmatrix} \sigma_x \\ \sigma_y \\ \sigma_{yz} \\ \sigma_{zx} \\ \sigma_{xy} \end{Bmatrix} \text{ and } \begin{Bmatrix} \varepsilon_1 \\ \varepsilon_2 \\ \varepsilon_4 \\ \varepsilon_5 \\ \varepsilon_6 \end{Bmatrix} = [T] \begin{Bmatrix} \varepsilon_x \\ \varepsilon_y \\ \varepsilon_{yz} \\ \varepsilon_{xz} \\ \varepsilon_{xy} \end{Bmatrix} \tag{2. 18}$$

Where

$$[T] = \begin{bmatrix} m^2 & n^2 & 0 & 0 & 2mn \\ n^2 & m^2 & 0 & 0 & -2mn \\ 0 & 0 & m & -n & 0 \\ 0 & 0 & n & m & 0 \\ -mn & mn & 0 & 0 & (m^2 - n^2) \end{bmatrix} \tag{2. 19}$$

Multiplying (2. 18) by $[T]^{-1}$, the relationships can be written as

$$\begin{Bmatrix} \sigma_x \\ \sigma_y \\ \sigma_{yz} \\ \sigma_{zx} \\ \sigma_{xy} \end{Bmatrix} = [T]^{-1} \begin{Bmatrix} \sigma_1 \\ \sigma_2 \\ \sigma_4 \\ \sigma_5 \\ \sigma_6 \end{Bmatrix} \text{ and } \begin{Bmatrix} \varepsilon_x \\ \varepsilon_y \\ \varepsilon_{yz} \\ \varepsilon_{xz} \\ \varepsilon_{xy} \end{Bmatrix} = [T]^{-1} \begin{Bmatrix} \varepsilon_1 \\ \varepsilon_2 \\ \varepsilon_4 \\ \varepsilon_5 \\ \varepsilon_6 \end{Bmatrix} \tag{2. 20}$$

The $[T]^{-1}$ matrix is obtained by replacing θ by -θ in $[T]$, and is given by

$$[T]^{-1} = \begin{bmatrix} m^2 & n^2 & 0 & 0 & -2mn \\ n^2 & m^2 & 0 & 0 & 2mn \\ 0 & 0 & m & n & 0 \\ 0 & 0 & -n & m & 0 \\ mn & -mn & 0 & 0 & (m^2 - n^2) \end{bmatrix} \tag{2. 21}$$

Using Hooke´s law that relates stresses and strains, the general equations for a lamina of composite material in terms of the principal material directions (1, 2, 3), where 3 would represent the z-axis, are given by:

$$\begin{Bmatrix} \sigma_1 \\ \sigma_2 \\ \sigma_4 \\ \sigma_5 \\ \sigma_6 \end{Bmatrix} = \begin{bmatrix} Q_{11} & Q_{12} & 0 & 0 & 0 \\ Q_{12} & Q_{22} & 0 & 0 & 0 \\ 0 & 0 & 2Q_{44} & 0 & 0 \\ 0 & 0 & 0 & 2Q_{55} & 0 \\ 0 & 0 & 0 & 0 & 2Q_{66} \end{bmatrix} . \begin{Bmatrix} \varepsilon_1 \\ \varepsilon_2 \\ \varepsilon_4 \\ \varepsilon_5 \\ \varepsilon_6 \end{Bmatrix} \tag{2. 22}$$

Q_{ij} are defined in reference [2.4] and are given by:

$$\begin{cases} Q_{11} = E_1(1 - \nu_{23}\nu_{32})/\Delta \\ Q_{22} = E_2(1 - \nu_{31}\nu_{13})/\Delta \\ Q_{44} = \lambda G_{23} \\ Q_{55} = \lambda G_{13} \\ Q_{66} = \lambda G_{12} \\ Q_{12} = E_1(\nu_{21} + \nu_{31}\nu_{23})/\Delta \\ \quad\;\; = E_2(\nu_{12} + \nu_{32}\nu_{13})/\Delta \end{cases} \tag{2. 23}$$

where $\Delta = 1 - \nu_{12}\nu_{21} - \nu_{23}\nu_{32} - \nu_{31}\nu_{13} - 2\nu_{21}\nu_{32}\nu_{13}$.

Displacements in the *z*-direction are not considered, therefore $\nu_{23} = \nu_{32} = \nu_{31} = \nu_{13} = 0$ and (2. 23) comes

$$\begin{cases} Q_{11} = \dfrac{E_1}{1-\nu_{12}\nu_{21}} \\ Q_{22} = \dfrac{E_2}{1-\nu_{12}\nu_{21}} \\ Q_{12} = \dfrac{\nu_{21}E_1}{1-\nu_{12}\nu_{21}} \\ Q_{44} = \lambda G_{23} \\ Q_{55} = \lambda G_{13} \\ Q_{66} = G_{12} \end{cases} \tag{2. 24}$$

Here, E_1 and E_2 are the major and minor Young's moduli; ν_{12} and ν_{21} are the Poisson's ratios; G_{12} is the shear modulus. [2.4] 1 and 2 denote the principal directions of the plate layer. A shear correction factor, λ=5/6, that accounts for the fact that the shear stresses are not constant across the section, was introduced in (2. 24).

Multiplying equation (2. 20) by $[T]$ and substituting in equation (2. 22), we have

$$[T]\begin{Bmatrix} \sigma_x \\ \sigma_y \\ \sigma_{yz} \\ \sigma_{zx} \\ \sigma_{xy} \end{Bmatrix} = \begin{bmatrix} Q_{11} & Q_{12} & 0 & 0 & 0 \\ Q_{12} & Q_{22} & 0 & 0 & 0 \\ 0 & 0 & 2Q_{44} & 0 & 0 \\ 0 & 0 & 0 & 2Q_{55} & 0 \\ 0 & 0 & 0 & 0 & 2Q_{66} \end{bmatrix} [T]\begin{Bmatrix} \varepsilon_x \\ \varepsilon_y \\ \varepsilon_{yz} \\ \varepsilon_{xz} \\ \varepsilon_{xy} \end{Bmatrix}$$

which is equivalent to

$$\begin{Bmatrix} \sigma_x \\ \sigma_y \\ \sigma_{yz} \\ \sigma_{zx} \\ \sigma_{xy} \end{Bmatrix} = [T]^{-1}\begin{bmatrix} Q_{11} & Q_{12} & 0 & 0 & 0 \\ Q_{12} & Q_{22} & 0 & 0 & 0 \\ 0 & 0 & 2Q_{44} & 0 & 0 \\ 0 & 0 & 0 & 2Q_{55} & 0 \\ 0 & 0 & 0 & 0 & 2Q_{66} \end{bmatrix} [T]\begin{Bmatrix} \varepsilon_x \\ \varepsilon_y \\ \varepsilon_{yz} \\ \varepsilon_{xz} \\ \varepsilon_{xy} \end{Bmatrix}$$

by multiplying both members by $[T]^{-1}$. This is equivalent to

$$\begin{Bmatrix}\sigma_x\\ \sigma_y\\ \sigma_{yz}\\ \sigma_{zx}\\ \sigma_{xy}\end{Bmatrix}=\begin{bmatrix}\overline{Q}_{11} & \overline{Q}_{12} & 0 & 0 & \overline{Q}_{16}\\ \overline{Q}_{12} & \overline{Q}_{22} & 0 & 0 & \overline{Q}_{26}\\ 0 & 0 & \overline{Q}_{44} & \overline{Q}_{45} & 0\\ 0 & 0 & \overline{Q}_{45} & \overline{Q}_{55} & 0\\ \overline{Q}_{16} & \overline{Q}_{26} & 0 & 0 & \overline{Q}_{66}\end{bmatrix}\begin{Bmatrix}\varepsilon_x\\ \varepsilon_y\\ 2\varepsilon_{yz}\\ 2\varepsilon_{xz}\\ 2\varepsilon_{xy}\end{Bmatrix}, \tag{2. 25}$$

Considering $\varepsilon_{yz}=\frac{1}{2}\gamma_{yz}$, $\varepsilon_{xz}=\frac{1}{2}\gamma_{xz}$, and $\varepsilon_{xy}=\frac{1}{2}\gamma_{xy}$, equation (2. 25) comes

$$\begin{Bmatrix}\sigma_x\\ \sigma_y\\ \sigma_{yz}\\ \sigma_{zx}\\ \sigma_{xy}\end{Bmatrix}=\begin{bmatrix}\overline{Q}_{11} & \overline{Q}_{12} & 0 & 0 & \overline{Q}_{16}\\ \overline{Q}_{12} & \overline{Q}_{22} & 0 & 0 & \overline{Q}_{26}\\ 0 & 0 & \overline{Q}_{44} & \overline{Q}_{45} & 0\\ 0 & 0 & \overline{Q}_{45} & \overline{Q}_{55} & 0\\ \overline{Q}_{16} & \overline{Q}_{26} & 0 & 0 & \overline{Q}_{66}\end{bmatrix}\begin{Bmatrix}\varepsilon_x\\ \varepsilon_y\\ \gamma_{yz}\\ \gamma_{xz}\\ \gamma_{xy}\end{Bmatrix} \tag{2. 26}$$

where $\left[\overline{Q}\right]=[T]^{-1}[Q][T]$ is given by

$$\begin{aligned}
\overline{Q}_{11}&=Q_{11}m^4+2(Q_{12}+2Q_{66})m^2n^2+Q_{22}n^4\\
\overline{Q}_{12}&=(Q_{11}+Q_{22}-4Q_{66})m^2n^2+Q_{12}(m^4+n^4)\\
\overline{Q}_{16}&=-mn^3Q_{22}+m^3nQ_{11}-mn(m^2-n^2)(Q_{12}+2Q_{66})\\
\overline{Q}_{22}&=Q_{11}n^4+2(Q_{12}+2Q_{66})m^2n^2+Q_{22}m^4\\
\overline{Q}_{26}&=-m^3nQ_{22}+mn^3Q_{11}+mn(m^2-n^2)(Q_{12}+2Q_{66})\\
\overline{Q}_{44}&=Q_{44}m^2+Q_{55}n^2\\
\overline{Q}_{45}&=(Q_{55}-Q_{44})mn\\
\overline{Q}_{55}&=Q_{55}m^2+Q_{44}n^2\\
\overline{Q}_{66}&=Q_{11}+Q_{22}-2Q_{12})m^2n^2+Q_{66}(m^2-n^2)^2
\end{aligned} \tag{2. 27}$$

Equation (2. 26) can be written as

$$\begin{Bmatrix}\sigma_x\\ \sigma_y\\ \sigma_{xy}\end{Bmatrix}=\begin{bmatrix}\overline{Q}_{11} & \overline{Q}_{12} & \overline{Q}_{16}\\ \overline{Q}_{12} & \overline{Q}_{22} & \overline{Q}_{26}\\ \overline{Q}_{16} & \overline{Q}_{26} & \overline{Q}_{66}\end{bmatrix}\begin{Bmatrix}\varepsilon_x\\ \varepsilon_y\\ \gamma_{xy}\end{Bmatrix} \qquad (2.\ 28)$$

$$\begin{Bmatrix}\sigma_{yz}\\ \sigma_{zx}\end{Bmatrix}=\begin{bmatrix}\overline{Q}_{44} & \overline{Q}_{45}\\ \overline{Q}_{45} & \overline{Q}_{55}\end{bmatrix}\begin{Bmatrix}\gamma_{yz}\\ \gamma_{zx}\end{Bmatrix}$$

At this point the quantities Q_{ij} and $\overline{Q}_{ij}$ can be determined relating stresses and strains in either coordinate system. Equations (2. 28) are the constitutive equations of laminae.

In the following, N is the number of laminae that composes the laminate. For the k^{th} laminae, equation (2. 26) can be written as

$$\begin{Bmatrix}\sigma_x\\ \sigma_y\\ \sigma_{yz}\\ \sigma_{zx}\\ \sigma_{xy}\end{Bmatrix}_k=\left[\overline{Q}\right]_k\begin{Bmatrix}\varepsilon_x\\ \varepsilon_y\\ \gamma_{yz}\\ \gamma_{xz}\\ \gamma_{xy}\end{Bmatrix}_k \qquad (2.\ 29)$$

where all matrices must have the subscript k due to the orientation of the particular lamina with respect to the plate x-y coordinates and its unique $\left[\overline{Q}\right]$.

Consider equations (2. 1) to (2. 13), and a laminated plate, elastic, with uniform thickness h, and each layer of the plate is homogeneous and orthotropic; h_k is the vectorial distance from the mid-plane, to the upper surface of the k^{th} lamina.

2.2 - *Moment-Curvature and stress relations*

The in-plane stress resultants $\{T_x,\ T_y,\ T_{xy}\}$ and the moments $\{M_x,\ M_y,\ M_{xy}\}$, per unit length are defined by:

$$\{T_x,\ T_y,\ T_{xy}\}=\int_{-\frac{h}{2}}^{\frac{h}{2}}\{\sigma_x,\ \sigma_y,\ \tau_{xy}\}dz\,, \qquad (2.\ 30)$$

$$\left\{M_x, \quad M_y, \quad M_{xy}\right\} = \int_{-\frac{h}{2}}^{\frac{h}{2}} \left\{\sigma_x, \quad \sigma_y, \quad \tau_{xy}\right\} z dz \tag{2. 31}$$

The shear stress resultants are

$$\left\{Q_x, \quad Q_y\right\} = \int_{-\frac{h}{2}}^{\frac{h}{2}} \left\{\tau_{xz}, \quad \tau_{yz}\right\} dz \tag{2. 32}$$

For a laminated plate, the stress components can be integrated across each lamina and added together as follows, employing equations (2. 29), (2. 5) and (2. 6),

$$\left\{T_x, \quad T_y, \quad T_{xy}\right\} = \sum_{k=1}^{N} \int_{h_{k-1}}^{h_k} \left\{\sigma_x, \quad \sigma_y, \quad \tau_{xy}\right\} dz =$$

$$= \sum_{k=1}^{N} \left\{ \int_{h_{k-1}}^{h_k} \left[\overline{Q}\right]_k \left\{\varepsilon_x^0, \quad \varepsilon_y^0, \quad \tau_{xy}^0\right\}_k dz + \int_{h_{k-1}}^{h_k} \left[\overline{Q}\right]_k \left\{k_x, \quad k_y, \quad k_{xy}\right\}_k z dz \right\} \tag{2. 33}$$

Since the derivatives of u_0 and v_0 (mid-surface displacements) and the $\overline{Q}$'s are not functions of z, (2. 33) can be rewritten as:

$$\left\{T_x, \quad T_y, \quad T_{xy}\right\} =$$

$$= \sum_{k=1}^{N} \left\{ \left[\overline{Q}\right]_k \left\{\varepsilon_x^0, \quad \varepsilon_y^0, \quad \tau_{xy}^0\right\}_k \int_{h_{k-1}}^{h_k} dz + \left[\overline{Q}\right]_k \left\{k_x, \quad k_y, \quad k_{xy}\right\}_k \int_{h_{k-1}}^{h_k} z dz \right\} \tag{2. 34}$$

or, in reduced form,

$$[T] = [A][\varepsilon_0] + [B][k] \tag{2. 35}$$

where

$$A_{ij} = \sum_{k=1}^{N} (\overline{Q}_{ij})_k \left[h_k - h_{k-1}\right], \; [i,j = 1,2,6] \tag{2. 36}$$

$$B_{ij} = \tfrac{1}{2} \sum_{k=1}^{N} (\overline{Q}_{ij})_k \left[h_k^2 - h_{k-1}^2\right], \; [i,j = 1,2,6] \tag{2. 37}$$

From equation (2. 31),

$$\left\{M_x, \quad M_y, \quad M_{xy}\right\} = \sum_{k=1}^{N} \int_{h_{k-1}}^{h_k} \left\{\sigma_x, \quad \sigma_y, \quad \tau_{xy}\right\} z dz =$$

$$= \sum_{k=1}^{N} \left\{ \int_{h_{k-1}}^{h_k} \left[\overline{Q}\right]_k \left\{\varepsilon_x^0, \quad \varepsilon_y^0, \quad \tau_{xy}^0\right\}_k z dz + \int_{h_{k-1}}^{h_k} \left[\overline{Q}\right]_k \left\{\kappa_x, \quad \kappa_y, \quad \kappa_{xy}\right\}_k z^2 dz \right\}$$

$$= \sum_{k=1}^{N} \left\{ \left[\overline{Q}\right]_k \left\{\varepsilon_x^0, \quad \varepsilon_y^0, \quad \tau_{xy}^0\right\}_k \int_{h_{k-1}}^{h_k} z dz + \left[\overline{Q}\right]_k \left\{\kappa_x, \quad \kappa_y, \quad \kappa_{xy}\right\}_k \int_{h_{k-1}}^{h_k} z^2 d \right. \tag{2. 38}$$

or, in reduced form[1],

$$[M] = [B][\varepsilon_0] + [D][\kappa] \tag{2. 39}$$

Where

$$D_{ij} = \tfrac{1}{3} \sum_{k=1}^{N} (\overline{Q}_{ij})_k \left[h_k^3 - h_{k-1}^3\right], [i,j = 1,2,6] \tag{2. 40}$$

From (2. 22), (2. 5), and (2. 30) to (2. 32),

$$\tau_{xz_k} = 2\overline{Q}_{55_k} \varepsilon_{xz} + 2\overline{Q}_{45_k} \varepsilon_{yz}$$

$$\tau_{yz_k} = 2\overline{Q}_{45_k} \varepsilon_{xz} + 2\overline{Q}_{44_k} \varepsilon_{yz}$$

hence

$$Q_x = 2\left(A_{55}\varepsilon_{xz} + A_{45}\varepsilon_{yz}\right) \tag{2. 41}$$

$$Q_y = 2\left(A_{45}\varepsilon_{xz} + A_{44}\varepsilon_{yz}\right) \tag{2. 42}$$

Combining (2.32) and (2.36),

$$\begin{cases} [T] = [A][\varepsilon_0] + [B][k] \\ [M] = [B][\varepsilon_0] + [D][k] \end{cases}, \tag{2. 43}$$

we have

$$\begin{Bmatrix} T \\ M \end{Bmatrix} = \begin{bmatrix} [A] & [B] \\ [B] & [D] \end{bmatrix} \{\varepsilon\} = [E]\{\varepsilon\} \tag{2. 44}$$

which is equivalent to

[1] The notation here used for the reduced form is equal to the representation of the mass matrix defined in section 2.3.

$$\begin{bmatrix} T_x \\ T_y \\ T_{xy} \\ \hline M_x \\ M_y \\ M_{xy} \end{bmatrix} = \left[\begin{array}{ccc|ccc} A_{11} & A_{12} & A_{16} & B_{11} & B_{12} & B_{16} \\ A_{12} & A_{22} & A_{26} & B_{12} & B_{22} & B_{26} \\ A_{16} & A_{26} & A_{66} & B_{16} & B_{26} & B_{66} \\ \hline B_{11} & B_{12} & B_{16} & D_{11} & D_{12} & D_{16} \\ B_{12} & B_{22} & B_{26} & D_{12} & D_{22} & D_{26} \\ B_{16} & B_{26} & B_{66} & D_{16} & D_{26} & D_{66} \end{array}\right] \begin{bmatrix} \varepsilon_x^0 \\ \varepsilon_y^0 \\ \tau_{xy}^0 \\ \hline \kappa_x \\ \kappa_y \\ \kappa_{xy} \end{bmatrix} \tag{2. 45}$$

where $[\mathrm{A}]$ is the extensional stiffness matrix relating in-plane stress resultants (N's) to the mid-surface strains (ε_0's); $[D]$ is the flexural stiffness matrix relating the stress couples (M's) to the curvatures (k's), and $[B]$ is the bending-stretching matrix and relates M's to ε_0's and N's to k's. The model presented is valid for laminated plates which may be not symmetrical about their mid-surface plane.

2.3 - *Equations of Motion*

The equations of motion of the plate are derived by equating the sum of the virtual work of the inertia forces, of the elastic restoring forces, and of external forces to zero. In-plane and transverse external forces are considered.

Combining equations (2. 4), (2. 5) and (2. 6), the strains are expressed as

$$\begin{Bmatrix} \varepsilon_x \\ \varepsilon_y \\ \varepsilon_{xy} \end{Bmatrix} = \begin{bmatrix} 1 & 0 & 0 & -z & 0 & 0 \\ 0 & 1 & 0 & 0 & -z & 0 \\ 0 & 0 & 1 & 0 & 0 & -z \end{bmatrix} \{\varepsilon\} \tag{2. 46}$$

Where

$$\{\varepsilon\} = \begin{Bmatrix} \varepsilon_0^p \\ \varepsilon_0^b \end{Bmatrix} + \begin{Bmatrix} \varepsilon_L^p \\ 0 \end{Bmatrix} \tag{2. 47}$$

The linear membrane and bending strains, $\{\varepsilon_0^p\}$ and $\{\varepsilon_0^b\}$, and the geometrically non-linear membrane strain, $\{\varepsilon_L^p\}$, are defined as

$$\left\{\varepsilon_0^p\right\}=\begin{Bmatrix} u_{,x} \\ v_{,y} \\ u_{,y}+v_{,x} \end{Bmatrix},\ \left\{\varepsilon_0^b\right\}=\begin{Bmatrix} -\dfrac{\partial\Phi_y^0}{\partial x} \\ \dfrac{\partial\Phi_x^0}{\partial y} \\ -\dfrac{\partial\Phi_y^0}{\partial y}+\dfrac{\partial\Phi_x^0}{\partial x} \end{Bmatrix},\ \left\{\varepsilon_L^p\right\}=\begin{Bmatrix} \left(w_{,x}\right)^2/2 \\ \left(w_{,x}\right)^2/2 \\ w_{,x}w_{,y} \end{Bmatrix} \tag{2. 48}$$

Or, in terms of shape functions and generalized displacements, using relation (2. 8),

$$\left\{\varepsilon_0^p\right\}=\begin{bmatrix} \left\{N_{,x}^u\right\}^T & 0 \\ 0 & \left\{N_{,y}^u\right\}^T \\ \left\{N_{,y}^u\right\}^T & \left\{N_{,x}^u\right\}^T \end{bmatrix}\begin{Bmatrix} q_u \\ q_v \end{Bmatrix} \tag{2. 49}$$

$$\left\{\varepsilon_0^b\right\}=\begin{bmatrix} -\left\{N_{,x}^{\Phi_y}\right\}^T & 0 \\ 0 & \left\{N_{,y}^{\Phi_x}\right\}^T \\ -\left\{N_{,y}^{\Phi_y}\right\}^T & \left\{N_{,x}^{\Phi_x}\right\}^T \end{bmatrix}\begin{Bmatrix} q_{\Phi_y} \\ q_{\Phi_x} \end{Bmatrix} \tag{2. 50}$$

$$\left\{\varepsilon_L^p\right\}=\begin{bmatrix} \frac{1}{2}\left\{q_w\right\}^T\left\{N_{,x}^w\right\}\left\{N_{,x}^w\right\}^T\left\{q_w\right\} \\ \frac{1}{2}\left\{q_w\right\}^T\left\{N_{,y}^w\right\}\left\{N_{,y}^w\right\}^T\left\{q_w\right\} \\ \left\{q_w\right\}^T\left\{N_{,x}^w\right\}\left\{N_{,y}^w\right\}^T\left\{q_w\right\} \end{bmatrix} \tag{2. 51}$$

The transverse shear strains, $\left\{\gamma_{zx}\right\}$ and $\left\{\gamma_{yz}\right\}$ are defined as

$$\begin{Bmatrix} \gamma_{yz} \\ \gamma_{zx} \end{Bmatrix}=\begin{Bmatrix} w_{,y}^0-\Phi_x \\ w_{,x}^0+\Phi_y \end{Bmatrix}=\begin{bmatrix} \left\{N_{,y}^w\right\}^T & 0 & -\left\{N^{\Phi_x}\right\}^T \\ \left\{N_{,x}^w\right\}^T & \left\{N^{\Phi_y}\right\}^T & 0 \end{bmatrix}\begin{Bmatrix} q_w \\ q_{\Phi_y} \\ q_{\Phi_x} \end{Bmatrix} \tag{2. 52}$$

The principle of virtual work states that:

$$\delta W_{in}+\delta W_v+\delta W_{ex}=0 \tag{2. 53}$$

where δW_{in}, δW_v and δW_{ex} are, respectively, the work done by the inertia, internal and external forces due to virtual displacements $\{\delta d\}$. $\{\delta d\}$ is given by

$$\{\delta d\} = \begin{Bmatrix} \delta u \\ \delta v \\ \delta w \\ \delta \Phi_x \\ \delta \Phi_y \end{Bmatrix} = [N]\{\delta q\} \tag{2. 54}$$

Making use of d'Alembert principle, we obtain the following expression for the virtual work of the inertia forces:

$$\delta W_{in} = -\rho h \int_\Omega \{\delta d\}^T \{\ddot{d}\} d\Omega = \{\delta q\}^T \left(-\rho h \int_\Omega [N]^T [N] d\Omega \{\ddot{q}\}\right) = -\{\delta q\}^T [M]\{\ddot{q}\}$$

(2. 55)

Where $[M]$ is the mass matrix:

$$[M] = \rho h \int_\Omega [N]^T [N] d\Omega =$$

$$= \begin{bmatrix} \rho h \int_\Omega \{N^u\}^T \{N^u\}^T d\Omega & 0 & 0 & 0 & 0 \\ 0 & \rho h \int_\Omega \{N^u\}^T \{N^u\}^T d\Omega & 0 & 0 & 0 \\ 0 & 0 & \rho h \int_\Omega \{N^w\}^T \{N^w\}^T d\Omega & 0 & 0 \\ 0 & 0 & 0 & \frac{\rho h^3}{12} \int_\Omega \{N^{\Phi_y}\}^T \{N^{\Phi_y}\}^T d\Omega & 0 \\ 0 & 0 & 0 & 0 & \frac{\rho h^3}{12} \int_\Omega \{N^{\Phi_x}\}^T \{N^{\Phi_x}\}^T d\Omega \end{bmatrix} =$$

(2. 56)

where ρ is the mass density of the material that constitutes the plate, $\{\ddot{q}\} = \dfrac{d^2\{q\}}{dt^2}$ and Ω represents the area of the plate.

This is equivalent to, in simplified notation,

$$[M]=\begin{bmatrix} [M_p] & 0 & 0 & 0 & 0 \\ 0 & [M_p] & 0 & 0 & 0 \\ 0 & 0 & [M_b] & 0 & 0 \\ 0 & 0 & 0 & [M_{Ry}] & 0 \\ 0 & 0 & 0 & 0 & [M_{Rx}] \end{bmatrix} \tag{2. 57}$$

where $[M_p]$ and $[M_b]$ are the in-plane and out-of-plane inertia matrices, $[M_{Ry}]$ and $[M_{Rx}]$ are due to the rotatory inertia.

The variation δW_v may be expressed as:

$$\delta W_v = -\delta\int_\Omega \{\varepsilon\}^T \begin{Bmatrix} T \\ M \end{Bmatrix} d\Omega - \int_\Omega \{\delta\gamma\}^T \{Q\}\, d\Omega \tag{2. 58}$$

Substituting equations (2. 47) and (2. 44) in (2. 58),

$$\delta W_v = -\delta\int_\Omega \left(\begin{Bmatrix} \varepsilon_0^p \\ \varepsilon_0^b \end{Bmatrix}^T + \begin{Bmatrix} \varepsilon_L^p \\ 0 \end{Bmatrix}^T \right) [E] \left(\begin{Bmatrix} \varepsilon_0^p \\ \varepsilon_0^b \end{Bmatrix} + \begin{Bmatrix} \varepsilon_L^p \\ 0 \end{Bmatrix} \right) d\Omega - \int_\Omega \left(\{\delta\gamma\}^T \{Q\}\, d\Omega \right) \tag{2. 59}$$

$$= -\delta\int_\Omega \left(\begin{Bmatrix} \varepsilon_0^p \\ \varepsilon_0^b \end{Bmatrix}^T [E] + \begin{Bmatrix} \varepsilon_L^p \\ 0 \end{Bmatrix}^T [E] \right) \left(\begin{Bmatrix} \varepsilon_0^p \\ \varepsilon_0^b \end{Bmatrix} + \begin{Bmatrix} \varepsilon_L^p \\ 0 \end{Bmatrix} \right) d\Omega - \int_\Omega \{\delta\gamma\}^T \{Q\}\, d\Omega$$

$$= -\delta\int_\Omega \left(\begin{Bmatrix} \varepsilon_0^p \\ \varepsilon_0^b \end{Bmatrix}^T [E] \begin{Bmatrix} \varepsilon_0^p \\ \varepsilon_0^b \end{Bmatrix} + \begin{Bmatrix} \varepsilon_0^p \\ \varepsilon_0^b \end{Bmatrix}^T [E] \begin{Bmatrix} \varepsilon_L^p \\ 0 \end{Bmatrix} + \begin{Bmatrix} \varepsilon_L^p \\ 0 \end{Bmatrix}^T [E] \begin{Bmatrix} \varepsilon_0^p \\ \varepsilon_0^b \end{Bmatrix} + \begin{Bmatrix} \varepsilon_L^p \\ 0 \end{Bmatrix}^T [E] \begin{Bmatrix} \varepsilon_L^p \\ 0 \end{Bmatrix} \right) d\Omega$$

$$-\int_\Omega \{\delta\gamma\}^T \{Q\}\, d\Omega =$$

$$= \begin{Bmatrix} \delta u \\ \delta v \\ \delta w \\ \delta\phi_x \\ \delta\phi_y \end{Bmatrix}^T \int_\Omega [N]^T \begin{Bmatrix} P_u(x,y,t) \\ P_v(x,y,t) \\ P_w(x,y,t) \\ 0 \\ 0 \end{Bmatrix} d\Omega \tag{2. 60}$$

Where $P_u(x,y,t)$, $P_v(x,y,t)$ and $P_w(x,y,t)$ are the distributed forces (N/m^2) applied to the plate in the *x*, *y*, *z* directions, respectively. The linear stiffness matrix $[K_1]$, non-

linear stiffness matrices, $[K_2],[K_3]$ and $[K_4]$ and the vector of external forces $\{P\}$ are defined as follows:

$$\delta\int_\Omega\left(\begin{Bmatrix}\varepsilon_0^p\\ \varepsilon_0^b\end{Bmatrix}^T[E]\begin{Bmatrix}\varepsilon_0^p\\ \varepsilon_0^b\end{Bmatrix}\right)d\Omega-\int_\Omega\{\delta\gamma\}^T\{Q\}\,d\Omega$$

$$=\delta\int_\Omega\left(\begin{Bmatrix}\varepsilon_0^p\\ \varepsilon_0^b\end{Bmatrix}^T\begin{bmatrix}[A] & [B]\\ [B] & [D]\end{bmatrix}\begin{Bmatrix}\varepsilon_0^p\\ \varepsilon_0^b\end{Bmatrix}\right)d\Omega-\int_\Omega\{\delta\gamma\}^T\{Q\}\,d\Omega$$

$$=\{\delta q\}^T[K_1]\{q\}, \tag{2. 61}$$

$$\delta\int_\Omega\left(\begin{Bmatrix}\varepsilon_0^p\\ \varepsilon_0^b\end{Bmatrix}^T[E]\begin{Bmatrix}\varepsilon_L^p\\ 0\end{Bmatrix}\right)d\Omega=\delta\int_\Omega\left(\begin{Bmatrix}\varepsilon_0^p\\ \varepsilon_0^b\end{Bmatrix}^T\begin{bmatrix}[A] & [B]\\ [B] & [D]\end{bmatrix}\begin{Bmatrix}\varepsilon_L^p\\ 0\end{Bmatrix}\right)d\Omega$$

$$=\{\delta q\}^T[K_2]\{q\}, \tag{2. 62}$$

$$\delta\int_\Omega\left(\begin{Bmatrix}\varepsilon_L^p\\ 0\end{Bmatrix}[E]\begin{Bmatrix}\varepsilon_0^p\\ \varepsilon_0^b\end{Bmatrix}^T\right)d\Omega=\delta\int_\Omega\left(\begin{Bmatrix}\varepsilon_L^p\\ 0\end{Bmatrix}\begin{bmatrix}[A] & [B]\\ [B] & [D]\end{bmatrix}\begin{Bmatrix}\varepsilon_0^p\\ \varepsilon_0^b\end{Bmatrix}^T\right)d\Omega$$

$$=\{\delta q\}^T[K_3]\{q\} \tag{2. 63}$$

$$\delta\int_\Omega\left(\begin{Bmatrix}\varepsilon_L^p\\ 0\end{Bmatrix}^T[E]\begin{Bmatrix}\varepsilon_L^p\\ 0\end{Bmatrix}\right)d\Omega=\delta\int_\Omega\left(\begin{Bmatrix}\varepsilon_L^p\\ 0\end{Bmatrix}^T\begin{bmatrix}[A] & [B]\\ [B] & [D]\end{bmatrix}\begin{Bmatrix}\varepsilon_L^p\\ 0\end{Bmatrix}\right)d\Omega$$

$$=\{\delta q\}^T[K_4]\{q\} \tag{2. 64}$$

$$\{\delta q\}^T\int_\Omega[N]^T\begin{Bmatrix}P_u(x,y,t)\\ P_v(x,y,t)\\ P_w(x,y,t)\\ 0\\ 0\end{Bmatrix}d\Omega=\{\delta q\}^T\{P\}, \tag{2. 65}$$

where $\{P\} = \begin{Bmatrix} P_u(x,y,t) \\ P_v(x,y,t) \\ P_w(x,y,t) \\ 0 \\ 0 \end{Bmatrix}$.

Therefore, equation (2. 59) may be expressed as

$$\delta W_v = -\{\delta q\}^T \left([K_1]+[K_2]+[K_3]+[K_4]\right)\{q\} \tag{2. 66}$$

The generalized excitation forces δW_{ex} can be expressed in terms of the actual forces and the shape functions of the HFEM, by means of the virtual work executed by these forces. For example, if $P_j(t)$ represents a transverse concentrated force acting at the point $x = x_j$ and $P_d(x,y,t)$ represents a transverse distributed force, the virtual work of the external forces is given by:

$$\delta W_{ex} = \int_\Omega \left[P_j(t)\delta(x-x_j)\delta(y-y_j) + P_d(x,y,t)\right]\delta w(x,t)d\Omega = \{\delta q_w\}^T \{P_w(t)\} \tag{2. 67}$$

where $\delta(x-x_j)$ represents a spatial Dirac delta functions given by

$$\begin{aligned} &\delta(x-x_j) \qquad x \neq x_j \\ &\int_0^L \delta(x-x_j)dx = 1 \end{aligned} \tag{2. 68}$$

So that $P_j(t)\delta(x-x_j)\delta(y-y_j)$ has units of distributed force (N/m^2).

Substituting equations (2. 61)-(2. 65) into equation (2. 60) and allowing the virtual generalized displacements to be arbitrary, gives the time domain equations of motion in generalized coordinates:

$$-\{\delta q\}^T [M]\{\ddot{q}\} - \{\delta q\}^T \left([K_1]+[K_2]+[K_3]+[K_4]\right)\{q\} + \{\delta q\}^T \{P(t)\} = 0 \tag{2. 69}$$

This is equivalent to,

$$\{\delta q\}^T\left(-[M]\{\ddot{q}\}-\left([K_1]+[K_2]+[K_3]+[K_4]\right)\{q\}+\{P(t)\}\right)=0$$

$$\Leftrightarrow [M]\{\ddot{q}\}+[K_1]\{q\}+\left([K_2]+[K_3]+[K_4]\right)\{q\}=\{P(t)\}$$

$$\Leftrightarrow [M]\{\ddot{q}\}+[Kl]\{q\}+[Knl]\{q\}=\{P\} \qquad (2.\ 70)$$

In a more detailed form, equation (2. 70) may be written as follows:

$$\begin{bmatrix} [M_p] & 0 & 0 & 0 & 0 \\ 0 & [M_p] & 0 & 0 & 0 \\ 0 & 0 & [M_b] & 0 & 0 \\ 0 & 0 & 0 & [M_{Ry}] & 0 \\ 0 & 0 & 0 & 0 & [M_{Rx}] \end{bmatrix} \begin{Bmatrix} \ddot{q}_u \\ \ddot{q}_v \\ \ddot{q}_w \\ \ddot{q}_{\Phi_y} \\ \ddot{q}_{\Phi_x} \end{Bmatrix} +$$

$$+\begin{bmatrix} [K_1^{p11}] & [K_1^{p12}] & 0 & [K_1^{pb11}] & [K_1^{pb12}] \\ [K_1^{p21}] & [K_1^{p22}] & 0 & [K_1^{pb21}] & [K_1^{pb22}] \\ 0 & 0 & [K_1^{\gamma 11}] & [K_1^{\gamma 12}] & [K_1^{\gamma 13}] \\ [K_1^{bp11}] & [K_1^{bp12}] & [K_1^{\gamma 21}] & [K_1^{b11}]+[K_1^{\gamma 22}] & [K_1^{b12}]+[K_1^{\gamma 23}] \\ [K_1^{bp21}] & [K_1^{bp22}] & [K_1^{\gamma 31}] & [K_1^{b21}]+[K_1^{\gamma 32}] & [K_1^{b22}]+[K_1^{\gamma 33}] \end{bmatrix} \begin{Bmatrix} q_u \\ q_v \\ q_w \\ q_{\Phi_y} \\ q_{\Phi_x} \end{Bmatrix}$$

$$+\begin{bmatrix} 0 & 0 & [K_2^{11}] & 0 & 0 \\ 0 & 0 & [K_2^{21}] & 0 & 0 \\ [K_3^{11}] & [K_3^{12}] & [K_2^{31}]+[K_3^{13}]+[K_4] & 0 & 0 \\ 0 & 0 & 0 & 0 & 0 \\ 0 & 0 & 0 & 0 & 0 \end{bmatrix} \begin{Bmatrix} q_u \\ q_v \\ q_w \\ q_{\Phi_y} \\ q_{\Phi_x} \end{Bmatrix} = \begin{Bmatrix} \{P_u\} \\ \{P_v\} \\ \{P_w\} \\ 0 \\ 0 \end{Bmatrix}, \qquad (2.\ 71)$$

Where

$$\begin{bmatrix} [K_1^{p11}] & [K_1^{p12}] \\ [K_1^{p21}] & [K_1^{p22}] \end{bmatrix}, \begin{bmatrix} [K_1^{b11}] & [K_1^{b12}] \\ [K_1^{b21}] & [K_1^{b22}] \end{bmatrix}, \begin{bmatrix} [K_1^{pb11}] & [K_1^{pb12}] \\ [K_1^{pb21}] & [K_1^{pb22}] \end{bmatrix}, \begin{bmatrix} [K_1^{bp11}] & [K_1^{bp12}] \\ [K_1^{bp21}] & [K_1^{bp22}] \end{bmatrix},$$

$\begin{bmatrix} [K_1^{\gamma 11}] & [K_1^{\gamma 12}] & [K_1^{\gamma 13}] \\ [K_1^{\gamma 21}] & [K_1^{\gamma 22}] & [K_1^{\gamma 23}] \\ [K_1^{\gamma 31}] & [K_1^{\gamma 32}] & [K_1^{\gamma 33}] \end{bmatrix}$, $\begin{bmatrix} [K_2^{11}] \\ [K_2^{21}] \\ [K_2^{31}] \end{bmatrix}$ and $\begin{bmatrix} [K_3^{11}] & [K_3^{12}] & [K_3^{13}] \end{bmatrix}$ indicate the area which $[K_1^p]$,$[K_1^b]$, $[K_1^{pb}]$,$[K_1^{bp}]$, $[K_1^\gamma]$, $[K_2]$ and $[K_3]$occupy, respectively. $[K_1^p]$is the in-plane linear stiffness matrix, $[K_1^b]$ is the out-plane linear stiffness matrix, $[K_1^{pb}]$and$[K_1^{bp}]$ are the in-plane/bending coupling matrices, and $[K_1^\gamma]$is the shear linear stiffness matrix; they form the linear $[K_1]$ matrix. $[K_2]$, $[K_3]$ and $[K_4]$represent the nonzero part of the non-linear stiffness matrices and $\{P\} = \{\{P_u\} \quad \{P_v\} \quad \{P_w\} \quad 0 \quad 0\}^T$ is the vector of generalized external forces. These matrices are defined in the following sections, with the exception of$[K_3]$. As is demonstrated in reference [2.1], by comparing the form of $[K_3]$ and$[K_2]$, $[K_3]$=$2[K_2]^T$.

From equation (2. 71), the system can be split in two parts:

$$\begin{bmatrix} [M_p] & 0 & 0 & 0 & 0 \\ 0 & [M_p] & 0 & 0 & 0 \end{bmatrix} \begin{Bmatrix} \ddot{q}_u \\ \ddot{q}_v \\ \ddot{q}_w \\ \ddot{q}_{\Phi_y} \\ \ddot{q}_{\Phi_x} \end{Bmatrix} +$$

$$\begin{bmatrix} [K_1^{p11}] & [K_1^{p12}] & 0 & [K_1^{pb11}] & [K_1^{pb12}] \\ [K_1^{p21}] & [K_1^{p22}] & 0 & [K_1^{pb21}] & [K_1^{pb22}] \end{bmatrix} \begin{Bmatrix} q_u \\ q_v \\ q_w \\ q_{\Phi_y} \\ q_{\Phi_x} \end{Bmatrix} +$$

$$+\begin{bmatrix} 0 & 0 & \left[K_2^{11}\right] & 0 & 0 \\ 0 & 0 & \left[K_2^{21}\right] & 0 & 0 \end{bmatrix}\begin{Bmatrix} q_u \\ q_v \\ q_w \\ q_{\Phi_y} \\ q_{\Phi_x} \end{Bmatrix} = \begin{Bmatrix} \{P_u\} \\ \{P_v\} \end{Bmatrix} \tag{2. 72}$$

And

$$\begin{bmatrix} \left[M_b\right] & 0 & 0 \\ 0 & \left[M_{Ry}\right] & 0 \\ 0 & 0 & \left[M_{Rx}\right] \end{bmatrix}\begin{Bmatrix} \ddot{q}_w \\ \ddot{q}_{\Phi_y} \\ \ddot{q}_{\Phi_x} \end{Bmatrix} +$$

$$+\begin{bmatrix} 0 & 0 & \left[K_1^{\gamma 11}\right] & \left[K_1^{\gamma 12}\right] & \left[K_1^{\gamma 13}\right] \\ \left[K_1^{bp11}\right] & \left[K_1^{bp12}\right] & \left[K_1^{\gamma 21}\right] & \left[K_1^{b11}\right]+\left[K_1^{\gamma 22}\right] & \left[K_1^{b12}\right]+\left[K_1^{\gamma 23}\right] \\ \left[K_1^{bp21}\right] & \left[K_1^{bp22}\right] & \left[K_1^{\gamma 31}\right] & \left[K_1^{b21}\right]+\left[K_1^{\gamma 32}\right] & \left[K_1^{b22}\right]+\left[K_1^{\gamma 33}\right] \end{bmatrix}\begin{Bmatrix} q_u \\ q_v \\ q_w \\ q_{\Phi_y} \\ q_{\Phi_x} \end{Bmatrix} +$$

$$+\begin{bmatrix} \left[K_3^{11}\right] & \left[K_3^{12}\right] & \left[K_2^{31}\right]+\left[K_3^{13}\right]+\left[K_4\right] & 0 & 0 \\ 0 & 0 & 0 & 0 & 0 \\ 0 & 0 & 0 & 0 & 0 \end{bmatrix}\begin{Bmatrix} q_u \\ q_v \\ q_w \\ q_{\Phi_y} \\ q_{\Phi_x} \end{Bmatrix} = \begin{Bmatrix} \{P_w\} \\ 0 \\ 0 \end{Bmatrix} \tag{2. 73}$$

In not too thick plates and if the in-plane displacements are much smaller than the transverse displacements, the in-plane inertia can be neglected. Therefore, from (2.72), comes

$$\begin{bmatrix} \left[K_1^{p11}\right] & \left[K_1^{p12}\right] & 0 & \left[K_1^{pb11}\right] & \left[K_1^{pb12}\right] \\ \left[K_1^{p21}\right] & \left[K_1^{p22}\right] & 0 & \left[K_1^{pb21}\right] & \left[K_1^{pb22}\right] \end{bmatrix}\begin{Bmatrix} q_u \\ q_v \\ q_w \\ q_{\Phi_y} \\ q_{\Phi_x} \end{Bmatrix} +$$

$$+\begin{bmatrix} 0 & 0 & \left[K_2^{11}\right] & 0 & 0 \\ 0 & 0 & \left[K_2^{21}\right] & 0 & 0 \end{bmatrix}\begin{Bmatrix} q_u \\ q_v \\ q_w \\ q_{\Phi_y} \\ q_{\Phi_x} \end{Bmatrix} = \begin{Bmatrix} \{P_u\} \\ \{P_v\} \end{Bmatrix} \tag{2. 74}$$

Solving (2.74) for $\begin{Bmatrix} q_u \\ q_v \end{Bmatrix}$, comes

$$\begin{Bmatrix} q_u \\ q_v \end{Bmatrix} = \begin{bmatrix} \left[K_1^{p11}\right] & \left[K_1^{p12}\right] \\ \left[K_1^{p21}\right] & \left[K_1^{p22}\right] \end{bmatrix}^{-1} \begin{Bmatrix} \{P_u\} \\ \{P_v\} \end{Bmatrix} - \begin{bmatrix} \left[K_1^{p11}\right] & \left[K_1^{p12}\right] \\ \left[K_1^{p21}\right] & \left[K_1^{p22}\right] \end{bmatrix}^{-1} \begin{bmatrix} \left[K_1^{pb11}\right] & \left[K_1^{pb12}\right] \\ \left[K_1^{pb21}\right] & \left[K_1^{pb22}\right] \end{bmatrix} \begin{Bmatrix} q_{\Phi y} \\ q_{\Phi x} \end{Bmatrix}$$

$$-\begin{bmatrix} \left[K_1^{p11}\right] & \left[K_1^{p12}\right] \\ \left[K_1^{p21}\right] & \left[K_1^{p22}\right] \end{bmatrix}^{-1} \begin{bmatrix} \left[K_2^{11}\right] \\ \left[K_2^{21}\right] \end{bmatrix} \{q_w\} \tag{2. 75}$$

From (2.73),

$$\begin{bmatrix} \left[M_b\right] & 0 & 0 \\ 0 & \left[M_{Ry}\right] & 0 \\ 0 & 0 & \left[M_{Rx}\right] \end{bmatrix} \begin{Bmatrix} \ddot{q}_w \\ \ddot{q}_{\Phi_y} \\ \ddot{q}_{\Phi_x} \end{Bmatrix} + \begin{bmatrix} 0 & 0 & 0 & 0 & 0 \\ \left[K_1^{bp11}\right] & \left[K_1^{bp12}\right] & 0 & 0 & 0 \\ \left[K_1^{bp21}\right] & \left[K_1^{bp22}\right] & 0 & 0 & 0 \end{bmatrix} \begin{Bmatrix} q_u \\ q_v \\ q_w \\ q_{\Phi_y} \\ q_{\Phi_x} \end{Bmatrix} +$$

$$+\begin{bmatrix} 0 & 0 & \left[K_1^{\gamma 11}\right] & \left[K_1^{\gamma 12}\right] & \left[K_1^{\gamma 13}\right] \\ 0 & 0 & \left[K_1^{\gamma 21}\right] & \left[K_1^{b11}\right]+\left[K_1^{\gamma 22}\right] & \left[K_1^{b12}\right]+\left[K_1^{\gamma 23}\right] \\ 0 & 0 & \left[K_1^{\gamma 31}\right] & \left[K_1^{b21}\right]+\left[K_1^{\gamma 32}\right] & \left[K_1^{b22}\right]+\left[K_1^{\gamma 33}\right] \end{bmatrix} \begin{Bmatrix} q_u \\ q_v \\ q_w \\ q_{\Phi_y} \\ q_{\Phi_x} \end{Bmatrix} +$$

$$+\begin{bmatrix} \left[K_3^{11}\right] & \left[K_3^{12}\right] & \left[K_2^{31}\right]+\left[K_3^{13}\right]+\left[K_4\right] & 0 & 0 \\ 0 & 0 & 0 & 0 & 0 \\ 0 & 0 & 0 & 0 & 0 \end{bmatrix} \begin{Bmatrix} q_u \\ q_v \\ q_w \\ q_{\Phi_y} \\ q_{\Phi_x} \end{Bmatrix} = \begin{Bmatrix} \{P_w\} \\ 0 \\ 0 \end{Bmatrix} \Leftrightarrow$$

$$\begin{bmatrix} [M_b] & 0 & 0 \\ 0 & [M_{Ry}] & 0 \\ 0 & 0 & [M_{Rx}] \end{bmatrix} \begin{Bmatrix} \ddot{q}_w \\ \ddot{q}_{\Phi_y} \\ \ddot{q}_{\Phi_x} \end{Bmatrix} + \begin{bmatrix} 0 \\ \begin{bmatrix} [K_1^{bp11}] & [K_1^{bp12}] \\ [K_1^{bp21}] & [K_1^{bp22}] \end{bmatrix} \begin{Bmatrix} q_u \\ q_v \end{Bmatrix} \end{bmatrix} +$$

$$+ \begin{bmatrix} 0 & 0 & [K_1^{\gamma 11}] & [K_1^{\gamma 12}] & [K_1^{\gamma 13}] \\ 0 & 0 & [K_1^{\gamma 21}] & [K_1^{b11}]+[K_1^{\gamma 22}] & [K_1^{b12}]+[K_1^{\gamma 23}] \\ 0 & 0 & [K_1^{\gamma 31}] & [K_1^{b21}]+[K_1^{\gamma 32}] & [K_1^{b22}]+[K_1^{\gamma 33}] \end{bmatrix} \begin{Bmatrix} q_u \\ q_v \\ q_w \\ q_{\Phi_y} \\ q_{\Phi_x} \end{Bmatrix} +$$

$$+ \begin{bmatrix} [K_3^{11}] & [K_3^{12}] & 0 & 0 & 0 \\ 0 & 0 & 0 & 0 & 0 \\ 0 & 0 & 0 & 0 & 0 \end{bmatrix} \begin{Bmatrix} q_u \\ q_v \\ q_w \\ q_{\Phi_y} \\ q_{\Phi_x} \end{Bmatrix} +$$

$$+ \begin{bmatrix} 0 & 0 & [K_2^{31}]+[K_3^{13}]+[K_4] & 0 & 0 \\ 0 & 0 & 0 & 0 & 0 \\ 0 & 0 & 0 & 0 & 0 \end{bmatrix} \begin{Bmatrix} q_u \\ q_v \\ q_w \\ q_{\Phi_y} \\ q_{\Phi_x} \end{Bmatrix} = \begin{Bmatrix} \{P_w\} \\ 0 \\ 0 \end{Bmatrix} \Leftrightarrow$$

$$\begin{bmatrix} [M_b] & 0 & 0 \\ 0 & [M_{Ry}] & 0 \\ 0 & 0 & [M_{Rx}] \end{bmatrix} \begin{Bmatrix} \ddot{q}_w \\ \ddot{q}_{\Phi_y} \\ \ddot{q}_{\Phi_x} \end{Bmatrix} +$$

$$\begin{bmatrix} [K_1^{\gamma 11}] & [K_1^{\gamma 12}] & [K_1^{\gamma 13}] \\ [K_1^{\gamma 21}] & [K_1^{b11}]+[K_1^{\gamma 22}] & [K_1^{b12}]+[K_1^{\gamma 23}] \\ [K_1^{\gamma 31}] & [K_1^{b21}]+[K_1^{\gamma 32}] & [K_1^{b22}]+[K_1^{\gamma 33}] \end{bmatrix} \begin{Bmatrix} q_w \\ q_{\Phi_y} \\ q_{\Phi_x} \end{Bmatrix} +$$

$$\begin{bmatrix} [K_2^{31}]+[K_3^{13}]+[K_4] & 0 & 0 \\ 0 & 0 & 0 \\ 0 & 0 & 0 \end{bmatrix} \begin{Bmatrix} q_w \\ q_{\Phi_y} \\ q_{\Phi_x} \end{Bmatrix} = \begin{Bmatrix} \{P_w\} \\ 0 \\ 0 \end{Bmatrix} - \begin{bmatrix} \begin{bmatrix} [K_3^{11}] & [K_3^{12}] \end{bmatrix} \begin{Bmatrix} q_u \\ q_v \end{Bmatrix} \\ \begin{bmatrix} [K_1^{bp11}] & [K_1^{bp12}] \\ [K_1^{bp21}] & [K_1^{bp22}] \end{bmatrix} \begin{Bmatrix} q_u \\ q_v \end{Bmatrix} \end{bmatrix}$$

(2. 76)

Replacing (2.75) in (2. 76) the reduced equations of motion are obtained.

From (2. 70), the mass matrix $[M]$, the linear stiffness matrix $[Kl]$ and the non-linear stiffness matrix $[Knl]$ are given by:

$$[M]=\begin{bmatrix}[M_b] & 0 & 0\\ 0 & [M_{Ry}] & 0\\ 0 & 0 & [M_{Rx}]\end{bmatrix},$$

$$[Kl]=\begin{bmatrix}[K_1^{\gamma 11}] & [K_1^{\gamma 12}] & [K_1^{\gamma 13}]\\ [K_1^{\gamma 21}] & [K_1^{b11}]+[K_1^{\gamma 22}] & [K_1^{b12}]+[K_1^{\gamma 23}]\\ [K_1^{\gamma 31}] & [K_1^{b21}]+[K_1^{\gamma 32}] & [K_1^{b22}]+[K_1^{\gamma 33}]\end{bmatrix},$$

$$[Knl]=\begin{bmatrix}0 & 0 & [K_2^{31}]+[K_3^{13}]+[K_4] & 0 & 0\\ 0 & 0 & 0 & 0 & 0\\ 0 & 0 & 0 & 0 & 0\end{bmatrix},$$

the latter with terms which are either linear or quadratic functions of $\{q_w\}$. The vector of external forces $\{P\}$ is given by

$$\{P\}=\begin{Bmatrix}\{P_w\}-[K_3^{11}]\{q_u\}-[K_3^{12}]\{q_v\}\\ -[K_1^{bp11}]\{q_u\}-[K_1^{bp12}]\{q_v\}\\ -[K_1^{bp21}]\{q_u\}-[K_1^{bp22}]\{q_v\}\end{Bmatrix} \qquad (2.\ 77)$$

If a distributed force that impinges on the plate's surface in the *z* direction is considered, then $\{P_u\}=\{P_v\}=0$. Therefore, from equation (2.72), the new force vector is given by

$$\{P\}=\left\{\begin{array}{l}\{P_w\}+\begin{bmatrix}[K_3^{11}] & [K_3^{12}]\end{bmatrix}\begin{bmatrix}[K_1^{p11}] & [K_1^{p12}]\\ [K_1^{p21}] & [K_1^{p22}]\end{bmatrix}^{-1}\left(\begin{bmatrix}[K_1^{pb11}] & [K_1^{pb12}]\\ [K_1^{pb21}] & [K_1^{pb22}]\end{bmatrix}\begin{Bmatrix}q_{\Phi_y}\\ q_{\Phi_x}\end{Bmatrix}+\begin{bmatrix}[K_2^{11}]\\ [K_2^{21}]\end{bmatrix}\{q_w\}\right)\\ +\begin{bmatrix}[K_1^{bp11}] & [K_1^{bp12}]\\ [K_1^{bp21}] & [K_1^{bp22}]\end{bmatrix}\begin{bmatrix}[K_1^{p11}] & [K_1^{p12}]\\ [K_1^{p21}] & [K_1^{p22}]\end{bmatrix}^{-1}\left(\begin{bmatrix}[K_1^{pb11}] & [K_1^{pb12}]\\ [K_1^{pb21}] & [K_1^{pb22}]\end{bmatrix}\begin{Bmatrix}q_{\Phi_y}\\ q_{\Phi_x}\end{Bmatrix}-\begin{bmatrix}[K_2^{11}]\\ [K_2^{21}]\end{bmatrix}\{q_w\}\right)\end{array}\right\}$$

(2. 78)

2.4 - *Derivation of the Matrices Used in the Equations of Motion*

2.4.1 - *Linear stiffness matrix* $[K_1]$

From equation (2. 61),

$$\int_\Omega\left(\delta\begin{Bmatrix}\varepsilon_0^p\\ \varepsilon_0^b\end{Bmatrix}^T[E]\begin{Bmatrix}\varepsilon_0^p\\ \varepsilon_0^b\end{Bmatrix}\right)d\Omega=\int_\Omega\left(\delta\begin{Bmatrix}\varepsilon_0^p\\ \varepsilon_0^b\end{Bmatrix}^T\begin{bmatrix}[A] & [B]\\ [B] & [D]\end{bmatrix}\begin{Bmatrix}\varepsilon_0^p\\ \varepsilon_0^b\end{Bmatrix}\right)d\Omega=$$

$$=\int_\Omega\left(\delta\{\varepsilon_0^p\}^T[A]\{\varepsilon_0^p\}+\delta\{\varepsilon_0^b\}^T[B]\{\varepsilon_0^p\}+\delta\{\varepsilon_0^p\}^T[B]\{\varepsilon_0^b\}+\delta\{\varepsilon_0^b\}^T[D]\{\varepsilon_0^b\}\right)d\Omega$$

(2. 79)

The linear $[K_1]$ matrix consists of four independent parts. The in plane stiffness matrix, $\left[K_1^p\right]$, the bending stiffness matrix, $\left[K_1^b\right]$, and the coupling in-plane/bending matrices $\left[K_1^{pb}\right],\left[K_1^{bp}\right]$ which are obtained from (2. 79).

Therefore,

$$\int_\Omega\delta\{\varepsilon_0^p\}^T[\mathrm{A}]\{\varepsilon_0^p\}d\Omega=\int_\Omega\left(\delta\begin{bmatrix}\{N_{,x}^u\}^T & 0\\ 0 & \{N_{,y}^u\}^T\\ \{N_{,y}^u\}^T & \{N_{,x}^u\}^T\end{bmatrix}\begin{Bmatrix}q_u\\ q_v\end{Bmatrix}\right)^T[\mathrm{A}]\begin{bmatrix}\{N_{,x}^u\}^T & 0\\ 0 & \{N_{,y}^u\}^T\\ \{N_{,y}^u\}^T & \{N_{,x}^u\}^T\end{bmatrix}\begin{Bmatrix}q_u\\ q_v\end{Bmatrix}d\Omega=$$

$$= \begin{Bmatrix} \delta q_u \\ \delta q_v \end{Bmatrix}^T \int_\Omega \begin{bmatrix} \left\{N^u_{,x}\right\}^T & 0 \\ 0 & \left\{N^u_{,y}\right\}^T \\ \left\{N^u_{,y}\right\}^T & \left\{N^u_{,x}\right\}^T \end{bmatrix}^T \begin{bmatrix} \mathrm{A}_{11} & \mathrm{A}_{12} & \mathrm{A}_{16} \\ \mathrm{A}_{12} & \mathrm{A}_{22} & \mathrm{A}_{26} \\ \mathrm{A}_{16} & \mathrm{A}_{26} & \mathrm{A}_{66} \end{bmatrix} \begin{bmatrix} \left\{N^u_{,x}\right\}^T & 0 \\ 0 & \left\{N^u_{,y}\right\}^T \\ \left\{N^u_{,y}\right\}^T & \left\{N^u_{,x}\right\}^T \end{bmatrix} d\Omega \begin{Bmatrix} q_u \\ q_v \end{Bmatrix} =$$

$$= \begin{Bmatrix} \delta q_u \\ \delta q_v \end{Bmatrix}^T \int_\Omega \begin{bmatrix} \left\{N^u_{,x}\right\} & 0 & \left\{N^u_{,y}\right\} \\ 0 & \left\{N^u_{,y}\right\} & \left\{N^u_{,x}\right\} \end{bmatrix} \begin{bmatrix} \mathrm{A}_{11} & \mathrm{A}_{12} & \mathrm{A}_{16} \\ \mathrm{A}_{12} & \mathrm{A}_{22} & \mathrm{A}_{26} \\ \mathrm{A}_{16} & \mathrm{A}_{26} & \mathrm{A}_{66} \end{bmatrix} \begin{bmatrix} \left\{N^u_{,x}\right\}^T & 0 \\ 0 & \left\{N^u_{,y}\right\}^T \\ \left\{N^u_{,y}\right\}^T & \left\{N^u_{,x}\right\}^T \end{bmatrix} d\Omega \begin{Bmatrix} q_u \\ q_v \end{Bmatrix} =$$

$$= \begin{Bmatrix} \delta q_u \\ \delta q_v \end{Bmatrix}^T \int_\Omega \begin{bmatrix} \mathrm{A}_{11}\left\{N^u_{,x}\right\}\left\{N^u_{,x}\right\}^T + \mathrm{A}_{16}\left(\left\{N^u_{,y}\right\}\left\{N^u_{,x}\right\}^T + \left\{N^u_{,x}\right\}\left\{N^u_{,y}\right\}^T\right) + \mathrm{A}_{66}\left\{N^u_{,y}\right\}\left\{N^u_{,y}\right\}^T \\ \mathrm{A}_{12}\left\{N^u_{,y}\right\}\left\{N^u_{,x}\right\}^T + \mathrm{A}_{16}\left\{N^u_{,x}\right\}\left\{N^u_{,x}\right\}^T + \mathrm{A}_{26}\left\{N^u_{,y}\right\}\left\{N^u_{,y}\right\}^T + \mathrm{A}_{66}\left\{N^u_{,x}\right\}\left\{N^u_{,y}\right\}^T \\ \mathrm{A}_{12}\left\{N^u_{,x}\right\}\left\{N^u_{,y}\right\}^T + \mathrm{A}_{26}\left\{N^u_{,y}\right\}\left\{N^u_{,y}\right\}^T + \mathrm{A}_{16}\left\{N^u_{,x}\right\}\left\{N^u_{,x}\right\}^T + \mathrm{A}_{66}\left\{N^u_{,y}\right\}\left\{N^u_{,x}\right\}^T \\ \mathrm{A}_{22}\left\{N^u_{,y}\right\}\left\{N^u_{,y}\right\}^T + \mathrm{A}_{26}\left(\left\{N^u_{,x}\right\}\left\{N^u_{,y}\right\}^T + \left\{N^u_{,y}\right\}\left\{N^u_{,x}\right\}^T\right) + \mathrm{A}_{66}\left\{N^u_{,x}\right\}\left\{N^u_{,x}\right\}^T \end{bmatrix} d\Omega \begin{Bmatrix} q_u \\ q_v \end{Bmatrix} =$$

$$= \{\delta q\}^T \left[K_1^p\right] \{q\} \qquad (2.\,80)$$

The bending stiffness matrix $\left[K_1^b\right]$ is derived considering the virtual work $\int_\Omega \delta\left\{\varepsilon_0^b\right\}^T [\mathrm{D}]\left\{\varepsilon_0^b\right\} d\Omega$. Replacing $\left\{\varepsilon_0^b\right\}$ by $\begin{bmatrix} -\left\{N^{\Phi_y}_{,x}\right\}^T & 0 \\ 0 & \left\{N^{\Phi_x}_{,y}\right\}^T \\ -\left\{N^{\Phi_y}_{,y}\right\}^T & \left\{N^{\Phi_x}_{,x}\right\}^T \end{bmatrix} \begin{Bmatrix} q_{\Phi_y} \\ q_{\Phi_x} \end{Bmatrix}$ in the integral, comes

$$\begin{Bmatrix}\delta q_{\Phi_y}\\ \delta q_{\Phi_x}\end{Bmatrix}^T \int_\Omega \begin{bmatrix} -\left\{N_{,x}^{\Phi_y}\right\} & 0 & -\left\{N_{,y}^{\Phi_y}\right\} \\ 0 & \left\{N_{,y}^{\Phi_x}\right\} & \left\{N_{,x}^{\Phi_x}\right\} \end{bmatrix} \begin{bmatrix} D_{11} & D_{12} & D_{16} \\ D_{12} & D_{22} & D_{26} \\ D_{16} & D_{26} & D_{66} \end{bmatrix} \begin{bmatrix} -\left\{N_{,x}^{\Phi_y}\right\}^T & 0 \\ 0 & \left\{N_{,y}^{\Phi_x}\right\}^T \\ -\left\{N_{,y}^{\Phi_y}\right\}^T & \left\{N_{,x}^{\Phi_x}\right\}^T \end{bmatrix} d\Omega \begin{Bmatrix} q_{\Phi_y} \\ q_{\Phi_x} \end{Bmatrix} =$$

$$= \begin{Bmatrix}\delta q_{\Phi_y}\\ \delta q_{\Phi_x}\end{Bmatrix}^T \int_\Omega \begin{bmatrix} D_{11}\left\{N_{,x}^{\Phi_y}\right\}\left\{N_{,x}^{\Phi_y}\right\}^T + D_{16}\left(\left\{N_{,y}^{\Phi_y}\right\}\left\{N_{,x}^{\Phi_y}\right\}^T + \left\{N_{,x}^{\Phi_y}\right\}\left\{N_{,y}^{\Phi_y}\right\}^T\right) + D_{66}\left\{N_{,y}^{\Phi_y}\right\}\left\{N_{,y}^{\Phi_y}\right\}^T \\ -D_{12}\left\{N_{,y}^{\Phi_x}\right\}\left\{N_{,x}^{\Phi_y}\right\}^T - D_{16}\left\{N_{,x}^{\Phi_x}\right\}\left\{N_{,x}^{\Phi_y}\right\}^T - D_{26}\left\{N_{,y}^{\Phi_x}\right\}\left\{N_{,y}^{\Phi_y}\right\}^T - D_{66}\left\{N_{,x}^{\Phi_x}\right\}\left\{N_{,y}^{\Phi_y}\right\}^T \end{bmatrix}$$

$$\begin{bmatrix} -D_{12}\left\{N_{,x}^{\Phi_y}\right\}\left\{N_{,y}^{\Phi_x}\right\}^T - D_{26}\left\{N_{,y}^{\Phi_y}\right\}\left\{N_{,y}^{\Phi_x}\right\}^T - D_{16}\left\{N_{,x}^{\Phi_y}\right\}\left\{N_{,x}^{\Phi_x}\right\}^T - D_{66}\left\{N_{,y}^{\Phi_y}\right\}\left\{N_{,x}^{\Phi_x}\right\}^T \\ D_{22}\left\{N_{,y}^{\Phi_x}\right\}\left\{N_{,y}^{\Phi_x}\right\}^T + D_{26}\left(\left\{N_{,x}^{\Phi_x}\right\}\left\{N_{,y}^{\Phi_x}\right\}^T + \left\{N_{,y}^{\Phi_x}\right\}\left\{N_{,x}^{\Phi_x}\right\}^T\right) + D_{66}\left\{N_{,x}^{\Phi_x}\right\}\left\{N_{,x}^{\Phi_x}\right\}^T \end{bmatrix} d\Omega \begin{Bmatrix} q_{\Phi_y} \\ q_{\Phi_x} \end{Bmatrix} =$$

$$= \begin{Bmatrix}\delta q_{\Phi_y}\\ \delta q_{\Phi_x}\end{Bmatrix}^T \left[K_1^b\right] \begin{Bmatrix} q_{\Phi_y} \\ q_{\Phi_x} \end{Bmatrix}$$

(2. 81)

Matrix $\left[K_1^{pb}\right]$ is obtained from the integral $\int_\Omega \delta\left\{\varepsilon_0^p\right\}^T [B]\left\{\varepsilon_0^b\right\} d\Omega$. Replacing $\left\{\varepsilon_0^p\right\}^T$ and $\left\{\varepsilon_0^b\right\}$ in the integral, comes

$$\int_\Omega \left(\delta \begin{bmatrix} \left\{N_{,x}^u\right\}^T & 0 \\ 0 & \left\{N_{,y}^u\right\}^T \\ \left\{N_{,y}^u\right\}^T & \left\{N_{,x}^u\right\}^T \end{bmatrix} \begin{Bmatrix} q_u \\ q_v \end{Bmatrix} \right)^T \begin{bmatrix} \mathrm{B}_{11} & \mathrm{B}_{12} & \mathrm{B}_{16} \\ \mathrm{B}_{12} & \mathrm{B}_{22} & \mathrm{B}_{26} \\ \mathrm{B}_{16} & \mathrm{B}_{26} & \mathrm{B}_{66} \end{bmatrix} \begin{bmatrix} -\left\{N_{,x}^{\Phi_y}\right\}^T & 0 \\ 0 & \left\{N_{,y}^{\Phi_x}\right\}^T \\ -\left\{N_{,y}^{\Phi_y}\right\}^T & \left\{N_{,x}^{\Phi_x}\right\}^T \end{bmatrix} \begin{Bmatrix} q_{\Phi_y} \\ q_{\Phi_x} \end{Bmatrix} d\Omega =$$

$$= \begin{Bmatrix}\delta q_u\\ \delta q_v\end{Bmatrix}^T \int_\Omega \begin{bmatrix} \left\{N_{,x}^u\right\} & 0 & \left\{N_{,y}^u\right\} \\ 0 & \left\{N_{,y}^u\right\} & \left\{N_{,x}^u\right\} \end{bmatrix} \begin{bmatrix} \mathrm{B}_{11} & \mathrm{B}_{12} & \mathrm{B}_{16} \\ \mathrm{B}_{12} & \mathrm{B}_{22} & \mathrm{B}_{26} \\ \mathrm{B}_{16} & \mathrm{B}_{26} & \mathrm{B}_{66} \end{bmatrix} \begin{bmatrix} -\left\{N_{,x}^{\Phi_y}\right\}^T & 0 \\ 0 & \left\{N_{,y}^{\Phi_x}\right\}^T \\ -\left\{N_{,y}^{\Phi_y}\right\}^T & \left\{N_{,x}^{\Phi_x}\right\}^T \end{bmatrix} d\Omega \begin{Bmatrix} q_{\Phi_y} \\ q_{\Phi_x} \end{Bmatrix} =$$

$$= \begin{Bmatrix}\delta q_u\\ \delta q_v\end{Bmatrix}^T \int_\Omega \begin{bmatrix} \left(\left\{N_{,x}^u\right\}\mathrm{B}_{11} + \left\{N_{,y}^u\right\}\mathrm{B}_{16}\right)\left(-\left\{N_{,x}^{\Phi_y}\right\}^T\right) + \left(\left\{N_{,x}^u\right\}\mathrm{B}_{16} + \left\{N_{,y}^u\right\}\mathrm{B}_{66}\right)\left(-\left\{N_{,y}^{\Phi_y}\right\}^T\right) \\ \left(\left\{N_{,y}^u\right\}\mathrm{B}_{12} + \left\{N_{,x}^u\right\}\mathrm{B}_{16}\right)\left(-\left\{N_{,x}^{\Phi_y}\right\}^T\right) + \left(\left\{N_{,y}^u\right\}\mathrm{B}_{26} + \left\{N_{,x}^u\right\}\mathrm{B}_{66}\right)\left(-\left\{N_{,y}^{\Phi_y}\right\}^T\right) \end{bmatrix}$$

$$\begin{bmatrix} \left(\left\{N^{u}_{,x}\right\}\mathrm{B}_{12}+\left\{N^{u}_{,y}\right\}\mathrm{B}_{26}\right)\left\{N^{\Phi_x}_{,y}\right\}^{T}+\left(\left\{N^{u}_{,x}\right\}\mathrm{B}_{16}+\left\{N^{u}_{,y}\right\}\mathrm{B}_{66}\right)\left\{N^{\Phi_x}_{,x}\right\}^{T} \\ \left(\left\{N^{u}_{,y}\right\}\mathrm{B}_{22}+\left\{N^{u}_{,x}\right\}\mathrm{B}_{26}\right)\left\{N^{\Phi_x}_{,y}\right\}^{T}+\left(\left\{N^{u}_{,y}\right\}\mathrm{B}_{26}+\left\{N^{u}_{,x}\right\}\mathrm{B}_{66}\right)\left\{N^{\Phi_x}_{,x}\right\}^{T} \end{bmatrix} d\Omega \begin{Bmatrix} q_{\Phi_y} \\ q_{\Phi_x} \end{Bmatrix} =$$

$$= \begin{Bmatrix} \delta q_u \\ \delta q_v \end{Bmatrix}^{T} \int_{\Omega} \begin{bmatrix} -\mathrm{B}_{11}\left\{N^{u}_{,x}\right\}\left\{N^{\Phi_y}_{,x}\right\}^{T}-\mathrm{B}_{16}\left(\left\{N^{u}_{,y}\right\}\left\{N^{\Phi_y}_{,x}\right\}^{T}+\left\{N^{u}_{,x}\right\}\left\{N^{\Phi_y}_{,y}\right\}^{T}\right)-\mathrm{B}_{66}\left\{N^{u}_{,y}\right\}\left\{N^{\Phi_y}_{,y}\right\}^{T} \\ -\mathrm{B}_{12}\left\{N^{u}_{,y}\right\}\left\{N^{\Phi_y}_{,x}\right\}^{T}-\mathrm{B}_{16}\left\{N^{u}_{,x}\right\}\left\{N^{\Phi_y}_{,x}\right\}^{T}-\mathrm{B}_{26}\left\{N^{u}_{,y}\right\}\left\{N^{\Phi_y}_{,y}\right\}^{T}-\mathrm{B}_{66}\left\{N^{u}_{,x}\right\}\left\{N^{\Phi_y}_{,y}\right\}^{T} \\ \mathrm{B}_{12}\left\{N^{u}_{,x}\right\}\left\{N^{\Phi_x}_{,y}\right\}^{T}+\mathrm{B}_{26}\left\{N^{u}_{,y}\right\}\left\{N^{\Phi_x}_{,y}\right\}^{T}+\mathrm{B}_{16}\left\{N^{u}_{,x}\right\}\left\{N^{\Phi_x}_{,x}\right\}^{T}+\mathrm{B}_{66}\left\{N^{u}_{,y}\right\}\left\{N^{\Phi_x}_{,x}\right\}^{T} \\ \mathrm{B}_{22}\left\{N^{u}_{,y}\right\}\left\{N^{\Phi_x}_{,y}\right\}^{T}+\mathrm{B}_{26}\left(\left\{N^{u}_{,x}\right\}\left\{N^{\Phi_x}_{,y}\right\}^{T}+\left\{N^{u}_{,y}\right\}\left\{N^{\Phi_x}_{,x}\right\}^{T}\right)+\mathrm{B}_{66}\left\{N^{u}_{,x}\right\}\left\{N^{\Phi_x}_{,x}\right\}^{T} \end{bmatrix} d\Omega \begin{Bmatrix} q_{\Phi_y} \\ q_{\Phi_x} \end{Bmatrix} =$$

$$= \begin{Bmatrix} \delta q_u \\ \delta q_v \end{Bmatrix}^{T} \left[K_1^{pb}\right] \begin{Bmatrix} q_{\Phi_y} \\ q_{\Phi_x} \end{Bmatrix} \tag{2. 82}$$

Matrix $\left[K_1^{bp}\right]$ is obtained from the integral $\int_{\Omega} \delta\left\{\varepsilon_0^{b}\right\}^{T}[B]\left\{\varepsilon_0^{p}\right\} d\Omega$. Replacing $\left\{\varepsilon_0^{b}\right\}^{T}$ and $\left\{\varepsilon_0^{p}\right\}$ in the integral, comes

$$\int_{\Omega} \left(\delta \begin{bmatrix} -\left\{N^{\Phi_y}_{,x}\right\}^{T} & 0 \\ 0 & \left\{N^{\Phi_x}_{,y}\right\}^{T} \\ -\left\{N^{\Phi_y}_{,y}\right\}^{T} & \left\{N^{\Phi_x}_{,x}\right\}^{T} \end{bmatrix} \begin{Bmatrix} q_{\Phi_y} \\ q_{\Phi_x} \end{Bmatrix} \right)^{T} \begin{bmatrix} \mathrm{B}_{11} & \mathrm{B}_{12} & \mathrm{B}_{16} \\ \mathrm{B}_{12} & \mathrm{B}_{22} & \mathrm{B}_{26} \\ \mathrm{B}_{16} & \mathrm{B}_{26} & \mathrm{B}_{66} \end{bmatrix} \begin{bmatrix} \left\{N^{u}_{,x}\right\}^{T} & 0 \\ 0 & \left\{N^{u}_{,y}\right\}^{T} \\ \left\{N^{u}_{,y}\right\}^{T} & \left\{N^{u}_{,x}\right\}^{T} \end{bmatrix} \begin{Bmatrix} q_u \\ q_v \end{Bmatrix} d\Omega =$$

$$= \begin{Bmatrix} \delta q_{\Phi_y} \\ \delta q_{\Phi_x} \end{Bmatrix}^{T} \int_{\Omega} \begin{bmatrix} -\left\{N^{\Phi_y}_{,x}\right\} & 0 & -\left\{N^{\Phi_y}_{,y}\right\} \\ 0 & \left\{N^{\Phi_x}_{,y}\right\} & \left\{N^{\Phi_x}_{,x}\right\} \end{bmatrix} \begin{bmatrix} \mathrm{B}_{11} & \mathrm{B}_{12} & \mathrm{B}_{16} \\ \mathrm{B}_{12} & \mathrm{B}_{22} & \mathrm{B}_{26} \\ \mathrm{B}_{16} & \mathrm{B}_{26} & \mathrm{B}_{66} \end{bmatrix} \begin{bmatrix} \left\{N^{u}_{,x}\right\}^{T} & 0 \\ 0 & \left\{N^{u}_{,y}\right\}^{T} \\ \left\{N^{u}_{,y}\right\}^{T} & \left\{N^{u}_{,x}\right\}^{T} \end{bmatrix} d\Omega \begin{Bmatrix} q_u \\ q_v \end{Bmatrix} =$$

$$= \begin{Bmatrix} \delta q_{\Phi_y} \\ \delta q_{\Phi_x} \end{Bmatrix}^{T} \int_{\Omega} \begin{bmatrix} \left(-\left\{N^{\Phi_y}_{,x}\right\}\mathrm{B}_{11}-\left\{N^{\Phi_y}_{,y}\right\}\mathrm{B}_{16}\right)\left\{N^{u}_{,x}\right\}^{T}+\left(-\left\{N^{\Phi_y}_{,x}\right\}\mathrm{B}_{16}-\left\{N^{\Phi_y}_{,y}\right\}\mathrm{B}_{66}\right)\left\{N^{u}_{,y}\right\}^{T} \\ \left(\left\{N^{\Phi_x}_{,y}\right\}\mathrm{B}_{12}+\left\{N^{\Phi_x}_{,x}\right\}\mathrm{B}_{16}\right)\left\{N^{u}_{,x}\right\}^{T}+\left(\left\{N^{\Phi_x}_{,y}\right\}\mathrm{B}_{26}+\left\{N^{\Phi_x}_{,x}\right\}\mathrm{B}_{66}\right)\left\{N^{u}_{,y}\right\}^{T} \end{bmatrix}$$

$$\left(-\left\{N_{,x}^{\Phi_y}\right\}\mathrm{B}_{12}-\left\{N_{,y}^{\Phi_y}\right\}^T\mathrm{B}_{26}\right)\left\{N_{,y}^{u}\right\}^T+\left(-\left\{N_{,x}^{\Phi_y}\right\}\mathrm{B}_{16}-\left\{N_{,y}^{\Phi_y}\right\}\mathrm{B}_{66}\right)\left\{N_{,x}^{u}\right\}^T$$
$$\left(\left\{N_{,y}^{\Phi_x}\right\}\mathrm{B}_{22}+\left\{N_{,x}^{\Phi_x}\right\}^T\mathrm{B}_{26}\right)\left\{N_{,y}^{u}\right\}^T+\left(\left\{N_{,y}^{\Phi_x}\right\}\mathrm{B}_{26}+\left\{N_{,x}^{\Phi_x}\right\}\mathrm{B}_{66}\right)\left\{N_{,x}^{u}\right\}^T\Bigg]d\Omega\begin{Bmatrix}q_u\\q_v\end{Bmatrix}=$$

$$=\begin{Bmatrix}\delta q_{\Phi_y}\\\delta q_{\Phi_x}\end{Bmatrix}^T\int_\Omega\Bigg[-\mathrm{B}_{11}\left\{N_{,x}^{\Phi_y}\right\}\left\{N_{,x}^{u}\right\}^T-\mathrm{B}_{16}\left(\left\{N_{,y}^{\Phi_y}\right\}\left\{N_{,x}^{u}\right\}^T+\left\{N_{,x}^{\Phi_y}\right\}\left\{N_{,y}^{u}\right\}^T\right)-\mathrm{B}_{66}\left\{N_{,y}^{\Phi_y}\right\}\left\{N_{,y}^{u}\right\}^T$$
$$\mathrm{B}_{12}\left\{N_{,y}^{\Phi_x}\right\}\left\{N_{,x}^{u}\right\}^T+\mathrm{B}_{16}\left\{N_{,x}^{\Phi_x}\right\}\left\{N_{,x}^{u}\right\}^T+\mathrm{B}_{26}\left\{N_{,y}^{\Phi_x}\right\}\left\{N_{,y}^{u}\right\}^T+\mathrm{B}_{66}\left\{N_{,x}^{\Phi_x}\right\}\left\{N_{,y}^{u}\right\}^T$$
$$-\mathrm{B}_{12}\left\{N_{,x}^{\Phi_y}\right\}\left\{N_{,y}^{u}\right\}^T-\mathrm{B}_{26}\left\{N_{,y}^{\Phi_y}\right\}\left\{N_{,y}^{u}\right\}^T-\mathrm{B}_{16}\left\{N_{,x}^{\Phi_y}\right\}\left\{N_{,x}^{u}\right\}^T-\mathrm{B}_{66}\left\{N_{,y}^{\Phi_y}\right\}\left\{N_{,x}^{u}\right\}^T$$
$$\mathrm{B}_{22}\left\{N_{,y}^{\Phi_x}\right\}\left\{N_{,y}^{u}\right\}^T+\mathrm{B}_{26}\left(\left\{N_{,x}^{\Phi_x}\right\}\left\{N_{,y}^{u}\right\}^T+\left\{N_{,y}^{\Phi_x}\right\}\left\{N_{,x}^{u}\right\}^T\right)+\mathrm{B}_{66}\left\{N_{,x}^{\Phi_x}\right\}\left\{N_{,x}^{u}\right\}^T\Bigg]d\Omega\begin{Bmatrix}q_u\\q_v\end{Bmatrix}=$$

$$=\begin{Bmatrix}\delta q_{\Phi_y}\\\delta q_{\Phi_x}\end{Bmatrix}^T\left[K_1^{bp}\right]\begin{Bmatrix}q_u\\q_v\end{Bmatrix}\qquad(2.\ 83)$$

One verifies, as expected, that $\left[K_1^{bp}\right]=\left[K_1^{pb}\right]^T$.

2.4.2 – *Non-linear stiffness matrix* $\left[K_2\right]$ *and* $\left[K_3\right]$

In this section the non-linear stiffness matrix $\left[K_2\right]$ is derived. $\left[K_3\right]$ is proved to be twice the transpose of $\left[K_2\right]$, i.e., $\left[K_3\right]=2\left[K_2\right]^T$ [2.1]. Both $\left[K_2\right]$ and $\left[K_3\right]$ are linear functions of the generalised displacements.

Considering equation (2. 62),

$\int_\Omega\left(\delta\begin{Bmatrix}\varepsilon_0^p\\\varepsilon_0^b\end{Bmatrix}^T\left[E\right]\begin{Bmatrix}\varepsilon_L^p\\0\end{Bmatrix}\right)d\Omega=\left\{\delta q\right\}^T\left[K_2\right]\left\{q\right\}$. Therefore,

$$\int_\Omega\left(\delta\begin{Bmatrix}\varepsilon_0^p\\\varepsilon_0^b\end{Bmatrix}^T\left[E\right]\begin{Bmatrix}\varepsilon_L^p\\0\end{Bmatrix}\right)d\Omega=\int_\Omega\left(\delta\begin{Bmatrix}\varepsilon_0^p\\\varepsilon_0^b\end{Bmatrix}^T\begin{bmatrix}\left[\mathrm{A}\right]&\left[B\right]\\\left[B\right]&\left[D\right]\end{bmatrix}\begin{Bmatrix}\varepsilon_L^p\\0\end{Bmatrix}\right)d\Omega=$$

$$=\int_\Omega\left(\left\{\delta\varepsilon_0^p\right\}^T\left[\mathrm{A}\right]\left\{\varepsilon_L^p\right\}+\left\{\delta\varepsilon_0^b\right\}^T\left[\mathrm{B}\right]\left\{\varepsilon_L^p\right\}\right)d\Omega\qquad(2.\ 84)$$

From the definition of $\left\{\varepsilon_0^p\right\}$, $\left\{\varepsilon_0^b\right\}$ and $\left\{\varepsilon_L^p\right\}$, equations (2. 49), (2. 50) and (2. 51), results that

$$\int_{\Omega}\left(\left\{\delta\left(\begin{bmatrix}\{N^u_{,x}\}^T & 0\\ 0 & \{N^u_{,y}\}^T\\ \{N^u_{,y}\}^T & \{N^u_{,x}\}^T\end{bmatrix}\begin{Bmatrix}q_u\\ q_v\end{Bmatrix}\right)^T\begin{bmatrix}A_{11} & A_{12} & A_{16}\\ A_{12} & A_{22} & A_{26}\\ A_{16} & A_{26} & A_{66}\end{bmatrix}\begin{bmatrix}\frac{1}{2}\{q_w\}^T\{N^w_{,x}\}\{N^w_{,x}\}^T\{q_w\}\\ \frac{1}{2}\{q_w\}^T\{N^w_{,y}\}\{N^w_{,y}\}^T\{q_w\}\\ \{q_w\}^T\{N^w_{,x}\}\{N^w_{,y}\}^T\{q_w\}\end{bmatrix}+\right.$$

$$\left.+\delta\left(\begin{bmatrix}-\{N^{\Phi_y}_{,x}\}^T & 0\\ 0 & \{N^{\Phi_x}_{,y}\}^T\\ -\{N^{\Phi_y}_{,y}\}^T & \{N^{\Phi_x}_{,x}\}^T\end{bmatrix}\begin{Bmatrix}q_{\Phi_y}\\ q_{\Phi_x}\end{Bmatrix}\right)^T\begin{bmatrix}B_{11} & B_{12} & B_{16}\\ B_{12} & B_{22} & B_{26}\\ B_{16} & B_{26} & B_{66}\end{bmatrix}\begin{bmatrix}\frac{1}{2}\{q_w\}^T\{N^w_{,x}\}\{N^w_{,x}\}^T\{q_w\}\\ \frac{1}{2}\{q_w\}^T\{N^w_{,y}\}\{N^w_{,y}\}^T\{q_w\}\\ \{q_w\}^T\{N^w_{,x}\}\{N^w_{,y}\}^T\{q_w\}\end{bmatrix}\right\}\right)d\Omega$$

$$=\begin{Bmatrix}\delta q_u\\ \delta q_v\end{Bmatrix}^T\left[K_2^{pl}\right]\{q_w\}+\begin{Bmatrix}\delta q_{\Phi_y}\\ \delta q_{\Phi_x}\end{Bmatrix}^T\left[K_2^{bpl}\right]\{q_w\} \qquad (2.\,85)$$

Evaluating each term separately,

$$\begin{Bmatrix}\delta q_u\\ \delta q_v\end{Bmatrix}^T\left[K_2^{pl}\right]\{q_w\}=$$

$$=\int_{\Omega}\Big(\{\delta q_u\}^T\{N^u_{,x}\}A_{11}\tfrac{1}{2}\{q_w\}^T\{N^w_{,x}\}\{N^w_{,x}\}^T\{q_w\}+\{\delta q_v\}^T\{N^u_{,y}\}A_{12}\tfrac{1}{2}\{q_w\}^T\{N^w_{,x}\}\{N^w_{,x}\}^T\{q_w\}+$$
$$+\{\delta q_u\}^T\{N^u_{,y}\}A_{16}\tfrac{1}{2}\{q_w\}^T\{N^w_{,x}\}\{N^w_{,x}\}^T\{q_w\}+\{\delta q_v\}\{N^u_{,x}\}^T A_{16}\tfrac{1}{2}\{q_w\}^T\{N^w_{,x}\}\{N^w_{,x}\}^T\{q_w\}+$$
$$+\{\delta q_u\}^T\{N^u_{,x}\}A_{12}\tfrac{1}{2}\{q_w\}^T\{N^w_{,y}\}\{N^w_{,y}\}^T\{q_w\}+\{\delta q_v\}^T\{N^u_{,y}\}A_{22}\tfrac{1}{2}\{q_w\}^T\{N^w_{,y}\}\{N^w_{,y}\}^T\{q_w\}+$$
$$+\{\delta q_u\}^T\{N^u_{,y}\}A_{26}\tfrac{1}{2}\{q_w\}^T\{N^w_{,y}\}\{N^w_{,y}\}^T\{q_w\}+\{\delta q_v\}^T\{N^u_{,x}\}A_{26}\tfrac{1}{2}\{q_w\}^T\{N^w_{,y}\}\{N^w_{,y}\}^T\{q_w\}+$$
$$+\{\delta q_u\}^T\{N^u_{,x}\}A_{16}\{q_w\}^T\{N^w_{,x}\}\{N^w_{,y}\}^T\{q_w\}+\{\delta q_v\}^T\{N^u_{,y}\}A_{26}\{q_w\}^T\{N^w_{,x}\}\{N^w_{,y}\}^T\{q_w\}+$$
$$+\{\delta q_u\}\{N^u_{,y}\}^T A_{66}\{q_w\}^T\{N^w_{,x}\}\{N^w_{,y}\}^T\{q_w\}+\{\delta q_v\}\{N^u_{,x}\}^T A_{66}\{q_w\}^T\{N^w_{,x}\}\{N^w_{,y}\}^T\{q_w\}\Big)d\Omega=$$

Separating the terms with $\{q_u\}^T$ and $\{q_v\}^T$,

$$=\{\delta q_u\}^T\int_{\Omega}\tfrac{1}{2}\Big(\{N^u_{,x}\}A_{11}\{q_w\}^T\{N^w_{,x}\}\{N^w_{,x}\}^T+\{N^u_{,y}\}A_{16}\{q_w\}^T\{N^w_{,x}\}\{N^w_{,x}\}^T+$$
$$+\{N^u_{,x}\}A_{12}\{q_w\}^T\{N^w_{,y}\}\{N^w_{,y}\}^T+\{N^u_{,y}\}A_{26}\{q_w\}^T\{N^w_{,y}\}\{N^w_{,y}\}^T+$$
$$+2\{N^u_{,x}\}A_{16}\{q_w\}^T\{N^w_{,x}\}\{N^w_{,y}\}^T+2\{N^u_{,y}\}A_{66}\{q_w\}^T\{N^w_{,x}\}\{N^w_{,y}\}^T\Big)d\Omega\{q_w\}+$$

$$+\{\delta q_v\}^T \int_\Omega \tfrac{1}{2}\Big(\{N^u_{,y}\} A_{12} \{q_w\}^T \{N^w_{,x}\}\{N^w_{,x}\}^T + \{N^u_{,x}\} A_{16} \{q_w\}^T \{N^w_{,x}\}\{N^w_{,x}\}^T +$$
$$+\{N^u_{,y}\} A_{22} \{q_w\}^T \{N^w_{,y}\}\{N^w_{,y}\}^T + \{N^u_{,x}\} A_{26} \{q_w\}^T \{N^w_{,y}\}\{N^w_{,y}\}^T +$$
$$+2\{N^u_{,y}\} A_{26} \{q_w\}^T \{N^w_{,x}\}\{N^w_{,y}\}^T + 2\{N^u_{,x}\} A_{66} \{q_w\}^T \{N^w_{,x}\}\{N^w_{,y}\}^T \Big) d\Omega \{q_w\}$$
$$=\{\delta q_u\}^T \left[\overline{U}\right]\{q_w\} + \{\delta q_v\}^T \left[\overline{V}\right]\{q_w\} \qquad (2.\ 86)$$

Where

$$\left[\overline{U}\right] = \int_\Omega \tfrac{1}{2}\Big(\{N^u_{,x}\} A_{11} \{q_w\}^T \{N^w_{,x}\}\{N^w_{,x}\}^T + \{N^u_{,y}\} A_{16} \{q_w\}^T \{N^w_{,x}\}\{N^w_{,x}\}^T +$$
$$+\{N^u_{,x}\} A_{12} \{q_w\}^T \{N^w_{,y}\}\{N^w_{,y}\}^T + \{N^u_{,y}\} A_{26} \{q_w\}^T \{N^w_{,y}\}\{N^w_{,y}\}^T +$$
$$+2\{N^u_{,x}\} A_{16} \{q_w\}^T \{N^w_{,x}\}\{N^w_{,y}\}^T + 2\{N^u_{,y}\} A_{66} \{q_w\}^T \{N^w_{,x}\}\{N^w_{,y}\}^T \Big) d\Omega =$$
$$= \int_\Omega \tfrac{1}{2}\Big(\big(\{N^u_{,x}\} A_{11} + \{N^u_{,y}\} A_{16}\big)\{q_w\}^T \{N^w_{,x}\}\{N^w_{,x}\}^T +$$
$$+\big(\{N^u_{,x}\} A_{12} + \{N^u_{,y}\} A_{26}\big)\{q_w\}^T \{N^w_{,y}\}\{N^w_{,y}\}^T +$$
$$+2\big(\{N^u_{,x}\} A_{16} + \{N^u_{,y}\} A_{66}\big)\{q_w\}^T \{N^w_{,x}\}\{N^w_{,y}\}^T \Big) d\Omega$$

(2. 87)

$$\left[\overline{V}\right] = \int_\Omega \tfrac{1}{2}\Big(\{N^u_{,y}\} A_{12} \{q_w\}^T \{N^w_{,x}\}\{N^w_{,x}\}^T + \{N^u_{,x}\} A_{16} \{q_w\}^T \{N^w_{,x}\}\{N^w_{,x}\}^T +$$
$$+\{N^u_{,y}\} A_{22} \{q_w\}^T \{N^w_{,y}\}\{N^w_{,y}\}^T + \{N^u_{,x}\} A_{26} \{q_w\}^T \{N^w_{,y}\}\{N^w_{,y}\}^T +$$
$$+2\{N^u_{,y}\} A_{26} \{q_w\}^T \{N^w_{,x}\}\{N^w_{,y}\}^T + 2\{N^u_{,x}\} A_{66} \{q_w\}^T \{N^w_{,x}\}\{N^w_{,y}\}^T \Big) d\Omega =$$
$$= \int_\Omega \tfrac{1}{2}\Big(\big(\{N^u_{,y}\} A_{12} + \{N^u_{,x}\} A_{16}\big)\{q_w\}^T \{N^w_{,x}\}\{N^w_{,x}\}^T +$$
$$\big(\{N^u_{,y}\} A_{22} + \{N^u_{,x}\} A_{26}\big)\{q_w\}^T \{N^w_{,y}\}\{N^w_{,y}\}^T +$$
$$+2\big(\{N^u_{,y}\} A_{26} + \{N^u_{,x}\} A_{66}\big)\{q_w\}^T \{N^w_{,x}\}\{N^w_{,y}\}^T \Big) d\Omega$$

(2. 88)

The term $\begin{Bmatrix}\delta q_{\Phi_y}\\ \delta q_{\Phi_x}\end{Bmatrix}^T \left[K_2^{bpl}\right]\{q_w\}$, comes

$$\begin{Bmatrix}\delta q_{\Phi_y}\\ \delta q_{\Phi_x}\end{Bmatrix}^T \left[K_2^{bpl}\right]\{q_w\} =$$

$$= \int_\Omega \Big(-\left\{\delta q_{\Phi_y}\right\}^T \left\{N_{,x}^{\Phi_y}\right\} B_{11}\tfrac{1}{2}\{q_w\}^T \left\{N_{,x}^{w}\right\}\left\{N_{,x}^{w}\right\}^T \{q_w\} +$$

$$+\left\{\delta q_{\Phi_x}\right\}^T \left\{N_{,y}^{\Phi_x}\right\} B_{12}\tfrac{1}{2}\{q_w\}^T \left\{N_{,x}^{w}\right\}\left\{N_{,x}^{w}\right\}^T \{q_w\} -$$

$$-\left\{\delta q_{\Phi_y}\right\}^T \left\{N_{,y}^{\Phi_y}\right\} B_{16}\tfrac{1}{2}\{q_w\}^T \left\{N_{,x}^{w}\right\}\left\{N_{,x}^{w}\right\}^T \{q_w\} +$$

$$+\left\{\delta q_{\Phi_x}\right\}^T \left\{N_{,x}^{\Phi_x}\right\} B_{16}\tfrac{1}{2}\{q_w\}^T \left\{N_{,x}^{w}\right\}\left\{N_{,x}^{w}\right\}^T \{q_w\} -$$

$$-\left\{\delta q_{\Phi_y}\right\}^T \left\{N_{,x}^{\Phi_y}\right\} B_{12}\tfrac{1}{2}\{q_w\}^T \left\{N_{,y}^{w}\right\}\left\{N_{,y}^{w}\right\}^T \{q_w\} +$$

$$+\left\{\delta q_{\Phi_x}\right\}^T \left\{N_{,y}^{\Phi_x}\right\} B_{22}\tfrac{1}{2}\{q_w\}^T \left\{N_{,y}^{w}\right\}\left\{N_{,y}^{w}\right\}^T \{q_w\} -$$

$$-\left\{\delta q_{\Phi_y}\right\}^T \left\{N_{,y}^{\Phi_y}\right\} B_{26}\tfrac{1}{2}\{q_w\}^T \left\{N_{,y}^{w}\right\}\left\{N_{,y}^{w}\right\}^T \{q_w\} +$$

$$+\left\{\delta q_{\Phi_x}\right\}^T \left\{N_{,x}^{\Phi_x}\right\} B_{26}\tfrac{1}{2}\{q_w\}^T \left\{N_{,y}^{w}\right\}\left\{N_{,y}^{w}\right\}^T \{q_w\} -$$

$$-\left\{\delta q_{\Phi_y}\right\}^T \left\{N_{,x}^{\Phi_y}\right\} B_{16}\{q_w\}^T \left\{N_{,x}^{w}\right\}\left\{N_{,y}^{w}\right\}^T \{q_w\} +$$

$$+\left\{\delta q_{\Phi_x}\right\}^T \left\{N_{,y}^{\Phi_x}\right\} B_{26}\{q_w\}^T \left\{N_{,x}^{w}\right\}\left\{N_{,y}^{w}\right\}^T \{q_w\} -$$

$$-\left\{\delta q_{\Phi_y}\right\}^T \left\{N_{,y}^{\Phi_y}\right\} B_{66}\{q_w\}^T \left\{N_{,x}^{w}\right\}\left\{N_{,y}^{w}\right\}^T \{q_w\} +$$

$$+\left\{\delta q_{\Phi_x}\right\}^T \left\{N_{,x}^{\Phi_x}\right\} B_{66}\{q_w\}^T \left\{N_{,x}^{w}\right\}\left\{N_{,y}^{w}\right\}^T \{q_w\}\Big) d\Omega$$

Separating the terms with $\left\{\delta q_{\Phi_y}\right\}^T$ and $\left\{\delta q_{\Phi_x}\right\}^T$,

$$= \left\{\delta q_{\Phi_y}\right\}^T \int_\Omega \tfrac{1}{2}\Big(-\left\{N_{,x}^{\Phi_y}\right\} B_{11}\{q_w\}^T \left\{N_{,x}^{w}\right\}\left\{N_{,x}^{w}\right\}^T - \left\{N_{,y}^{\Phi_y}\right\} B_{16}\{q_w\}^T \left\{N_{,x}^{w}\right\}\left\{N_{,x}^{w}\right\}^T -$$

$$-\left\{N_{,x}^{\Phi_y}\right\} B_{12}\{q_w\}^T \left\{N_{,y}^{w}\right\}\left\{N_{,y}^{w}\right\}^T - \left\{N_{,y}^{\Phi_y}\right\} B_{26}\{q_w\}^T \left\{N_{,y}^{w}\right\}\left\{N_{,y}^{w}\right\}^T -$$

$$-2\left\{N_{,x}^{\Phi_y}\right\} B_{16}\{q_w\}^T \left\{N_{,x}^{w}\right\}\left\{N_{,y}^{w}\right\}^T - 2\left\{N_{,y}^{\Phi_y}\right\} B_{66}\tfrac{1}{2}\{q_w\}^T \left\{N_{,x}^{w}\right\}\left\{N_{,y}^{w}\right\}^T \Big) d\Omega \{q_w\} +$$

$$+\left\{\delta q_{\Phi_x}\right\}^T \tfrac{1}{2}\int_\Omega \Big(\left\{N_{,y}^{\Phi_x}\right\} B_{12}\{q_w\}^T \left\{N_{,x}^{w}\right\}\left\{N_{,x}^{w}\right\}^T + \left\{N_{,x}^{\Phi_x}\right\} B_{16}\{q_w\}^T \left\{N_{,x}^{w}\right\}\left\{N_{,x}^{w}\right\}^T +$$

$$+\left\{N_{,y}^{\Phi_x}\right\} B_{22}\{q_w\}^T \left\{N_{,y}^{w}\right\}\left\{N_{,y}^{w}\right\}^T + \left\{N_{,x}^{\Phi_x}\right\} B_{26}\{q_w\}^T \left\{N_{,y}^{w}\right\}\left\{N_{,y}^{w}\right\}^T +$$

$$+2\left\{N_{,y}^{\Phi_x}\right\} B_{26}\{q_w\}^T \left\{N_{,x}^{w}\right\}\left\{N_{,y}^{w}\right\}^T + 2\left\{N_{,x}^{\Phi_x}\right\} B_{66}\{q_w\}^T \left\{N_{,x}^{w}\right\}\left\{N_{,y}^{w}\right\}^T \Big) d\Omega \{q_w\} =$$

$$= \left\{\delta q_{\Phi_y}\right\}^T \left[\overline{Y}\right] \{q_w\} + \left\{\delta q_{\Phi_x}\right\}^T \left[\overline{Z}\right] \{q_w\} \tag{2. 89}$$

where

$$\begin{aligned}
&\left[\overline{Y}\right] = \int_\Omega \tfrac{1}{2}\Big(-\left\{N_{,x}^{\phi_y}\right\} B_{11} \{q_w\}^T \left\{N_{,x}^{w}\right\}\left\{N_{,x}^{w}\right\}^T - \left\{N_{,y}^{\phi_y}\right\} B_{16} \{q_w\}^T \left\{N_{,x}^{w}\right\}\left\{N_{,x}^{w}\right\}^T - \\
&-\left\{N_{,x}^{\phi_y}\right\} B_{12} \{q_w\}^T \left\{N_{,y}^{w}\right\}\left\{N_{,y}^{w}\right\}^T - \left\{N_{,y}^{\phi_y}\right\} B_{26} \{q_w\}^T \left\{N_{,y}^{w}\right\}\left\{N_{,y}^{w}\right\}^T - \\
&-2\left\{N_{,x}^{\phi_y}\right\} B_{16} \{q_w\}^T \left\{N_{,x}^{w}\right\}\left\{N_{,y}^{w}\right\}^T - 2\left\{N_{,y}^{\phi_y}\right\} B_{66} \{q_w\}^T \left\{N_{,x}^{w}\right\}\left\{N_{,y}^{w}\right\}^T \Big) d\Omega = \\
&= \int_\Omega \tfrac{1}{2}\Big(\Big(-\left\{N_{,x}^{\phi_y}\right\} B_{11} - \left\{N_{,y}^{\phi_y}\right\} B_{16}\Big)\{q_w\}^T \left\{N_{,x}^{w}\right\}\left\{N_{,x}^{w}\right\}^T + \\
&+\Big(-\left\{N_{,x}^{\phi_y}\right\} B_{12} - \left\{N_{,y}^{\phi_y}\right\} B_{26}\Big)\{q_w\}^T \left\{N_{,y}^{w}\right\}\left\{N_{,y}^{w}\right\}^T + \\
&2\Big(-\left\{N_{,x}^{\phi_y}\right\} B_{16} - \left\{N_{,y}^{\phi_y}\right\} B_{66}\Big)\{q_w\}^T \left\{N_{,x}^{w}\right\}\left\{N_{,y}^{w}\right\}^T \Big) d\Omega
\end{aligned} \tag{2. 90}$$

$$\begin{aligned}
&\left[\overline{Z}\right] = \int_\Omega \tfrac{1}{2}\Big(\left\{N_{,y}^{\Phi_x}\right\} B_{12} \{q_w\}^T \left\{N_{,x}^{w}\right\}\left\{N_{,x}^{w}\right\}^T + \left\{N_{,x}^{\Phi_x}\right\} B_{16} \{q_w\}^T \left\{N_{,x}^{w}\right\}\left\{N_{,x}^{w}\right\}^T + \\
&+\left\{N_{,y}^{\Phi_x}\right\} B_{22} \{q_w\}^T \left\{N_{,y}^{w}\right\}\left\{N_{,y}^{w}\right\}^T + \left\{N_{,x}^{\Phi_x}\right\} B_{26} \{q_w\}^T \left\{N_{,y}^{w}\right\}\left\{N_{,y}^{w}\right\}^T + \\
&+2\left\{N_{,y}^{\Phi_x}\right\} B_{26} \{q_w\}^T \left\{N_{,x}^{w}\right\}\left\{N_{,y}^{w}\right\}^T + 2\left\{N_{,x}^{\Phi_x}\right\} B_{66} \{q_w\}^T \left\{N_{,x}^{w}\right\}\left\{N_{,y}^{w}\right\}^T \Big) d\Omega = \\
&= \int_\Omega \tfrac{1}{2}\Big(\Big(\left\{N_{,y}^{\Phi_x}\right\} B_{12} + \left\{N_{,x}^{\Phi_x}\right\} B_{16}\Big)\{q_w\}^T \left\{N_{,x}^{w}\right\}\left\{N_{,x}^{w}\right\}^T + \\
&+\Big(\left\{N_{,y}^{\Phi_x}\right\} B_{22} + \left\{N_{,x}^{\Phi_x}\right\} B_{26}\Big)\{q_w\}^T \left\{N_{,y}^{w}\right\}\left\{N_{,y}^{w}\right\}^T + \\
&+2\Big(\left\{N_{,y}^{\Phi_x}\right\} B_{26} + \left\{N_{,x}^{\Phi_x}\right\} B_{66}\Big)\{q_w\}^T \left\{N_{,x}^{w}\right\}\left\{N_{,y}^{w}\right\}^T \Big) d\Omega
\end{aligned} \tag{2. 91}$$

Summing the two integrals obtained, from equation (2. 84) results:

$$\left\{\delta q\right\}^T \left[K_2\right] \{q\} =$$

$$= \left\{\delta q_u\right\}^T \left[\overline{U}\right] \{q_w\} + \left\{\delta q_v\right\}^T \left[\overline{V}\right] \{q_w\} + \left\{\delta q_{\Phi_y}\right\}^T \left[\overline{Y}\right] \{q_w\} + \left\{\delta q_{\Phi_x}\right\}^T \left[\overline{Z}\right] \{q_w\} =$$

$$= \begin{Bmatrix} \delta q_u \\ \delta q_v \\ \delta q_{\Phi_y} \\ \delta q_{\Phi_x} \end{Bmatrix}^T \begin{Bmatrix} [\overline{U}] \\ [\overline{V}] \\ [\overline{Y}] \\ [\overline{Z}] \end{Bmatrix} \{q_w\} = \begin{Bmatrix} \delta q_u \\ \delta q_v \\ \delta q_{\Phi_y} \\ \delta q_{\Phi_x} \end{Bmatrix}^T [K_2]\{q_w\}$$

The non-zero part of the non-linear stiffness matrix $[K_2]$ is:

$$[K_2] = \begin{Bmatrix} [\overline{U}] \\ [\overline{V}] \\ [\overline{Y}] \\ [\overline{Z}] \end{Bmatrix} \tag{2. 92}$$

2.4.3 – *Non-linear stiffness matrix* $[K_4]$

In this section the non-linear stiffness matrix, $[K_4]$ is derived. The $[K_4]$ matrix is a quadratic function of the transverse displacement *w* and depends only upon the out-of-plane shape functions and corresponding generalised displacements $\{q_w\}$. Within the three non-linear stiffness matrices, $[K_4]$ is the main source of geometric non-linearity.

From equation (2. 64),

$$\int_\Omega \left(\delta \begin{Bmatrix} \varepsilon_L^p \\ 0 \end{Bmatrix}^T [E] \begin{Bmatrix} \varepsilon_L^p \\ 0 \end{Bmatrix} \right) d\Omega = \{\delta q\}^T [K_4]\{q\} =$$

$$= \int_\Omega \left(\delta \begin{Bmatrix} \varepsilon_L^p \\ 0 \end{Bmatrix}^T \begin{bmatrix} [A] & [B] \\ [B] & [D] \end{bmatrix} \begin{Bmatrix} \varepsilon_L^p \\ 0 \end{Bmatrix} \right) d\Omega = \int_\Omega \left(\delta \{\varepsilon_L^p\}^T [A] \{\varepsilon_L^p\} \right) d\Omega$$

(2. 93)

From the definition of $\left\{\varepsilon_L^p\right\}$ in equation (2. 51), results that

$$\int_\Omega \delta\left(\left\{\varepsilon_L^p\right\}^T [A]\left\{\varepsilon_L^p\right\}\right) d\Omega =$$

$$= \tfrac{1}{2}\left\{\delta q_w\right\}^T \int_\Omega \left(\begin{bmatrix} \{q_w\}^T \{N_{,x}^w\}\{N_{,x}^w\}^T \\ \{q_w\}^T \{N_{,y}^w\}\{N_{,y}^w\}^T \\ 2\{q_w\}^T \{N_{,x}^w\}\{N_{,y}^w\}^T \end{bmatrix}^T \begin{bmatrix} A_{11} & A_{12} & A_{16} \\ A_{12} & A_{22} & A_{26} \\ A_{16} & A_{26} & A_{66} \end{bmatrix} \begin{bmatrix} \frac{1}{2}\{q_w\}^T \{N_{,x}^w\}\{N_{,x}^w\}^T \{q_w\} \\ \frac{1}{2}\{q_w\}^T \{N_{,y}^w\}\{N_{,y}^w\}^T \{q_w\} \\ \{q_w\}^T \{N_{,x}^w\}\{N_{,y}^w\}^T \{q_w\} \end{bmatrix} \right) d\Omega$$

$$= \tfrac{1}{2}\left\{\delta q_w\right\}^T \int_\Omega \left(\begin{bmatrix} \{q_w\}^T \{N_{,x}^w\}\{N_{,x}^w\}^T A_{11} + \{q_w\}^T \{N_{,y}^w\}\{N_{,y}^w\}^T A_{12} + 2\{q_w\}^T \{N_{,x}^w\}\{N_{,y}^w\}^T A_{16} \\ \{q_w\}^T \{N_{,x}^w\}\{N_{,x}^w\}^T A_{12} + \{q_w\}^T \{N_{,y}^w\}\{N_{,y}^w\}^T A_{22} + 2\{q_w\}^T \{N_{,x}^w\}\{N_{,y}^w\}^T A_{26} \\ \{q_w\}^T \{N_{,x}^w\}\{N_{,x}^w\}^T A_{16} + \{q_w\}^T \{N_{,y}^w\}\{N_{,y}^w\}^T A_{26} + 2\{q_w\}^T \{N_{,x}^w\}\{N_{,y}^w\}^T A_{66} \end{bmatrix}^T \times \right.$$

$$\left. \times \begin{bmatrix} \frac{1}{2}\{q_w\}^T \{N_{,x}^w\}\{N_{,x}^w\}^T \{q_w\} \\ \frac{1}{2}\{q_w\}^T \{N_{,y}^w\}\{N_{,y}^w\}^T \{q_w\} \\ \{q_w\}^T \{N_{,x}^w\}\{N_{,y}^w\}^T \{q_w\} \end{bmatrix} \right) d\Omega$$

$$= \tfrac{1}{2}\left\{\delta q_w\right\}^T \int_\Omega \left(\left(\{q_w\}^T \{N_{,x}^w\}\{N_{,x}^w\}^T A_{11} + \{q_w\}^T \{N_{,y}^w\}\{N_{,y}^w\}^T A_{12} + 2\{q_w\}^T \{N_{,x}^w\}\{N_{,y}^w\}^T A_{16} \right) \times \right.$$

$$\times \tfrac{1}{2}\{q_w\}^T \{N_{,x}^w\}\{N_{,x}^w\}^T \{q_w\} + \left(\{q_w\}^T \{N_{,x}^w\}\{N_{,x}^w\}^T A_{12} + \{q_w\}^T \{N_{,y}^w\}\{N_{,y}^w\}^T A_{22} + \right.$$

$$\left. + 2\{q_w\}^T \{N_{,x}^w\}\{N_{,y}^w\}^T A_{26} \right) \times \tfrac{1}{2}\{q_w\}^T \{N_{,y}^w\}\{N_{,y}^w\}^T \{q_w\} +$$

$$\left(\{q_w\}^T \{N_{,x}^w\}\{N_{,x}^w\}^T A_{16} + \{q_w\}^T \{N_{,y}^w\}\{N_{,y}^w\}^T A_{26} + 2\{q_w\}^T \{N_{,x}^w\}\{N_{,y}^w\}^T A_{66} \right) \times$$

$$\left. \times \{q_w\}^T \{N_{,x}^w\}\{N_{,y}^w\}^T \{q_w\} \right) d\Omega$$

$$
\begin{aligned}
&= \tfrac{1}{2}\{\delta q_w\}^T \int_\Omega \Big(\Big(\{q_w\}^T \left\{N^w_{,x}\right\}\left\{N^w_{,x}\right\}^T A_{11} + \{q_w\}^T \left\{N^w_{,y}\right\}\left\{N^w_{,y}\right\}^T A_{12} + 2\{q_w\}^T \left\{N^w_{,x}\right\}\left\{N^w_{,y}\right\}^T A_{16} \Big) \times \\
&\times \tfrac{1}{2}\{q_w\}^T \left\{N^w_{,x}\right\}\left\{N^w_{,x}\right\}^T + \Big(\{q_w\}^T \left\{N^w_{,x}\right\}\left\{N^w_{,x}\right\}^T A_{12} + \{q_w\}^T \left\{N^w_{,y}\right\}\left\{N^w_{,y}\right\}^T A_{22} + \\
&+ 2\{q_w\}^T \left\{N^w_{,x}\right\}\left\{N^w_{,y}\right\}^T A_{26} \Big) \times \tfrac{1}{2}\{q_w\}^T \left\{N^w_{,y}\right\}\left\{N^w_{,y}\right\}^T + \\
&\Big(\{q_w\}^T \left\{N^w_{,x}\right\}\left\{N^w_{,x}\right\}^T A_{16} + \{q_w\}^T \left\{N^w_{,y}\right\}\left\{N^w_{,y}\right\}^T A_{26} + 2\{q_w\}^T \left\{N^w_{,x}\right\}\left\{N^w_{,y}\right\}^T A_{66} \Big) \times \\
&\times \{q_w\}^T \left\{N^w_{,x}\right\}\left\{N^w_{,y}\right\}^T \Big) d\Omega \{q_w\} \\
&= \{\delta q\}^T [K_4] \{q\}
\end{aligned}
\tag{2. 94}
$$

2.4.4 - *Shear Linear Stiffness Matrix* $\left[K_1^\gamma\right]$

From equation (2. 59), and considering $\begin{Bmatrix} Q_x \\ Q_y \end{Bmatrix} = \begin{bmatrix} \overline{Q}_{44} & \overline{Q}_{45} \\ \overline{Q}_{45} & \overline{Q}_{55} \end{bmatrix} \begin{Bmatrix} \gamma_{yz} \\ \gamma_{zx} \end{Bmatrix}$,

$$
\int_\Omega \left(\{\delta\gamma\}^T \{Q\}\, d\Omega \right) = \int_\Omega \delta \begin{Bmatrix} \gamma_{zx} \\ \gamma_{yz} \end{Bmatrix}^T \begin{bmatrix} \overline{Q}_{44} & \overline{Q}_{45} \\ \overline{Q}_{45} & \overline{Q}_{55} \end{bmatrix} \begin{Bmatrix} \gamma_{yz} \\ \gamma_{zx} \end{Bmatrix} d\Omega
$$

From $\begin{Bmatrix} \gamma_{yz} \\ \gamma_{zx} \end{Bmatrix} = \begin{bmatrix} \left\{N^w_{,y}\right\}^T & 0 & -\left\{N^{\Phi_x}\right\}^T \\ \left\{N^w_{,x}\right\}^T & \left\{N^{\Phi_y}\right\}^T & 0 \end{bmatrix} \begin{Bmatrix} q_w \\ q_{\Phi_y} \\ q_{\Phi_x} \end{Bmatrix}$, the integral becomes

$$\int_\Omega \delta\left(\begin{bmatrix} \{N^w_{,y}\}^T & 0 & -\{N^{\Phi_x}\}^T \\ \{N^w_{,x}\}^T & \{N^{\Phi_y}\}^T & 0 \end{bmatrix}\begin{Bmatrix} q_w \\ q_{\Phi_y} \\ q_{\Phi_x} \end{Bmatrix}\right)^T \begin{bmatrix} \{N^w_{,y}\}^T & 0 & -\{N^{\Phi_x}\}^T \\ \{N^w_{,x}\}^T & \{N^{\Phi_y}\}^T & 0 \end{bmatrix}\begin{Bmatrix} q_w \\ q_{\Phi_y} \\ q_{\Phi_x} \end{Bmatrix} d\Omega =$$

$$= \begin{Bmatrix} \delta q_w \\ \delta q_{\Phi_y} \\ \delta q_{\Phi_x} \end{Bmatrix}^T \int_\Omega \begin{bmatrix} \{N^w_{,y}\}\overline{Q}_{44}\{N^w_{,y}\}^T + \{N^w_{,x}\}\overline{Q}_{45}\{N^w_{,y}\}^T + \{N^w_{,y}\}\overline{Q}_{45}\{N^w_{,x}\}^T + \{N^w_{,x}\}\overline{Q}_{55}\{N^w_{,x}\}^T & \{N^w_{,y}\}\overline{Q}_{45}\{N^{\Phi_y}\}^T + \{N^w_{,x}\}\overline{Q}_{55}\{N^{\Phi_y}\}^T & -\{N^w_{,y}\}\overline{Q}_{44}\{N^{\Phi_x}\}^T - \{N^w_{,x}\}\overline{Q}_{45}\{N^{\Phi_x}\}^T \\ \{N^{\Phi_y}\}\overline{Q}_{45}\{N^w_{,y}\}^T + \{N^{\Phi_y}\}\overline{Q}_{55}\{N^w_{,x}\}^T & \{N^{\Phi_y}\}\overline{Q}_{55}\{N^{\Phi_y}\}^T & -\{N^{\Phi_y}\}\overline{Q}_{45}\{N^{\Phi_x}\}^T \\ -\{N^{\Phi_x}\}\overline{Q}_{45}\{N^w_{,y}\}^T - \{N^{\Phi_x}\}\overline{Q}_{55}\{N^w_{,x}\}^T & -\{N^{\Phi_x}\}\overline{Q}_{55}\{N^{\Phi_y}\}^T & \{N^{\Phi_x}\}\overline{Q}_{45}\{N^{\Phi_x}\}^T \end{bmatrix} d\Omega \begin{Bmatrix} q_w \\ q_{\Phi_y} \\ q_{\Phi_x} \end{Bmatrix}$$

$$= \{\delta q\}^T \left[K_1^\gamma\right]\{q\} \qquad (2.\ 95)$$

3. *DISPLACEMENT SHAPE FUNCTIONS*

As referred in section 2.1, a matrix of shape functions is considered, and four sets of shape functions are required: one set of in-plane shape functions, one set of out-of-plane shape functions, one set of rotation about *x* shape functions and one set of rotation about *y* shape functions (2. 10)-(2. 13).

The HFEM relies on the utilization of high order shape functions and ill-conditioning is common in high order polynomials. For this reason, trigonometric shape functions are suggested in [2.7]. Nevertheless, with the Rodrigue's form of Legendre polynomials no ill-condition problems were met and it was decided to continue using them. Thus, the in-plane shape functions are given by

$$g_{r-2} = \sum_{n=0}^{INT(r/2)} \frac{(-1)^n (2r-2n-5)!!}{2^n n!(r-2n-1)!}\xi^{r-2n-1}, r > 2 \qquad (2.\ 96)$$

And the out-of-plane shape functions are given by

$$f_r = \sum_{n=0}^{INT(r/2)} \frac{(-1)^n (2r-2n-7)!!}{2^n n!(r-2n-1)!} \xi^{r-2n-1}, r > 4 \qquad (2.97)$$

where $r!! = r(r\text{-}2)\ldots(2 \text{ or } 1)$, $0!! = (-1)!! = 1$ and $INT(r/2)$ denotes the integer part of $r/2$. The rotation shape functions about *x* and *y* are equal to the in-plane shape functions.

In APPENDIX A, the first out-of-plane and in-plane shape functions are plotted; the shape functions f_r, $1 \le r \le 4$ are cubic polynomials not represented.

It can be seen from the plots that:

(i) the in-plane shape functions have zero displacements at $\xi = -1$ and $\xi = 1$; the Legendre $(r > 4)$ out-of-plane shape functions have both zero displacements and slope at these points. These shape functions satisfy fully clamped boundary conditions;

(ii) the odd number in-plane and Legendre out-of-plane shape functions are symmetric, while the even number are anti-symmetric. The adequate shape functions regarding the symmetries of the problem under study can be chosen, thus reducing the number of degrees of freedom.

4. *NEWMARK METHOD*

In the previous sections, a finite element model was derived and the undamped equations of motion were obtained. Introducing damping matrix $[C]$, these equations may be written as:

$$[M]\{\ddot{q}\}+[C]\{\dot{q}\}+[K]\{q\}=\{P\} \tag{2. 98}$$

Where $[M]$ and $[K]$ are the mass and stiffness matrices; $\{P\}$ is the vector of externally applied loads.

The equations of motion are integrated in time domain, directly, that is without transformation of co-ordinates [2.6]. In essence, direct numerical integration is based in two ideas. First, instead of trying to satisfy (2. 98) at any time *t*, it is aimed to satisfy (2. 98) only at discrete time intervals Δt apart. The second idea in which a direct integration method is based is that a variation of displacements and accelerations within each time interval Δt is assumed.

In the following, displacement and acceleration vectors at time 0 are denoted by $\{\ddot{q}\}^0$ and $\{\dot{q}\}^0$, respectively, are known, and let the solution to the differential equation (2. 98) be required from time 0 to time t_f, in intervals of Δt.

To determine the solution of the displacements and accelerations at time $t+\Delta t$, the equations (2. 98) at time $t+\Delta t$ are also considered:

$$[M]\{\ddot{q}\}^{t+\Delta t}+[C]\{\dot{q}\}^{t+\Delta t}+[K]\{q\}^{t+\Delta t}=\{P\}^{t+\Delta t} \tag{2.99}$$

It is assumed that the accelerations within each time interval, Δt are given by

$$\{\ddot{q}\}=\{\ddot{q}\}^t+\frac{1}{\Delta t}\left(\{\ddot{q}\}^{t+\Delta t}-\{\ddot{q}\}^t\right)\tau \quad ,0\le\tau\le\Delta t \tag{2.100}$$

Integrating (2.100) gives

$$\{\dot{q}\}=\{\dot{q}\}^t+\{\ddot{q}\}^t\tau+\frac{1}{2\Delta t}\left(\{\ddot{q}\}^{t+\Delta t}-\{\ddot{q}\}^t\right)\tau^2 \tag{2.101}$$

since $\{\dot{q}\}=\{\dot{q}\}^t$ when $\tau=0$. Integrating again gives

$$\{q\} = \{q\}^t + \{\dot{q}\}^t \tau + \frac{1}{2}\{\ddot{q}\}^t \tau^2 + \frac{1}{6\Delta t}\left(\{\ddot{q}\}^{t+\Delta t} - \{\ddot{q}\}^t\right)\tau^3 \tag{2.102}$$

since $\{q\} = \{q\}^t$ when $\tau = 0$.

Evaluating (2.101) and (2.102) at $\tau = \Delta t$ gives

$$\{\dot{q}\}^{t+\Delta t} = \{\dot{q}\}^t + \frac{\Delta t}{2}\left(\{\ddot{q}\}^t + \{\ddot{q}\}^{t+\Delta t}\right) \tag{2.103}$$

and

$$\{q\}^{t+\Delta t} = \{q\}^t + \{\dot{q}\}^t \Delta t + \frac{(\Delta t)^2}{6}\left(2\{\ddot{q}\}^t + \{\ddot{q}\}^{t+\Delta t}\right) \tag{2.104}$$

In the Newmark method, equations (2.103) and (2.104) are assumed to take the form [2.6]

$$\{\dot{q}\}^{t+\Delta t} = \{\dot{q}\}^t + \Delta t\left[(1-\alpha)\{\ddot{q}\}^t + \alpha\{\ddot{q}\}^{t+\Delta t}\right] \tag{2.105}$$

and

$$\{q\}^{t+\Delta t} = \{q\}^t + \{\dot{q}\}^t \Delta t + (\Delta t)^2\left[\left(\frac{1}{2}-\delta\right)\{\ddot{q}\}^t + \delta\{\ddot{q}\}^{t+\Delta t}\right] \tag{2.106}$$

Taking $\alpha = \frac{1}{2}$ and $\delta = \frac{1}{4}$ corresponds to assuming that the acceleration is constant and equal to the average value $\left(\{\ddot{q}\}^t + \{\ddot{q}\}^{t+\Delta t}\right)/2$ within the interval $(t, t+\Delta t)$.

The response at time $t+\Delta t$ is obtained by evaluating the equation of motion at time $t+\Delta t$, that is

$$[M]\{\ddot{q}\}^{t+\Delta t} + [C]\{\dot{q}\}^{t+\Delta t} + [K]\{q\}^{t+\Delta t} = \{P\}^{t+\Delta t} \tag{2.107}$$

In order to obtain an equation for $\{q\}^{t+\Delta t}$, equation (2.106) is solved for $\{\ddot{q}\}^{t+\Delta t}$ which gives

$$\{\ddot{q}\}^{t+\Delta t} = \frac{1}{\delta(\Delta t)^2}\left(\{q\}^{t+\Delta t} - \{q\}^{t}\right) - \frac{1}{\delta \Delta t}\{\dot{q}\}^{t} - \left(\frac{1}{2\delta} - 1\right)\{\ddot{q}\}^{t} \tag{2.108}$$

Replacing $\{\ddot{q}\}^{t+\Delta t}$, given in (2.108) in (2.105) gives

$$\{\dot{q}\}^{t+\Delta t} = \frac{\alpha}{\delta \Delta t}\left(\{q\}^{t+\Delta t} - \{q\}^{t}\right) + \left(1 - \frac{\alpha}{\delta}\right)\{\dot{q}\}^{t} + \Delta t\left(1 - \frac{\alpha}{2\delta}\right)\{\ddot{q}\}^{t} \tag{2.109}$$

Substituting (2.108) and (2.109) into (2.107),

$$\begin{aligned}
&[M]\left(\frac{1}{\delta(\Delta t)^2}\left(\{q\}^{t+\Delta t} - \{q\}^{t}\right) - \frac{1}{\delta \Delta t}\{\dot{q}\}^{t} - \left(\frac{1}{2\delta} - 1\right)\{\ddot{q}\}^{t}\right) + \\
&+[C]\left(\frac{\alpha}{\delta \Delta t}\left(\{q\}^{t+\Delta t} - \{q\}^{t}\right) + \left(1 - \frac{\alpha}{\delta}\right)\{\dot{q}\}^{t} + \Delta t\left(1 - \frac{\alpha}{2\delta}\right)\{\ddot{q}\}^{t}\right) + \\
&+[K]\{q\}^{t+\Delta t} = \{P\}^{t+\Delta t} \Leftrightarrow \\
&\Leftrightarrow \frac{1}{\delta(\Delta t)^2}[M]\left(\{q\}^{t+\Delta t} - \{q\}^{t}\right) - \frac{1}{\delta \Delta t}[M]\{\dot{q}\}^{t} - \left(\frac{1}{2\delta} - 1\right)[M]\{\ddot{q}\}^{t} + \\
&+\frac{\alpha}{\delta \Delta t}[C]\left(\{q\}^{t+\Delta t} - \{q\}^{t}\right) + \left(1 - \frac{\alpha}{\delta}\right)[C]\{\dot{q}\}^{t} + \Delta t\left(1 - \frac{\alpha}{2\delta}\right)[C]\{\ddot{q}\}^{t} + \\
&+[K]\{q\}^{t+\Delta t} = \{P\}^{t+\Delta t}
\end{aligned} \tag{2.110}$$

Solving for $\{q\}^{t+\Delta t}$,

$$\begin{aligned}
&\left(\frac{1}{\delta(\Delta t)^2}[M] + \frac{\alpha}{\delta(\Delta t)^2}[C] + [K]\right)\{q\}^{t+\Delta t} = \\
&\{P\}^{t+\Delta t} + \frac{1}{\delta(\Delta t)^2}[M]\{q\}^{t} + \frac{1}{\delta \Delta t}[M]\{\dot{q}\}^{t} + \left(\frac{1}{2\delta} - 1\right)[M]\{\ddot{q}\}^{t} + \\
&+\frac{\alpha}{\delta \Delta t}[C]\{q\}^{t} - \left(1 - \frac{\alpha}{\delta}\right)[C]\{\dot{q}\}^{t} - \Delta t\left(1 - \frac{\alpha}{2\delta}\right)[C]\{\ddot{q}\}^{t}
\end{aligned}$$

Placing together terms in $\{\ddot{q}\}^{t}$, $\{\dot{q}\}^{t}$ and $\{q\}^{t}$, in the second member,

$$\left(\frac{1}{\delta(\Delta t)^2}[M]+\frac{\alpha}{\delta\Delta t}[C]+[K]\right)\{q\}^{t+\Delta t}=$$
$$=\{P\}^{t+\Delta t}+\left(\frac{1}{\delta(\Delta t)^2}[M]+\frac{\alpha}{\delta\Delta t}[C]+[K]\right)\{q\}^{t}+ \qquad (2.111)$$
$$\left(\frac{1}{\delta\Delta t}[M]-\left(1-\frac{\alpha}{\delta}\right)[C]\right)\{q\}^{t}+\left(\left(\frac{1}{2\delta}-1\right)[M]-\Delta t\left(1-\frac{\alpha}{2\delta}\right)[C]\right)\{\ddot{q}\}$$

If $\{q\}^t$, $\{\dot{q}\}^t$ and $\{\ddot{q}\}^t$ are known, then $\{q\}^{t+\Delta t}$ can be calculated using (2.111). Equations (2.108) and (2.109) can be used to determine $\{\ddot{q}\}^{t+\Delta t}$ and $\{\dot{q}\}^{t+\Delta t}$. The time history of the response is obtained from time 0 to time t_f, in intervals of Δt.

Therefore, from equations (2.108), (2.109) and (2.111) the Newmark Method is given by

$$\left(a_1[M]+a_2[C]+[K]\right)\{q\}^{t+\Delta t}=\{P\}^{t+\Delta t}+\left(a_1[M]+a_2[C]\right)\{q\}^{t}+$$
$$+\left(a_3[M]-a_4[C]\right)\{\dot{q}\}^{t}++\left(a_5[M]-a_6[C]\right)\{\ddot{q}\}^{t}$$

$$\{\ddot{q}\}^{t+\Delta t}=a_1\left(\{q\}^{t+\Delta t}-\{q\}^{t}\right)-a_3\{\dot{q}\}^{t}-a_5\{\ddot{q}\}^{t} \qquad (2.112)$$
$$\{\dot{q}\}^{t+\Delta t}=a_2\left(\{q\}^{t+\Delta t}-\{q\}^{t}\right)+a_4\{\dot{q}\}^{t}+a_6\{\ddot{q}\}^{t}$$

where

$$a_1=\frac{1}{\delta(\Delta t)^2}, \qquad a_2=\frac{\alpha}{\delta\Delta t},$$
$$a_3=\frac{1}{\delta\Delta t}, \qquad a_4=\left(1-\frac{\alpha}{\delta}\right), \qquad (2.113)$$
$$a_5=\left(\frac{1}{2\delta}-1\right), \qquad a_6=\Delta t\left(1-\frac{\alpha}{2\delta}\right)$$

The set of linear equations given in (2.112) is solved in order to determine $\{q\}^{t+\Delta t}$.

In reference [2.6] the stability of the method is investigated and it is stated that the method is unconditionally stable if

$$\alpha \geq 0,50 \text{ and } \delta \geq 0,25\left(0,5+\delta\right)^2 \tag{2.114}$$

Unless α is taken to be $\frac{1}{2}$, the method introduces artificial damping, which can be negative (when $\alpha < \frac{1}{2}$). In the Newmark integration scheme, as an unconditionally stable method (choosing parameters verifying (2.114), the time step Δt is based upon the period corresponding to the highest frequency likely to contribute to the response, ω_n. According to reference [2.6], good accuracy is obtained with a time step given by $\omega_n \Delta t = \pi/50$.

The Newmark method can be extended to non-linear dynamic analysis. This requires that iteration must be performed at each time step in order to satisfy equilibrium. Also, the non-linear stiffness matrix must be formed and triangularized at each iteration or at selective points in time.

5. *CLOSING COMMENTS*

The mathematical model of the *p*-version HEFM for asymmetrically laminated rectangular plates is given in this chapter. The equations of motion are obtained and the matrices in the equations of motion are derived for the asymmetrically laminated rectangular plates, with a detailed description of the matrices involved. All these matrices are finally expressed as the integration of shape functions and their derivatives. In the implementation of the model, the differentiation and the integration of the polynomials will be calculated symbolically to find out the exact values via symbolic computation method using *MAPLE*.

The model is derived in time domain by applying the finite element method, the principle of virtual work and the d'Alembert's principle. Because the problems to be analysed do not involve singularities and the geometry of the plate is very regular, only one element was used. The model developed in this chapter is applied to the study of the geometrical non-linear vibrations of plates in following chapters.

Chapter 3

TOOLS TO ANALYSE MOTIONS

1. *INTRODUCTION*

In Chapter 2, the mathematical model of the p-version of the FEM has been derived including geometrical non-linearity for thick, asymmetric composite laminated rectangular plates. In order to solve the non-linear equations of motion, the Newmark method was presented. In this chapter different tools that can be used to characterize the responses of non-linear systems are presented.

In non-linear vibrations, there are several parameters that influence the time dependence of the response: time variation, space dependence and amplitude of the external excitation, properties of the structure, initial and boundary conditions, etc. Depending on these parameters, the oscillations may be periodic – including harmonic, sub-harmonic and super-harmonic – quasi-periodic or even chaotic [3.1, 3.7].

Unlike equilibrium equations, periodic solutions are characterized by one basic frequency ω. The spectrum of a periodic signal consists of a spike at the frequency 0 and spikes at integer multiples of ω.

A quasi-periodic solution is a dynamic solution characterized by two or more incommensurate[1] frequencies. Although the waveform of a quasi-periodic signal may look complex because of the presence of many sinusoids in it, calculating its spectrum would reveal its simplicity. In principle, the spectrum can be used to distinguish a quasi-periodic signal from a periodic signal in that the spikes in the spectrum of a quasi-periodic signal are not spaced at integer multiples of a particular

[1] Two frequencies ω_1 and ω_2 are said to be incommensurate if ω_1 / ω_2 is an irrational number.

frequency [3.2]. Poincaré Maps are also used to determine the stability of a quasi-periodic solution.

Chaotic solutions will also be studied in this thesis; there is no precise definition for a chaotic solution because it cannot be represented through standard mathematical functions. A chaotic solution is an aperiodic solution which is endowed with some special characteristics. From a practical point of view, chaos can be defined as a bounded steady-state behaviour that is not an equilibrium solution or a periodic solution or a quasi-periodic solution. The attractor associated with a chaotic motion in state space is not a simple geometrical object like a finite number of points, a closed curve or a torus. Chaotic attractors are complicated geometrical objects that possess fractal dimensions. The spectrum of a chaotic signal contains spikes that indicate the predominant frequencies of the signal [3.2].

In this chapter, tools such as Fourier spectra [3.2], Poincaré Maps [3.3, 3.5] and Lyapunov exponents [3.3, 3.5], which are used to characterize the responses of non-linear systems, will be presented.

2. *FOURIER SPECTRA*

The Fourier or frequency spectra help in distinguishing among periodic, quasi-periodic, and chaotic motions and are typically used to study stationary signals. The frequency spectrum can be either amplitude or a power spectrum. In an amplitude spectrum, the Fourier amplitude is displayed at each frequency. On the other hand, in a power spectrum, the square of the Fourier amplitude per unit time is displayed at each frequency [3.2].

The Fourier transform of a signal $x(t)$ is defined as

$$X(\omega) = \int_{-\infty}^{+\infty} x(t) e^{-2i\pi\omega t} dt \tag{3.4}$$

where ω denotes the frequency, $X(\omega)$ is an integrable[2] complex quantity.

In theory, the Fourier transform can be used to determine the frequency content of a signal $X(\omega)$ if it is known for $-\infty < \omega < +\infty$ and is integrable. However, a stationary signal that exists for all ω is not integrable. Besides, in practice, $X(\omega)$ is known for only a finite length of time T_c and hence the so called finite Fourier transform is used:

$$X(\omega, T_c) = \int_0^{T_c} x(t) e^{-2i\pi\omega t} dt \tag{3.5}$$

where, again, $X(\omega, T_c)$ is a complex quantity.

Fourier methods will only be employed to determine the harmonic content of periodic oscillations. The finite Fourier transform provides a mechanism for representing a signal as the sum of simple sine and cosine functions, which correspond to discrete lines in the frequency spectrum. In this work, the signal is a time series obtained from the numerical integration of the equations of motion. This time series is collected over a finite time T_c and consists of a discrete number of points obtained at a chosen sampling frequency. The period of the stationary motions is related with the excitation period, and one easily selects a length of numerical data that coincides with the period. These data is modelled as a sum of sine and cosine functions of time *t* [3.2]. To obtain the frequency spectra of quasi-periodic and chaotic oscillations, other tools of signal processing, like the power spectral density function are recommended.

The Fourier transform of discrete data is obtained using the discrete Fourier transform (DFT). It is a procedure for modifying the Fourier transform so as to permit its computation on a digital computer. Hence, a discrete Fourier transform is an approximation of the continuous Fourier transform. A special case of the DFT transform is the fast Fourier transform (FFT) It is essentially an efficient computational scheme that takes advantage of certain symmetry properties in the

[2] $X(\omega)$ is integrable if $\int_{-\infty}^{+\infty} |x(t)| dt < +\infty$

cosine and sine functions at their points of evaluation in order to achieve speed over conventional methods [3.2].

Suppose that we sample a periodic, continuous time function $X(t)$ at a sequence of N points with equal time intervals of length Δ seconds, starting at time t_0, with period $N\Delta$; the discrete Fourier transform is given by

$$X(t) = \frac{1}{N}\left[c_1 + 2\sum_{n=2}^{(N+1)/2} c_{2n-2} cos\left[\frac{2\pi(n-1)(t-t_0)}{N\Delta}\right] - 2\sum_{n=2}^{(N+1)/2} c_{2n-1} sin\left[\frac{2\pi(n-1)(t-t_0)}{N\Delta}\right]\right] \tag{3.6}$$

and the coefficients c_k, $k = 1,..., N/2$ are given by

$$\begin{aligned} c_1 &= \sum_{n=1}^{N} s_n \\ c_{2m-1} &= -\sum_{n=1}^{N} s_n sin\left[\frac{2\pi(m-1)(n-1)}{N}\right], \quad m = 2,..., N/2 \\ c_{2m-2} &= \sum_{n=1}^{N} s_n cos\left[\frac{2\pi(m-1)(n-1)}{N}\right], \quad m = 2,..., (N/2)+1 \end{aligned} \tag{3.7}$$

If N is odd, c_m is defined from 2 to $\frac{N+1}{2}$. The dominant frequencies correspond to the higher values of P_k, where P_k are the components of a vector $\{P\}$ of length $N/2$ as follows

$$\begin{aligned} P_1 &= |c_1| \\ P_k &= \sqrt{c_{2k-2}^2 + c_{2k-1}^2} \quad k = 2,..., (N+1)/2 \end{aligned} \tag{3.8}$$

These values correspond to the energy spectrum of the signal. In particular, P_k corresponds to the energy level at frequency $\frac{k-1}{N\Delta}$, $k = 1, 2,..., \frac{N+1}{2}$.

The time series of a periodic motion has the appearance of a uniform trace, and the corresponding spectrum has one basic frequency. If the response spectrum of a system excited by a harmonic excitation contains solely a line at the excitation frequency, the motion is a linear periodic motion. On the other hand, if the response spectrum contains lines at frequencies which are multiples of the excitation

frequency, then the motion is non-linear periodic. The spectrum of a periodic motion consists of a single basic frequency. When the spectrum has *n* basic frequencies (i.e., *n* incommensurate frequencies), the corresponding motion is no longer periodic and is called an *n*-period quasi-periodic motion. The spectrum of a chaotic motion has a continuous or broadband character [3.5].

The spectra of random motions such as noise also have continuous or broadband character, but chaotic motions can be distinguished from noise by using the character of the spectrum and tools, such as dimension calculations and Lyapunov exponents. For the spectrum associated with a chaotic motion, the Fourier amplitudes are frequency dependent in the broadband region. These amplitudes scale as $1/\omega^{\alpha}$, where ω is the frequency and α is a positive integer. For the spectrum associated with a random motion, the Fourier amplitudes in the broadband region are either frequency independent or frequency dependent and do not follow the $1/\omega^{\alpha}$ scaling law [3.2].

The Fourier analysis is not well suited for signals with transient effects that occur over a short period of time because it is not localized in time. This problem can partly be overcome by conducting Fourier analysis in different time windows. The location of the time window adds a time dimension to the overall analysis. For a signal with short-lived transient events, it is desirable to use functions such as wavelets, that are localized in time and frequency to represent the signal rather than sine and cosine functions that extend over all time [3.2].

3. *POINCARÉ MAPS*

In this section, we consider periodic solutions of dynamical systems, especially continuous-time systems. For continuous values of time, the evolution of a system is governed by either an autonomous or a non-autonomous system of differential equations. Only non-autonomous systems are studied. In these systems the equations are of the form

$$\{\dot{x}\} = \{F(\{x\}, t)\} \tag{3.9}$$

Where $\{x\}$ is finite dimensional, $\{x\} \in \mathbb{R}^n$, $t \in \mathbb{R}$ and $\{F\}$ explicitly depends on *t*. The vector $\{F\}$ is often referred to as vector field, the vector $\{x\}$ is called state vector because it describes the state of the system, and the space $\mathbb{R}^n$ in which $\{x\}$ evolves is called a state space. A state space is called a phase space when one-half of the states are displacements and the other one-half are velocities [3.2].

Let the initial state of the system at time t_0 be $\{x_0\}$, and let *I* represent a time interval that includes t_0. In general, a projection of a solution $\{x(t, t_0, x_0)\}$ of (3.9) onto the *n*-dimensional state space is referred to as trajectory or an orbit of the system trough the point $\{x\} = \{x_0\}$. In other words, the solution could be thought of as a point that moves along a trajectory, occupying different positions at different times similar to the way a planet moves through the space. An orbit is represented by $\gamma(\{x_0\})$ or Γ. The orbit obtained for times $t \geq 0$ passing through the point $\{x_0\}$ at $t = 0$ is called a positive orbit and is denoted by $\gamma^+(\{x_0\})$; the orbit obtained for times $t \leq 0$ is called a negative orbit and is denoted by $\gamma^-(\{x_0\})$. Also, $\Gamma = \gamma^+(\{x_0\}) \cup \gamma^-(\{x_0\})$, where the symbol $\cup$ stands for the union operator.

Equation (3.9) is also referred to as an evolving equation. Let the evolution of the system described by this equation be controlled by a set of parameters *E*. To make this parameter dependence explicit, we describe the evolution by

$$\{\dot{x}\} = \{F(\{x\}, t; E)\} \tag{3.10}$$

where *E* is a vector of control parameters. Formally, $E \in \mathbb{R}^n$ and the vector function $\{F\}$ can be represented as $\{F\} : \mathbb{R}^n \times \mathbb{R}^1 \times \mathbb{R}^m \to \mathbb{R}^n$.

Next, some facts from the theory of ordinary-differential equations are stated [3.4]. If the scalar components of $\{F\}$ are C^0 in a domain D of the $(\{x\}, t)$ space, then a solution $\{x(t, t_0, x_0)\}$ satisfying the conditions $\{x\} = \{x_0\}$ at $t = t_0$ exists in a small

time interval around t_0 in D. Moreover, if the scalar components of $\{F\}$ are C^1 in D, then the solution $\{x(t,t_0,\{x_0\})\}$ is unique in a small time interval around t_0. If the existence and uniqueness of solutions of a system of the form (3.10) are ensured, then this system is deterministic. This means that two integral curves starting from two different initial conditions cannot intersect each other in the extended state space.

Equation (2.71) depends explicitly on time; therefore it represents a non-autonomous system.

A dynamic solution $\{x\} = \{X(t)\}$ of a continuous time system is periodic with least period T if $\{X(t+h)\} = \{X(t)\}$ and $\{X(t+\tau)\} \neq \{X(t)\}$ for $0 < \tau < T$. For these solutions, Poincaré introduced the notion of orbital stability.

Let Γ_1 represent the orbit of u and Γ_2 represent the orbit of v for all times. The periodic solutions u and v have different periods T_1 and T_2, and hence, the corresponding motions evolve on different time scales. The orbit Γ_1 is said to be orbitally stable if, given a small number $\varepsilon > 0$, there exists $\delta = \delta(\varepsilon) > 0$ such that if $\|u(t=0) - v(t=\tau)\| < \delta$ for some τ, then there exist t_1 and t_2 for which $\|u(t_1) - v(t_2)\| < \varepsilon$. Further, if Γ_2 tends to Γ_1 as $t \to \infty$, then we say Γ_1 is asymptotically stable. In Poincaré stability, we examine how "close" orbits are in the state space.

In the following chapter Poincaré maps are used to determine if the solutions are periodic, quasi-periodic or chaotic [3.3].

A Poincaré section is a hypersurface[3] in the state space that is transverse to the flow of a given system of equations. The state space is given by

$$\{nx(t)\}.\{F(\{x\};t)\} \neq 0 \tag{3.11}$$

[3] In a *n*-dimensional space, a hypersurface is a surface whose dimension is less than *n*.

where $\{nx(t)\}$ is a vector normal to the selection located at $\{x\}$, $\{F(x;t)\}$ is the vector field describing the flow, and the dot indicates the dot product. A Poincaré section is denoted by Σ. Although the time interval between two successive intersections of a trajectory with a chosen Poincaré section is not constant in all situations, we can collect the points on the Poincaré section by stroboscopically monitoring the state variables at intervals of the period T [3.5].

In Poincaré Maps, a finite number of points corresponds to a periodic motion, an infinite number of points filling up a closed curve corresponds to quasi-periodic motion, and an infinite number of orderly distributed points (usually) corresponds to chaotic motion.

4. *LYAPUNOV EXPONENTS*

For a dynamical system, sensitivity to initial conditions is quantified by the Lyapunov exponents. For example, consider two trajectories with nearby initial conditions on an attractor. When the attractor is chaotic, the trajectories diverge, on average, at an exponential rate characterized by the largest Lyapunov exponent [3.6]. Considering the non-autonomous system given in (3.9), a particular trajectory $\{\tilde{x}_1(t)\}$ and a neighbour of that trajectory (defined by the diameter, of the sphere) at some instance of time t_0, the purpose is to evaluate how another trajectory $\{\tilde{x}_2(t)\}$ diverges from $\{\tilde{x}_1(t)\}$, as the system evolves. This way, the Lyapunov exponent evaluates the time evolution of a sphere's axes.

The variation of the diameter may be expressed as $d(t) = d_0 2^{\lambda t}$ [3.5]. Therefore,

$$\lambda = \frac{1}{t}\log_2\left(\frac{d(t)}{d(0)}\right)$$

If the exponent λ is negative or equal to zero, then the trajectory $\{\tilde{x}_2(t)\}$ does not diverge from $\{\tilde{x}_1(t)\}$; on the other hand, if λ is positive, the trajectory $\{\tilde{x}_2(t)\}$ diverges exponentially from the original orbit, characterizing chaos [3.5].

This concept is also generalized for the spectrum of Lyapunov exponents, $\lambda_i, i = 1, 2, ..., n$, by considering a small n-dimensional sphere of initial conditions, where n is the number of equations (or, equivalently, the number of state variables) used to describe the system. As time progresses, the sphere evolves into an ellipsoid whose principal axes expand (or contract) at rates given by the Lyapunov exponents [3.6]:

$$\lambda_i = \lim_{t\to\infty}\left[\frac{1}{t}\log_2\left(\frac{d_i(t)}{d_i(0)}\right)\right],\ i = 1,..,n$$

where $d_i(t)$ measures the growth of an infinitesimal *n*-sphere of initial conditions at $t = 0$ in terms of the i'th ellipsoidal axis.

The presence of a positive exponent is sufficient to diagnose chaos and represents local instability in a particular direction. If more than one Lyapunov exponent is positive then there is hipercaos. Note that for the existence of an attractor, the overall dynamics must be dissipative, i.e., globally stable, and the total rate of contraction must outweigh the total rate of expansion. Thus, even when there are several positive Lyapunov exponents, the sum across the entire spectrum is negative.

Wolf et al [3.6] explain the Lyapunov spectrum by providing the following geometrical interpretation. First, arrange the *n* principal axes of the ellipsoid in the order of most rapidly expanding to most rapidly contracting. It follows that the associated Lyapunov exponents will be arranged such that

$$\lambda_1 \geq \lambda_2 \geq ... \geq \lambda_n$$

where λ_1 and λ_n correspond to the most rapidly expanding and contracting principal axes, respectively. Next, recognize that the length of the first principal axis is proportional to $2^{\lambda_1 t}$; the area determined by the first two principal axes is proportional to $2^{(\lambda_1+\lambda_2)t}$; and the volume determined by the first *k* principal axes is proportional to $2^{(\lambda_1+\lambda_2+...+\lambda_k)t}$. Thus, the Lyapunov spectrum can be defined such that the exponential growth of a *k*-volume element is given by the sum of the *k* largest Lyapunov exponents. Note that information created by the system is represented as a change in the volume defined by the expanding principal axes.

Next, the method used by Wolf et *al*. to compute the largest non-negative Lyapunov exponent is presented. It is based in evaluating distances between points and the trajectory. Given the time series $\{x(t)\}$, an n-dimensional phase portrait is reconstructed with delay coordinates [3.6], i.e., a point on the attractor is given by

$$\left\{\{x(t)\},\{x(t+\tau)\},...,\{x(t+(n-1)\tau)\}\right\},$$

where τ is the almost arbitrary delay time. Considering $\{Z(t_0)\}$ the nearest neighbour to the initial point $\{x(t_0)\}$ and L_0, the distance between $\{x(t_0)\}$ and $\{Z(t_0)\}$ is given by $L_0 = \left\|\{x(t_0)\}-\{Z(t_0)\}\right\|$ where $\|\ \|$ represents the Euclidean norm.

Defining an hipersphere with ray ε centred in $\{x(t_0)\}$ such that $\{Z(t_0)\}$ is inside the hipersphere, i.e., $L_0 = \left\|\{x(t_0)\}-\{Z(t_0)\}\right\| < \varepsilon$ the time evolution is followed from $\{x(t_0)\}$ to $\{Z(t_0)\}$ until, in an instant $t_1 = t_0 + \tau$ the distance between those points, $L_0^{'}$, is greater than ε. In that moment, $\{Z(t_0)\}$ is replaced by another neighbour, closer to $\{x(t_1)\}$, that is in the direction of the segment $L_0^{'}$ and such that

$L_1 = \left\|\{x(t_1)\}-\{Z(t_1)\}\right\| < \varepsilon$.

The process follows until all the points $\{x(t_i)\}$ are analysed. The largest positive Lyapunov exponent is obtained as an average of $\log_2\left(L_i'/L_i\right)$ along the trajectory, i.e.,

$$\lambda_1 = \frac{1}{t_M - t_0}\sum_{i=0}^{M-1}\log_2\left(\frac{L_i'}{L_i}\right)$$

where M is the number of times a new neighbour was chosen close to the trajectory.

In practice, where a finite number of points in the time series are considered and the presence of noise is usual, the selection of a neighbour point placed in the direction of the segment L_{i-1}' is not possible. The criterion is the selection of a point inside a cone of height ε with an angle of $\theta = \pi/9$ and the symmetry axes matches the segment L_{i-1}'. If no point is found, the angle is increased. Finally, the closest neighbour is chosen, regardless of θ and ε.

5. *CLOSING COMMENTS*

In this chapter three methods to determine the type of time domain solution were presented.

For the Fourier Spectra of a signal, periodic motion always shows up a discrete frequency spetrum. So does quasi-periodic motion, displaying the two or more incommensurate frequencies involved, and possibly sub-harmonics, higher harmonics, and linear combinations of these. Chaotic motion produces a continuous broadband spectrum with spikes at the dominating frequencies.

Representing motion in a Poincaré map, it is usually easy to distinguish periodic and non-periodic motion. Summing up the possible sets of Poincaré maps, a finite number of points corresponds to a periodic motion, an infinite number of points filling up a closed curve corresponds to quasi-periodic motion, and an infinite number of orderly distributed points (usually) corresponds to chaotic motion.

Finally, Lyapunov exponents essentially measure the average rates of convergence or divergence of nearby orbits in the phase space. A positive Lyapunov exponent is among the strongest indicators of chaotic motion. If $\lambda_i < 0,\ i = 1, n$ then the solution is an equilibrium point; if $\lambda_1 = 0$ and $\lambda_i < 0,\ i = 2, n$, then a periodic solution is obtained; if $\lambda_1 = \lambda_2 = 0$ and $\lambda_i < 0,\ i = 3, n$ then a quasi-periodic solution is obtained.

Chapter 4

FORCED VIBRATION ANALYSIS OF PLATES - TRANSVERSE FORCE

1. *INTRODUCTION*

In Chapter 2, the mathematical model of the p-version of the FEM has been derived including geometrical non-linearity for thick, asymmetric laminated rectangular plates. In this chapter, only symmetrically laminated plates, i.e,$[B]=0$, made of composite materials are studied. Before applying the model to geometrically non-linear analysis, it is worth applying the model to linear free vibration analysis. The excitation used in the forced vibration is a harmonic plane wave. The convergence of the model developed is studied. Results are also presented for non-linear forced vibrations. Fully clamped symmetrically laminated rectangular plates are here analysed. A different number of in-plane and out-of-plane shape functions are considered and the obtained results are compared with numerical results from the literature.

The study of linear dynamic behaviour of plates is not a new topic. Leissa [4.1] gave an extensive study of plate vibration. Lin and Kin [4.2] used classical laminated plate theory to compute the natural frequencies of un-symmetrically laminated, rectangular plates. Reddy [4.3] developed a finite element method based on a typical first order laminated theory and computed the natural frequencies of simply supported, anti-symmetric angle-ply, laminated plates. Bert and Mayberry [4.4] predicted the natural frequencies of un-symmetrically laminated plates with clamped edges using Raleigh-Ritz energy method. Chow, Liew and Lam [4.5] investigated the free vibration of symmetrically laminated plates with the Raleigh-Ritz method using admissible 2-D orthogonal polynomials. Some experimental work on the dynamic response of

laminated plates under acoustic excitation was carried out in the Institute of Sound and Vibration Research at Southampton University [4.14].

One of the main applications of laminated composite plates is that of skin-panels in aircraft. These panels, especially those near the jet engine's exhaust, work under high level acoustic pressure environment combined with pressure due to service loads. In this work, the dynamic response of laminated composite plates excited by harmonic plane waves is investigated. The Newmark method presented in Chapter 2 is applied to solve the equations of motion.

In order to analyse the time domain response of the plate's vibrations, the tools presented in Chapter 3 are used to determine the presence of a periodic, quasi-periodic or chaotic motion.

2. *PLATES ANALYSED*

Three symmetric, rectangular graphite/epoxy composite laminated plates are considered, therefore, there is no bending-twisting stiffness, i.e., $[B]=0$. Their geometrical and material properties are defined in Table 1 and in Table 2. It was assumed that G_{13} and G_{23} are equal to G_{12}.

Table 1- Geometrical properties of the plates

Plate	Number of lamina	Laminae orientation	*a*(m)	*b*(m)	*h*(m)
1	8	$(90,-45,45,0)_{sym.}$	0.48	0.32	0.001
2	5	$(\theta,-\theta,\theta,-\theta,\theta)$	0.3	0.3	0.001
3	3	(45,-45,45)	0.5	0.5	0.005

Table 2 – Material properties of the plates

Plate	E_{11} (N/m^2)	E_{22} (N/m^2)	G_{12} (N/m^2)	ρ (Kgm^{-3})	ν_{12}
1	120.5×10^9	9.63×10^9	3.58×10^9	1540	0.32
2	173.0×10^9	E11/15.4	$0.79\times$ E22	1540	0.3
3	206.84×10^9	5.171×10^9	2.5855×10^9	2564.856	0.25

The mode shapes of laminated composite rectangular plates depend not only upon the aspect ratio of the plates, but also on the elastic properties of the laminae and the orientations. For symmetrically laminated composite rectangular plates, the mode shape patterns are complicated by twisting-bending coupling. This coupling distorts the mode shapes of the plates. It is difficult to find a purely symmetric or antisymmetric mode in symmetrically laminated rectangular plates. Errors are inevitable if only symmetric or antisymmetric displacement functions are used in modelling a certain mode for this kind of plates.

3. *LINEAR VIBRATION ANALYSIS*

3.1 - *Convergence with the number of shape functions*

Consider a fully clamped rectangular carbon fibre reinforced symmetrically laminated plate. The plate displacement shape functions in the *x* and the *y* axes were defined in Chapter 2, as well as the rotations. These functions satisfy the fully clamped theoretical boundary conditions, i.e., zero displacement and zero slopes along the four plate edges; moreover they have been used and shown to be appropriate in previous studies on the vibration of fully clamped rectangular plates [4.8, 4.9, and 4.10]. The analytical expressions of the shape functions of the clamped-clamped plate are given in Chapter 2.

In this convergence study, a different number of in plane and out of plane shape functions are used in the model. In order to analyse the convergence of the linear frequencies, seven rotational shape functions are used in plates 1 and 3, and nine are considered in plate 2. The convergence of the model is assured comparing the values obtained for the natural frequencies, ω, with published results.

The influence of p_θ in the prediction of the linear frequencies is also considered, and the results are discussed for plate 1. In Tables 3 to 7, the convergence of the first four linear frequencies, ω_i, i=1,2,3,4, of the plates is studied:

Table 3- Natural frequencies of plate 1 with $p_i = p_\theta = 7$

p_o	4	5	6	7	8	9	10	11
DOF	114	123	134	147	162	179	198	219
ω_1	511.149	511.112	511.111	511.105	511.104	511.101	511.101	511.100
ω_2	645.189	644.977	644.967	644.959	644.956	644.953	644.951	644.948
ω_3	902.541	886.334	886.328	886.310	886.308	886.300	886.299	886.294
ω_4	1313.790	1307.348	1301.312	1301.272	1301.198	1301.154	1301.140	1301.111

Table 4 - Natural frequencies of plate 2 with $p_i = p_\theta = 7$, $\theta = 45^0$

p_o	4	5	6	7	8	9	10	11
DOF	114	123	134	147	162	179	198	219
ω_1	762.888	762.863	762.838	762.831	762.828	762.825	762.824	762.822
ω_2	1419.717	1419.674	1419.507	1419.505	1419.475	1419.474	1419.464	1419.463
ω_3	1647.676	1647.104	1646.861	1646.838	1646.809	1646.798	1646.789	1646.782
ω_4	2234.666	2219.137	2218.961	2218.928	2218.873	2218.860	2218.843	2218.835

Table 5 – Linear natural frequency parameter λ and linear frequencies of symmetrically five layer angle-ply $\left(\theta = 0^0\right)$, square plate 2 with fully clamped edges, $p_i = p_\theta = 9$, $\left(\lambda = \left(\rho h \omega^2 a^4 / D_0\right)^{1/2}\right.$, $\left. D_0 = \dfrac{E_{11} h^3}{12\left(1 - \upsilon_{12}\upsilon_{21}\right)}\right)$, (Graphite/Epoxy, $E_{11} / E_{22} = 15.4$, $G_{12} / E_{22} = 0.79$, $\upsilon_{12} = 0.30$)

p_o	4		5		6		7	
λ / ω	λ_i	ω_i	λ_i	ω_i	λ_i	ω_i	λ_i	ω_i
	23.840	812.856	23.839	812.819	23.839	812.819	23.839	812.816
	29.705	1012.815	29.704	1012.797	29.701	1012.677	29.700	1012.677
	42.813	1459.733	41.744	1423.701	41.744	1423.301	41.704	1421.928
	62.924	2145.456	62.922	2145.369	60.202	2052.649	60.202	2052.649
	64.563	2201.322	64.562	2201.293	62.900	2144.633	62.900	2144.627
p_o	8		9		10		11	
λ / ω	λ_i	ω_i	λ_i	ω_i	λ_i	ω_i	λ_i	ω_i
	23.839	812.816	23.839	812.811	23.839	812.811	23.839	812.809
	29.700	1012.677	29.700	1012.672	29.700	1012.671	29.700	102.668
	41.704	1421.928	41.703	1421.920	41.703	1421.920	41.703	1421.916
	60.146	2050.720	60.145	2050.711	60.145	2050.711	60.144	2050.674
	62.900	2144.627	62.900	2144.626	62.899	2144.603	62.899	2144.603

Table 6 - Natural frequencies of plate 3 with $p_i = p_\theta = 7$

p_o	4	5	6	7	8	9	10	11
DOF	114	123	134	147	162	179	198	219
ω_1	954.792	952.956	952.610	952.478	952.377	952.321	952.270	952.236
ω_2	1558.468	1557.922	1557.105	1556.940	1556.650	1556.603	1556.429	1556.402
ω_3	2234.674	2203.451	2196.995	2196.100	2195.495	2195.155	2194.925	2194.925
ω_4	2318.568	2273.654	2270.775	2269.591	2269.494	2268.938	2268.906	2268.572

From Tables 3 to 6, the convergence of the first four linear frequencies is assured for all the plates studied. In order to validate the model, in Tables 7, 8 and 9, the results obtained with the first order shear deformation model for thick plates, are compared with results obtained with the HFEM from the thin plate theory.

Table 7- Convergence of the first four linear frequencies (rad/s) of Plate 1, with the number of out of plane shape functions

** - Thin Plate theory* **- *First Order Shear Deformation Theory for thick plates*

Mode	[4.9]*	FSDT**					
	p_o=7, 49 DOF	p_o=5, p_i=7, p_θ=7, n=123	p_o=6, p_i=7, p_θ=7, n=134	p_o=7, p_i=7, p_θ=7, n=147	p_o=7, p_i=8, p_θ=7, n=162	p_o=8, p_i=8, p_θ=8, n=192	p_o=8, p_i=9, p_θ=9, n=226
1	511.390	511.112	511.111	511.105	511.104	511.091	511.087
2	645.281	644.977	644.967	644.959	644.956	644.895	644.881
3	886.217	886.334	886.328	886.310	886.308	886.167	885.628
4	-	1307.348	1301.312	1301.272	1301.198	1236.386	1235.338

Table 8 - Convergence of the first four linear frequencies (*rad/s*) of Plate 2, $\theta = 45^o$, with $p_i = p_\theta = 7$ and the number of out of plane shape functions

Mode	[4.10]	FSDT		
	p_o=7, 64 DOF	p_o=4, p_i=7, p_θ=7, n=114	p_o=5, p_i=7, p_θ=7, n=123	p_o=6, p_i=7, p_θ=7, n=134
1	763.0961	762.888	762.863	762.838
2	1419.927	1419.717	1419.674	1419.507
3	1647.361	1647.676	1647.104	1646.861
4	2219.133	2234.666	2219.137	2218.961

It can be seen from the two Tables that the linear frequencies for p_o differ very slightly. Increasing p_o, the linear frequency, decreases monotonically towards a certain value, i.e., the errors between them decrease with the increase of p_o. Excellent convergence properties of the HFEM in the linear frequency analysis of symmetrically laminated plates are observed.

Table 7 and 8, the linear frequencies are lower than those obtained in [4.9, 4.10]. Although more shape functions are used, with 192 DOF for plate 1, and 134 DOF for plate 2, the thick plate theory gives better approximations than the thin plate theory where the rotatory inertia and shear deformation are neglected.

Table 9 - Convergence of the first four linear frequencies (rad/s) of Plate 3, with $p_i = p_\theta = 7$ and the number of out of plane shape functions

Mode	[4.11]	FSDT		
	po=6, 36 DOF	*po =4, pi =7, p_θ=7, n=114*	*po =5, pi =7, p_θ=7, n=123*	*po =6, pi =7, p_θ=7, n=134*
1	1574.96	954.792	952.956	952.610
2	2577.55	1558.468	1557.922	1557.105
3	3671.02	2234.674	2203.451	2196.995
4	-	2318.568	2273.654	2270.775

Possible reasons for the large differences encountered in

Table 9 are not only the different theories employed, but also the material properties assumed here for G_{13} and G_{23}, shear moduli which are not necessary in [4.11].

In Tables 7, 8 and 9, the element defined can determine correctly the first four linear frequencies of thin plates.

3.2 - *The effect of b/h in the linear frequencies*

In Tables 10, 11 and 12 the thickness of plate 1, 2 and 3 is changed and the convergence of the first four linear frequencies, ω_i , i=1,2,3,4, of the plates is studied.

Table 10- Variation of the linear frequencies of vibration /different thickness of plate 1 with 134 DOF

ω_i Model	ω_1	ω_2	ω_3	ω_4
b/*h*= 10000	7.816	14.249	16.954	23.060
b/*h*= 1000	163.640	206.504	283.790	418.477
b/*h* = 100	1626.940	2052.411	2819.598	4045.113
b/*h* = 10	11205.824	14284.606	19578.063	23055.506

Table 11- Variation of the linear frequencies of vibration /different thickness of plate 2, $\theta = 45^o$ **, with 134 DOF**

ω_i Model	ω_1	ω_2	ω_3	ω_4
b/*h*= 1000	228.939	426.110	494.431	666.204
b/*h* = 100	2281.255	4238.556	4912.275	6614.088
b/*h* = 10	18111.411	31179.616	34244.400	44915.726

Table 12- Variation of the linear frequencies of vibration /different thickness of plate 3 with 134 DOF

w_i Model	ω_1	ω_2	ω_3	ω_4
b/*h*= 1000	96.557	158.203	225.939	231.694
b/*h* = 100	952.610	1557.105	2196.995	2270.775
b/*h* = 10	5557.992	8642.435	10187.659	12030.861

From the three tables above, for thin (b/h=1000) and moderately thick (b/h=100) plates, the linear frequencies obtained are smaller than those of thick (b/h=10) plates, as expected.

3.3 - *Influence of the fibre orientation in the prediction of the linear frequencies*

In this section, a fibre orientation study is carried out for plate 2. In Table 13, the results for 7 out-of-plane and 9 rotational shape functions are presented and compared with published results.

Table 13 – Linear natural frequency parameter λ of symmetrically five layer angle-ply, square plate 2 with fully clamped edges and different angle orientation

θ	Mode / Method	*1*	*2*	*3*	*4*
0º	FSDT	23.839	29.700	41.704	60.202
0º	CPT [4.14] [4.15]	23.852	29.715	41.721	60.229
30º	FSDT	22.704	36.526	53.967	57.118
30º	CPT [4.14]	22.713	36.546	54.012	57.156
45º	FSDT	22.372	41.621	48.282	65.032
45º	CPT [4.14]	22.381	41.645	48.316	65.086

Outstanding agreement for all the three groups of results with three different angles θ, can be clearly seen in this table. In all the cases, the frequency parameters given by the first order shear deformation model are smaller than those given in [4.14] and [4.15]. It may be due to the inclusion of in-plane displacements and transverse shear deformation in the model developed in this thesis, which could slightly reduce the stiffening effects caused by neglecting these factors.

4. *NON-LINEAR FORCED VIBRATION ANALYSIS*

4.1 - *Introduction*

In this section, the discussion of forced vibration of a rectangular plate is studied using the HFEM, and equation (2.71) is solved by the Newmark method. If a distributed force that impinges on the plate's surface only in the *z* direction is

considered, then $\{P_u\} = \{P_v\} = 0$ and the new force vector is given by equation (2.78).

In non-linear vibrations, there are several parameters that influence the time dependence of the response: time variation, space dependence and amplitude of the external excitation, properties of the structure, initial and boundary conditions, etc. Depending on these parameters, the oscillations may be periodic – including harmonic, sub-harmonic and super-harmonic – quasi-periodic or even chaotic [4.12].

Quasi-periodic motion has a finite number of frequency components where some of them are not related by a rational number; therefore, its time signal is non-repetitive. A chaotic signal is as well non-repetitive in the time domain and has a very wide frequency spectrum.

For various amplitudes and frequencies of excitation, time domain simulations of the response of the plates were carried out. A *FORTRAN* [4.13] Newmark integration routine was used.

Applying the principle of the virtual work, the generalised external forces in the transverse direction were obtained in Chapter 2. It is recalled that for a distributed transverse force in the z direction one has the following expression:

$$\{P\} = \int_{\Omega} \{N^w\} P_d(x, y, t) d\Omega \tag{4.1}$$

where $\{N^w\}$ is the out of plane shape function vector. If a harmonic plane wave impinges on the plate's surface in the normal direction then

$$P_d(x, y, t) = F \cos(\omega t - k), k \in \mathbb{R} \tag{4.2}$$

where F is the magnitude of the applied force, ω is the frequency of the harmonic wave and k is the phase. Substituting (4.2) in (4.1), we have

$$\begin{aligned} \{P\} &= F \int_{\Omega} \{N^w\} d\Omega \cos(\omega t - k) \\ &= \{\overline{f}\} \cos(\omega t - k) \end{aligned} \tag{4.3}$$

The generalised external force vector $\{\overline{f}\}$ has only a real part in the above equation. It is interesting to note that most of the components in $\{\overline{f}\}$ are zero. For a plate with fully clamped edges in which only the shape functions generated by equation (2.96) are used, only $\overline{f}(1)$ is different from zero. In this situation

$$\overline{f}(1) = F\frac{ab}{4}\int_{-1}^{1} f_4(\xi)\,d\xi\int_{-1}^{1} f_4(\eta)\,d\eta \tag{4.4}$$

in which, *a* and *b* are the in-plane dimensions of the plate, $f_4(\xi)$ and $f_4(\eta)$ are the first shape functions generated using equation (2.96).

4.2 - *Numerical results*

Plate 2 is excited by a harmonic wave of 4 *N*/m^2 and 123 DOF (pi=7, p_o=5, p_θ=7) are considered in the model. The fibres orientation varies from $\theta = 0^o$ to $\theta = 45^o$. The force applied to the plate is increased to 3000 *N/m^2* for $\theta = 30^o$ and $\theta = 45^o$; for $\theta = 0^o$ it is increased to 3300 *N/m^2*, and the results are discussed. For amplitudes of vibration of the order of the thickness of the plate, the solution was always periodic and highly dominated by the harmonic with frequency equal to the excitation frequency (principal harmonic).

Plate 1 is excited by a harmonic wave of 5 *N/m^2*, and 123 DOF are considered. The force applied to the plate is increased to 3000 *N/m^2*, at 511.112 *rad/s*. The results obtained are also discussed.

In Figure 1, the time domain response of the plate 2, $\theta = 45^o$ is presented for different values of α. Figure 2, shows that a closed path is obtained in the phase plane, therefore, the motion is periodic.

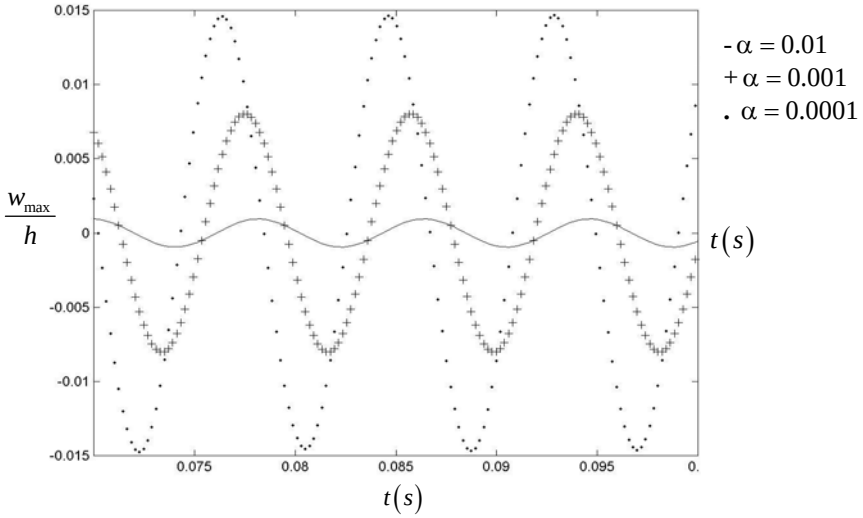

Figure 1 – Time domain response of Plate 2, $(45,-45,45,-45,45)$ due to harmonic excitation by a plane wave of 4 N/m^2

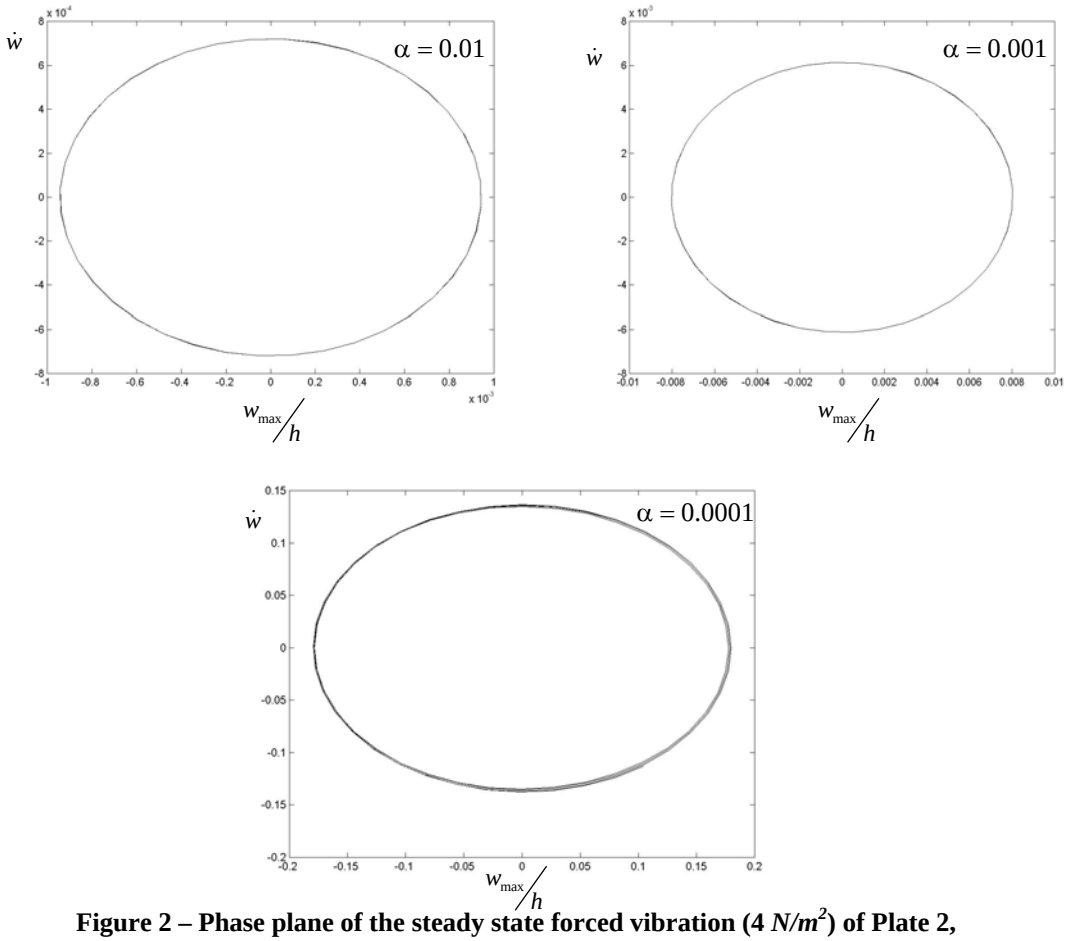

Figure 2 – Phase plane of the steady state forced vibration (4 N/m^2) of Plate 2, $(45,-45,45,-45,45)$ with different values of α

Considering these responses, the influence of the loss parameter in the vibration of plate 2 is investigated. In Figure 1, with $\alpha = 0.01$, the amplitude calculated at or near a point where it attains its maximum, $w_{\max}/h$, is given by 0.000941; with $\alpha = 0.001$, the value of $w_{\max}/h$ is 0.00801, and when $\alpha = 0.0001$, $w_{\max}/h$ is 0.01466. Therefore, diminishing the value of α implies an increase in the amplitude of vibration, as expected. In the following, α is 0.0001.

For plate 2, $\theta = 45^{o}$, and for plate 1, the Fourier spectra of the periodic responses due to a harmonic wave of 4 and 5 N/m^2 are defined. In Figures 3 and 4, the spectrum of the Fourier series of the plates excited at the first mode of vibration is presented. Once the spectrum consists of a single basic frequency, a periodic motion is achieved. The near absence of harmonics indicates that the plate is practically in the linear regime, which is a result of the small amplitudes of oscillation.

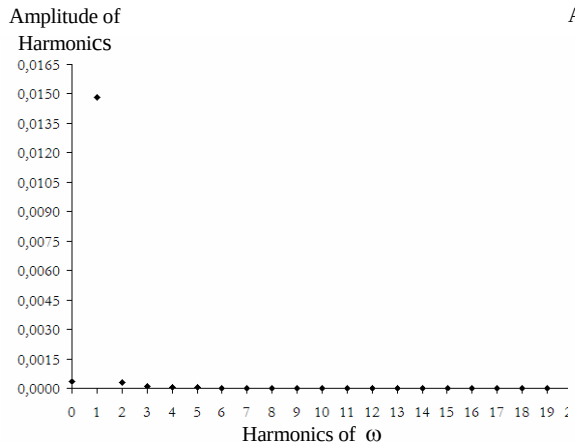

Figure 3 – Fourier spectrum of forced vibration of plate 2, (45,-45, 45,-45, 45) due to and harmonic excitation by a plane wave of 4 N/m^2

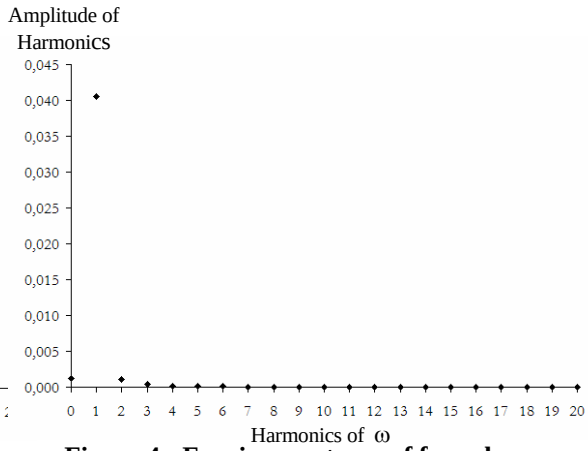

Figure 4 - Fourier spectrum of forced vibration of plate1, due to and harmonic excitation by a plane wave of 5 N/m^2

In Figures 5-16 the distributed force applied to plate 2 is increased; the response and the phase planes are presented.

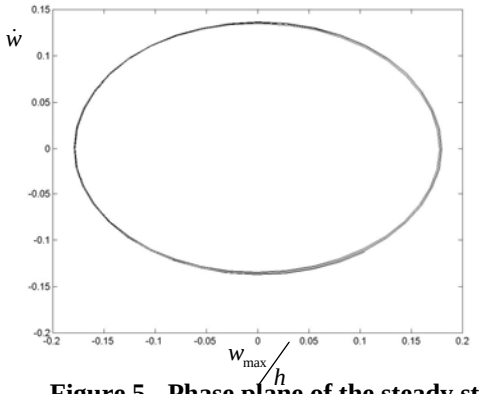

Figure 5 - Phase plane of the steady state forced vibration (50 *N/m*^{2}) of plate 2, (45,-45,45,-45,45) due to harmonic excitation by a plane wave

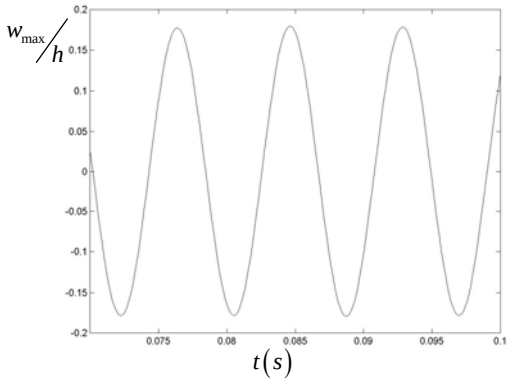

Figure 6 - Time domain response of Plate 2, (45,-45,45,-45,45) due to harmonic excitation by a plane wave of 50 *N/m*^{2}

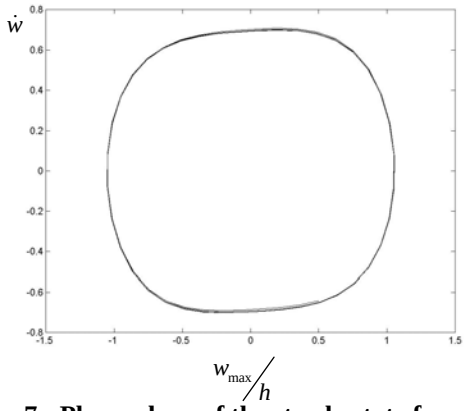

Figure 7 - Phase plane of the steady state forced vibration (500 N/m^2) of plate 2, (45,-45,45,-45,45) due to harmonic excitation by a plane wave

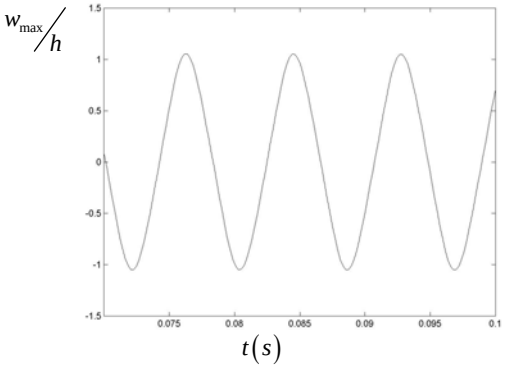

Figure 8 - Time domain response of Plate 2, (45,-45,45,-45,45) due to harmonic excitation by a plane wave of 500 N/m^2

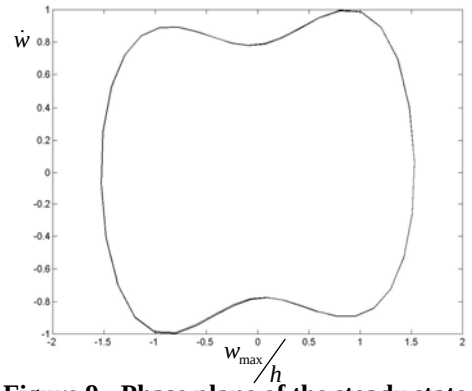

Figure 9 - Phase plane of the steady state forced vibration (1000 *N/m*^{2}) of plate 2, (45,-45,45,-45,45) due to harmonic excitation by a plane wave

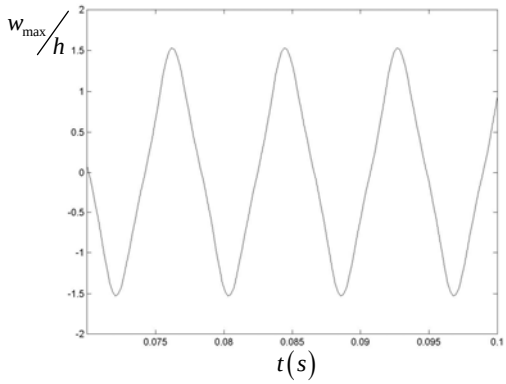

Figure 10 - Time domain response of Plate 2, (45,-45,45,-45,45) due to harmonic excitation by a plane wave of 1000 *N/m*^{2}

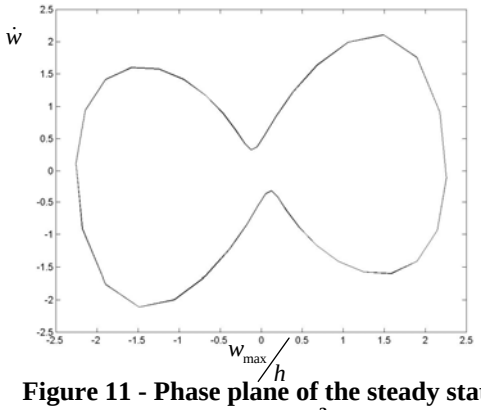

Figure 11 - Phase plane of the steady state forced vibration (2000 *N/m²*) of plate 2, (45,-45,45,-45,45) due to harmonic excitation by a plane wave

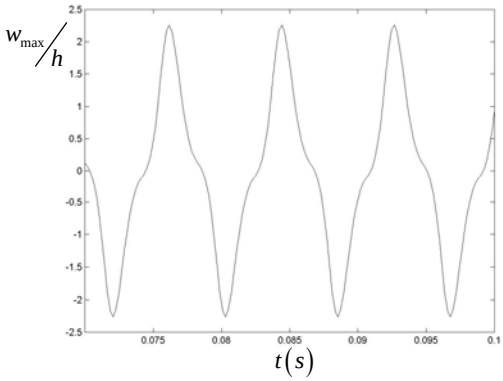

Figure 12 - Time domain response of Plate 2, (45,-45,45,-45,45) due to harmonic excitation by a plane wave of 2000 *N/m²*

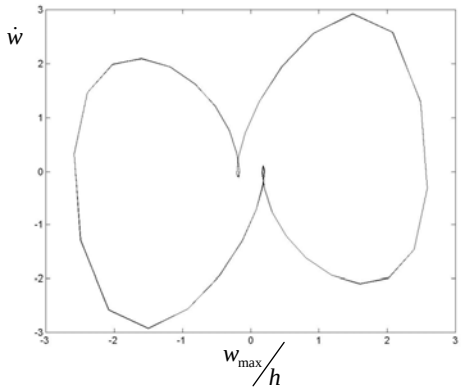

Figure 13 - Phase plane of the steady state forced vibration (2500 *N/m²*) of plate 2, (45,-45,45,-45,45) due to harmonic excitation by a plane wave

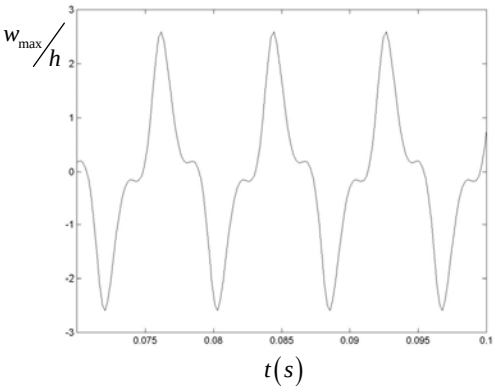

Figure 14 - Time domain response of Plate 2, (45,-45,45,-45,45) due to harmonic excitation by a plane wave of 2500 *N/m²*

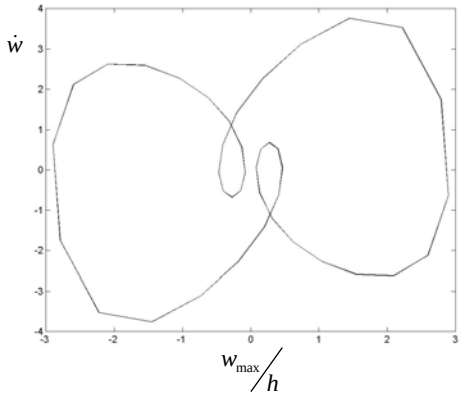

Figure 15 - Phase plane of the steady state forced vibration (3000 *N/m²*) of plate 2, (45,-45,45,-45,45) due to harmonic excitation by a plane wave

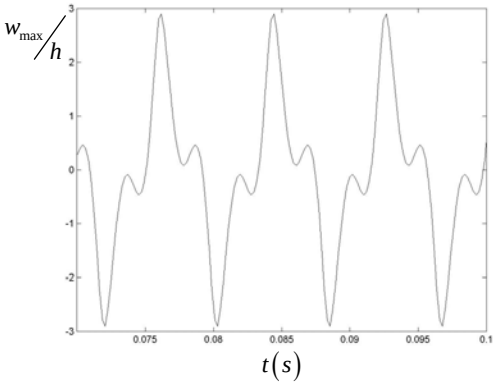

Figure 16 - Time domain response of Plate 2, (45,-45,45,-45,45) due to harmonic excitation by a plane wave of 3000 *N/m²*

Closed paths are obtained in the phase planes for all the forces applied, therefore periodic motions are achieved. The values of $w_{\max}/h$ are presented in Table 14, where P_d represents the distributed applied force.

Table 14 – Forced Vibration, Plate 2, $\theta = 45^{o}$, p_o=5

P_d $\left(N/m^2\right)$	$P_d = 4$	$P_d = 50$	$P_d = 500$	$P_d = 1000$	$P_d = 2000$	$P_d = 2500$	$P_d = 3000$
ω/ω_{l1}	$w_{\max}/h$						
1.0005	0.0147	0.1797	1.0536	1.5300	2.2628	2.5889	2.8998

The amplitude of vibration, $w_{\max}/h$, increases as the force applied to the plate increases, but the relation between them is not linear. Considering plate 2 with $\theta = 30^{o}$, the phase planes and the time domain responses for a force varying from 4 N/m^2 to 3000 N/m^2 are given by

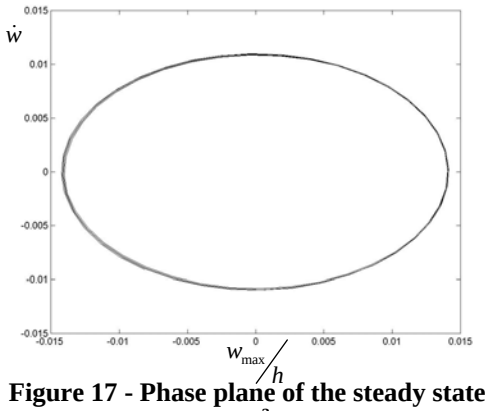

Figure 17 - Phase plane of the steady state forced vibration (4*N/m*^{2}) of plate 2, (30,- 30, 30,- 30, 30) due to harmonic excitation by a plane wave

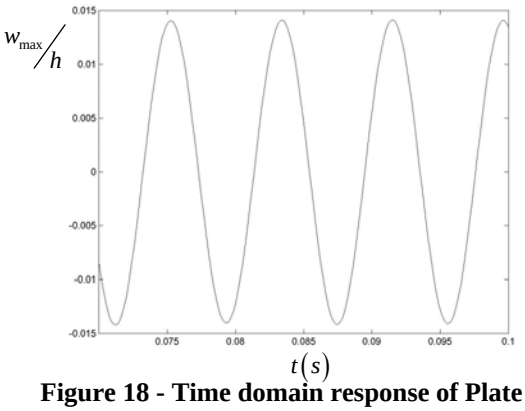

Figure 18 - Time domain response of Plate 2, (30,- 30, 30,- 30, 30) due to harmonic excitation by a plane wave of 4 *N/m*^{2}

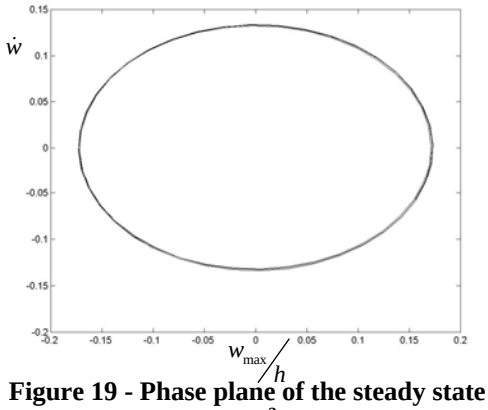

Figure 19 - Phase plane of the steady state forced vibration ($50N/m^2$) of plate 2, (30,- 30, 30,- 30, 30) due to harmonic excitation by a plane wave

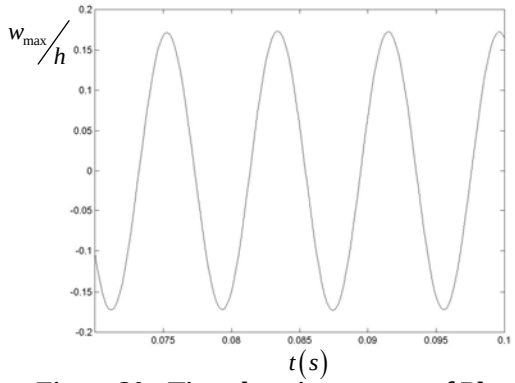

Figure 20 - Time domain response of Plate 2, (30,- 30, 30,- 30, 30) due to harmonic excitation by a plane wave of 50 N/m^2

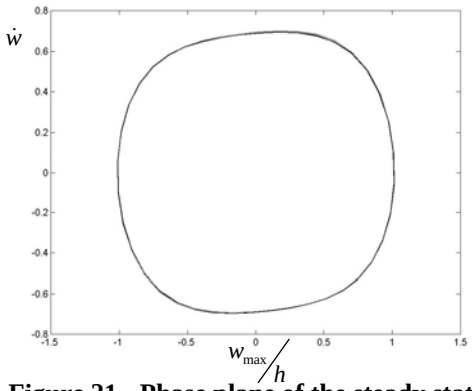

Figure 21 - Phase plane of the steady state forced vibration ($500N/m^2$) of plate 2, (30,- 30, 30,- 30, 30) due to harmonic excitation by a plane wave

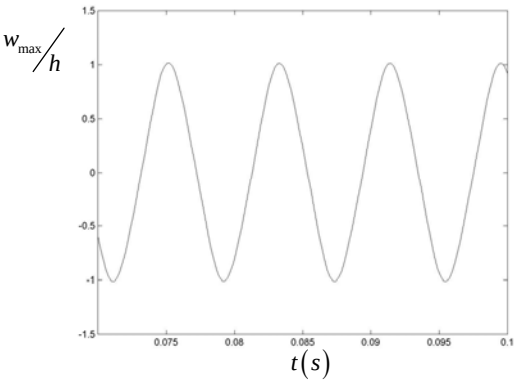

Figure 22 - Time domain response of Plate 2, (30,- 30, 30,- 30, 30) due to harmonic excitation by a plane wave of 500 N/m^2

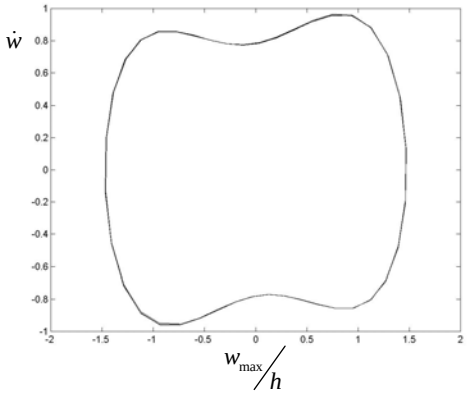

Figure 23 - Phase plane of the steady state forced vibration ($1000N/m^2$) of plate 2, (30,- 30, 30,- 30, 30) due to harmonic excitation by a plane wave

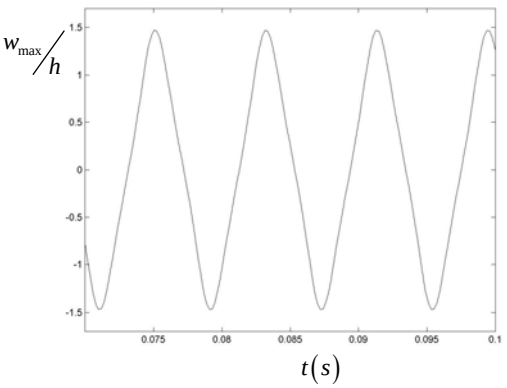

Figure 24 - Time domain response of Plate 2, (30,- 30, 30,- 30, 30) due to harmonic excitation by a plane wave of 1000 N/m^2

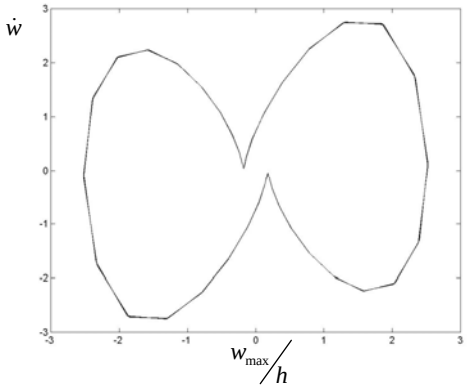

Figure 25 - Phase plane of the steady state forced vibration (2500*N/m*^{2}) of plate 2, (30,- 30, 30,- 30, 30) due to harmonic excitation by a plane wave

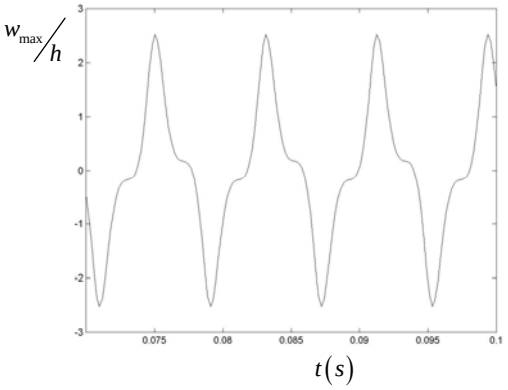

Figure 26 - Time domain response of Plate 2, (30,- 30, 30,- 30, 30) due to harmonic excitation by a plane wave of 2500 *N/m*^{2}

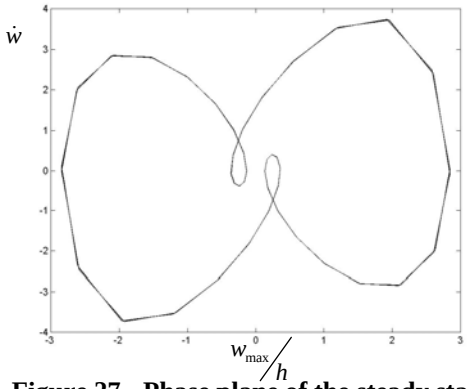

Figure 27 - Phase plane of the steady state forced vibration (3000*N/m*^{2}) of plate 2, (30,- 30, 30,- 30, 30) due to harmonic excitation by a plane wave

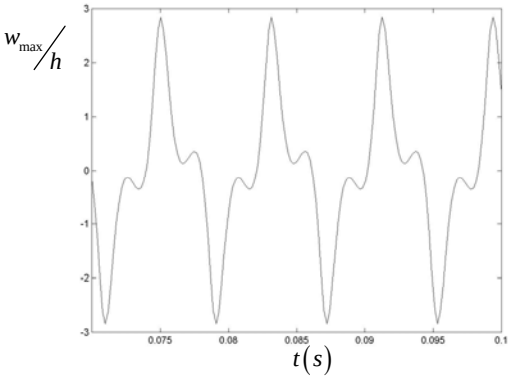

Figure 28 - Time domain response of Plate 2, (30,- 30, 30,- 30, 30) due to harmonic excitation by a plane wave of 3000 *N/m*^{2}

The amplitudes of vibration of plate 2, with $\theta = 30^o$ and for different distributed forces considered are presented in Table 15 and it can be seen that the amplitude of vibration increases as the force increases.

Table 15 - Forced Vibration, Plate 2, $\theta = 30^o$, p_o=5

P_d $\left(N/m^2\right)$	$P_d = 4$	$P_d = 50$	$P_d = 500$	$P_d = 1000$	$P_d = 2500$	$P_d = 3000$
ω/ω_{l1}	w_{max}/h					
1.0004	0.0141	0.1732	1.0147	1.4739	2.5232	2.8444

Comparing with the results obtained in Table 14, for $\theta = 30^o$ the amplitudes of vibration are lower than those obtained for $\theta = 45^o$.

Finally, the results obtained for plate 2 with $\theta = 0^o$ are given by:

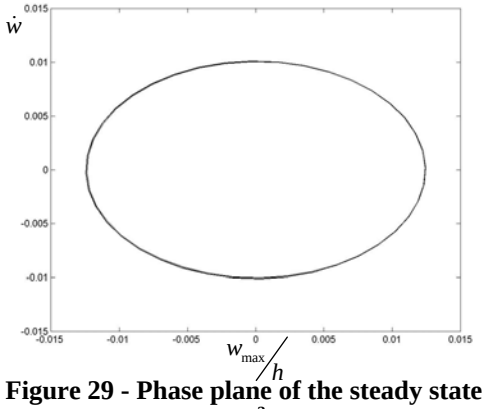

Figure 29 - Phase plane of the steady state forced vibration (4 N/m^2) of plate 2, (0,-0, 0, -0,0), due to harmonic excitation by a plane wave

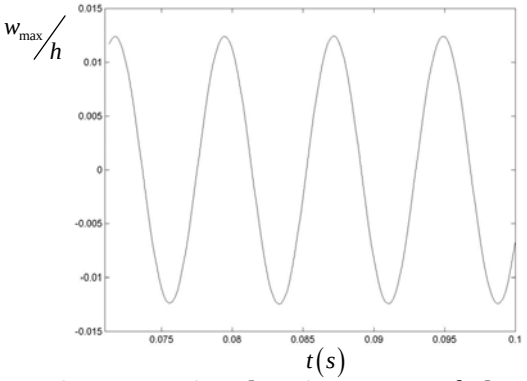

Figure 30 - Time domain response of Plate 2, (0,-0, 0, -0,0), due to harmonic excitation by a plane wave of 4 N/m^2

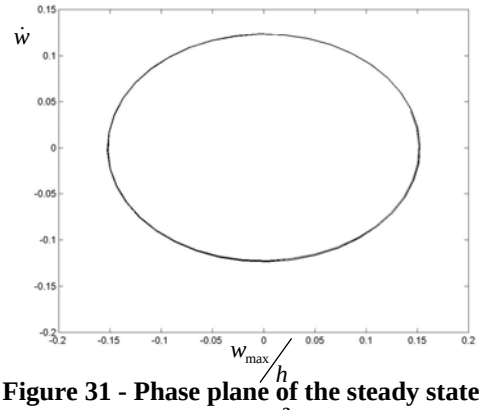

Figure 31 - Phase plane of the steady state forced vibration (50 N/m^2) of plate 2, (0,-0, 0, -0,0), due to harmonic excitation by a plane wave

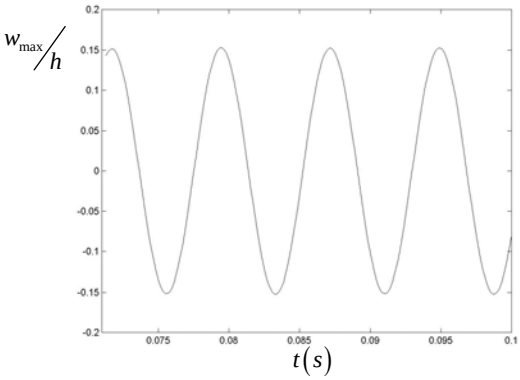

Figure 32 - Time domain response of Plate 2, (0,-0, 0, -0,0), due to harmonic excitation by a plane wave of 50 N/m^2

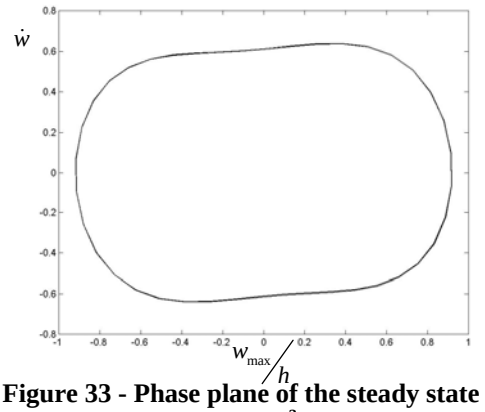

Figure 33 - Phase plane of the steady state forced vibration (500 N/m^2) of plate 2, (0,-0, 0, -0,0), due to harmonic excitation by a plane wave

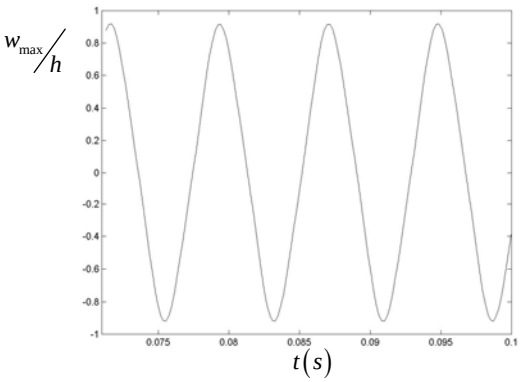

Figure 34 - Time domain response of Plate 2, (0,-0, 0, -0,0), due to harmonic excitation by a plane wave of 500 N/m^2

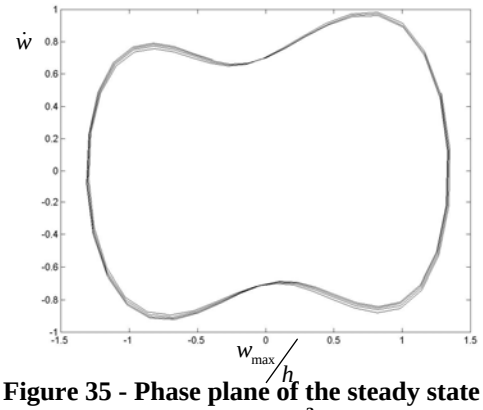

Figure 35 - Phase plane of the steady state forced vibration (1000 *N/m²*) of plate 2, (0,-0, 0, -0,0), due to harmonic excitation by a plane wave

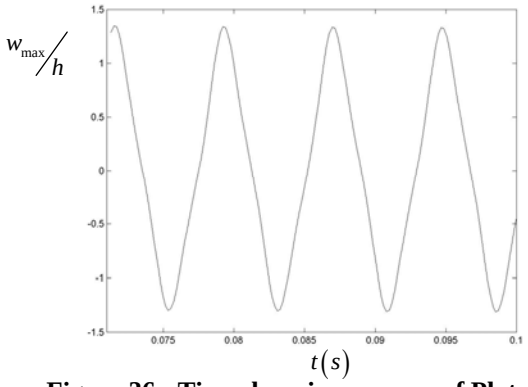

Figure 36 - Time domain response of Plate 2, (0,-0, 0, -0,0)., due to harmonic excitation by a plane wave of 1000 *N/m²*

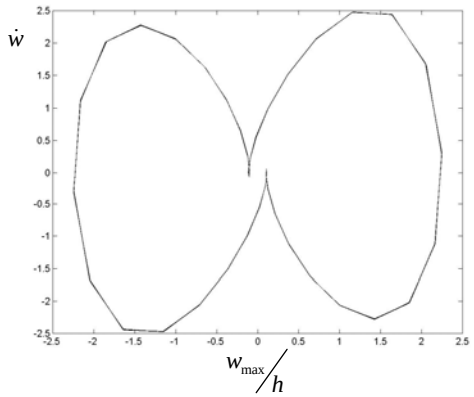

Figure 37 - Phase plane of the steady state forced vibration (2500 *N/m²*) of plate 2, (0,-0, 0, -0,0), due to harmonic excitation by a plane wave

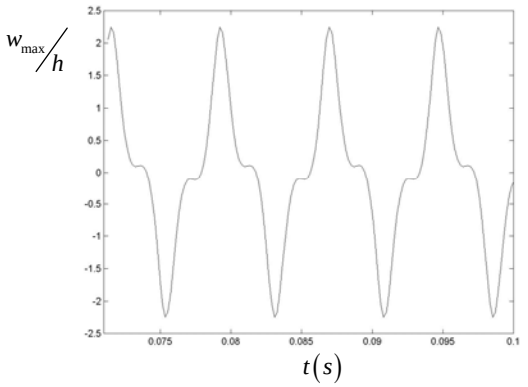

Figure 38 - Time domain response of Plate 2, (0,-0, 0, -0,0)., due to harmonic excitation by a plane wave of 2500 *N/m²*

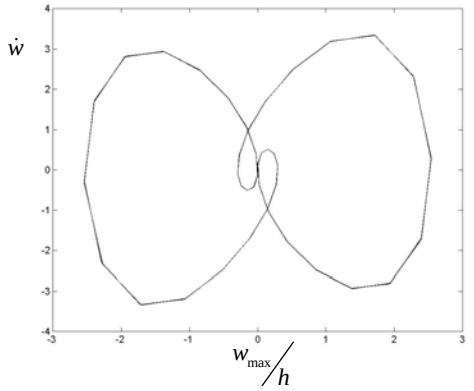

Figure 39 - Phase plane of the steady state forced vibration (3000 *N/m²*) of plate 2, (0,-0, 0, -0,0), due to harmonic excitation by a plane wave

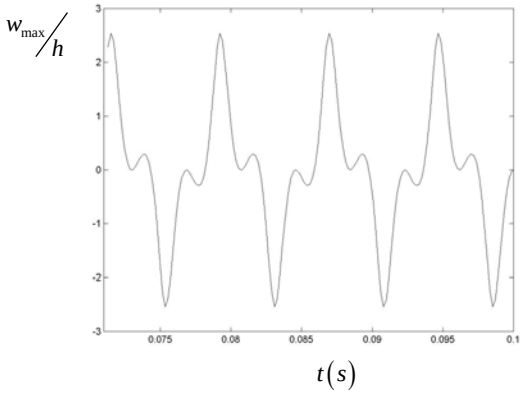

Figure 40 - Time domain response of Plate 2, (0,-0, 0, -0,0)., due to harmonic excitation by a plane wave of 3000 *N/m²*

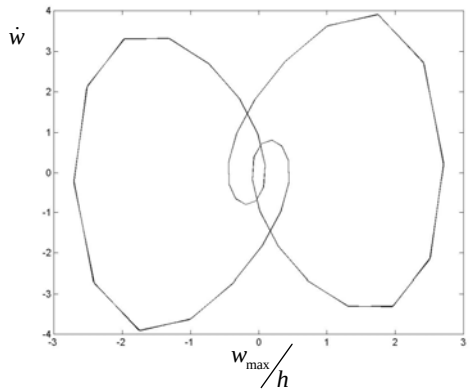

Figure 41 - Phase plane of the steady state forced vibration (3300 *N/m²*) of plate 2, (0,-0, 0, -0,0), due to harmonic excitation by a plane wave

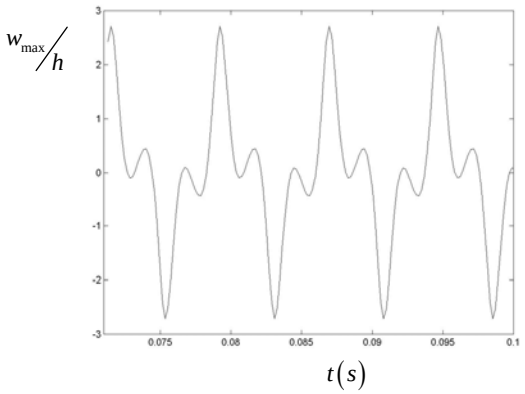

Figure 42 - Time domain response of Plate 2, (0,-0, 0, -0,0), due to harmonic excitation by a plane wave of 3300 *N/m²*

Table 16 - Forced Vibration, Plate 2,p_o=5

P_d (N/m^2)	$P_d = 4$	$P_d = 50$	$P_d = 500$	$P_d = 1000$	$P_d = 2500$	$P_d = 3000$	$P_d = 3300$
ω/ω_{l1}	w_{max}/h						
1.0002	0.0124	0.1524	0.9172	1.3322	2.2490	2.5414	2.7125

In

Table **16**, for plate 2 and for $\theta = 0^o$, the value of w_{max}/h increases as the force increases. Comparing with θ=30º and θ=45º, one sees that the lower vibration amplitudes occur for this orthotropic plate.

In figures 43-48, a periodic motion is achieved for Plate 1, $(90,-45, 45, 0)_{sym.}$, increasing the force applied from 5 *N/m²* to 1250 *N/m²*, and the results are given by:

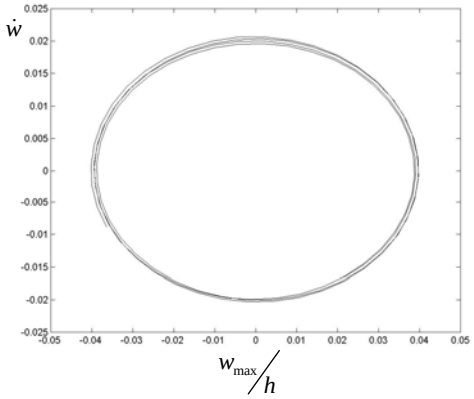

Figure 43 - Phase plane of the steady state forced vibration (5 N/m^2) of plate 1, (90,-45, 45, 0)$_{sym.}$, due to harmonic excitation by a plane wave.

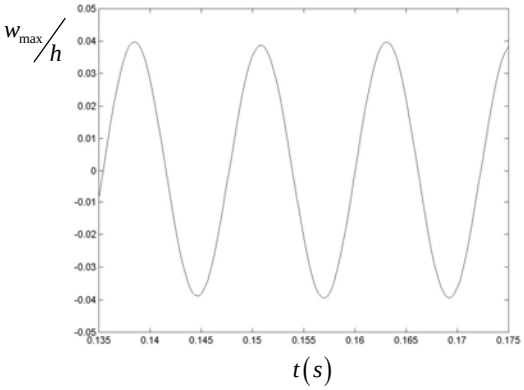

Figure 44 - Time domain response of Plate 1, (90,-45, 45, 0)$_{sym.}$, due to harmonic excitation by a plane wave of 5 N/m^2

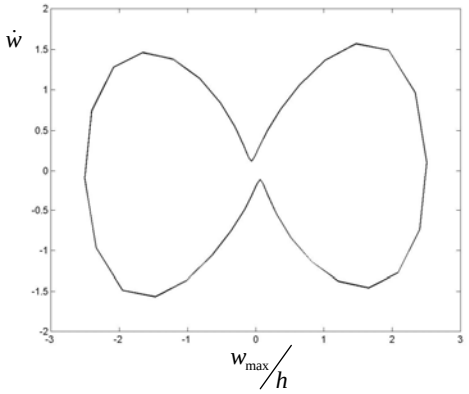

Figure 45 - Phase plane of the steady state forced vibration (1000 N/m^2) of plate 1, (90,-45, 45, 0)$_{sym.}$, due to harmonic excitation by a plane wave.

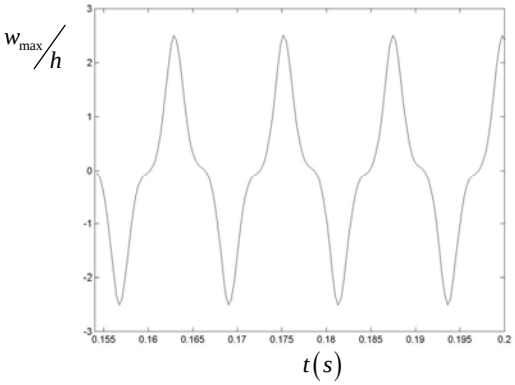

Figure 46 - Time domain response of Plate 1, (90,-45, 45, 0)$_{sym.}$, due to harmonic excitation by a plane wave of 1000 N/m^2

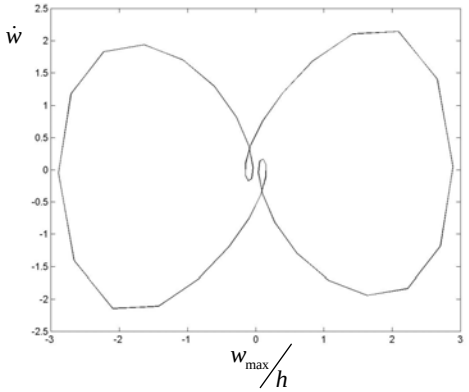

Figure 47 - Phase plane of the steady state forced vibration (1250 N/m^2) of plate 1, (90,-45, 45, 0)$_{sym.}$, due to harmonic excitation by a plane wave

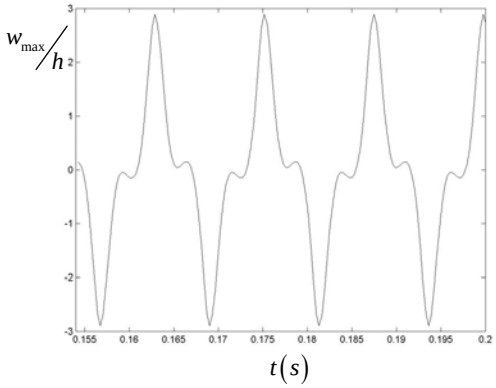

Figure 48 - Time domain response of Plate 1, (90,-45, 45, 0)$_{sym.}$, due to harmonic excitation by a plane wave of 1250 N/m^2

Table 17 shows that as the force increases, the amplitude of vibration also increases, as expected.

Table 17 - Forced Vibration, Plate 1,p_o=5

P_d $\left(N/m^2\right)$	$P_d = 5$	$P_d = 1000$	$P_d = 1250$
w/w_{l1}		$w_{\max}/h$	
1.0001	0.0397	2.5077	2.8924

Considering plate 2, with $\theta = 45^o$ excited by a plane wave of 4 *N/m²*, the Poincaré map is given by

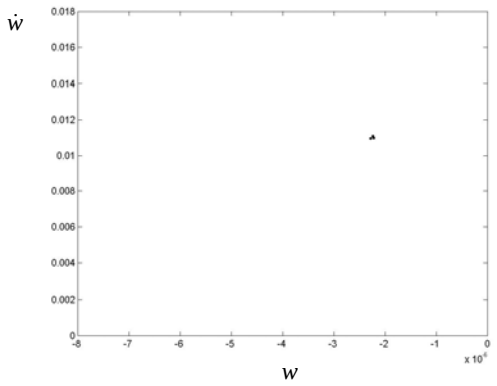

Figure 49 – Poincaré map of plate 2, $\theta = 45^\circ$ excited by a plane wave of 4 *N/m²*

The attractor is given by $(w, \dot{w}) = (\text{-2,22E-6;1,10E-2})$. Increasing the force applied to the plate, the Poincaré maps obtained are given by

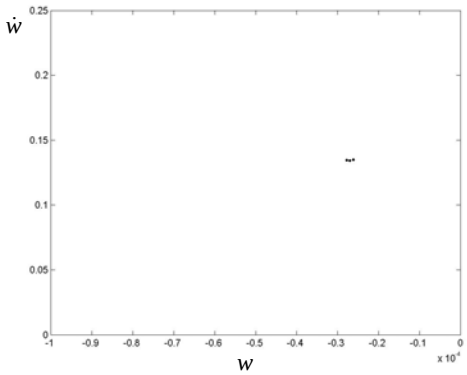

Figure 50 - Poincaré map of plate 2 $\theta = 45^\circ$ excited by a plane wave of 50 *N/m²*

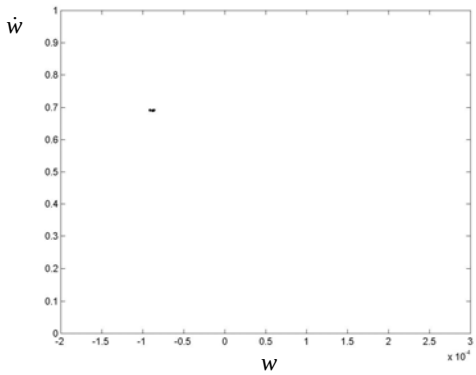

Figure 51 - Poincaré map of plate 2 $\theta = 45^\circ$ excited by a plane wave of 500 *N/m²*

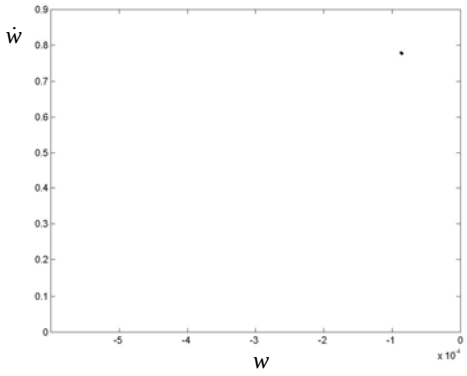

Figure 52 - Poincaré map of plate 2 $\theta = 45^{\circ}$ excited by a plane wave of 1000 N/m^2

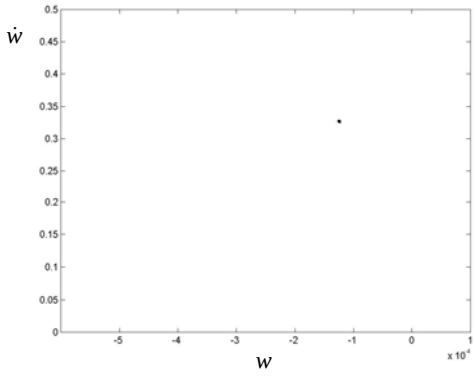

Figure 53 - Poincaré map of plate 2 $\theta = 45^{\circ}$ excited by a plane wave of 2000 N/m^2

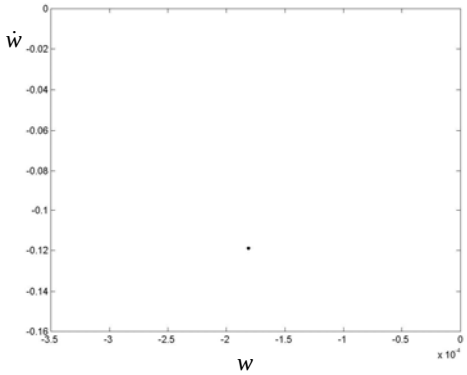

Figure 54 - Poincaré map of plate 2 $\theta = 45^{\circ}$ excited by a plane wave of 2500 N/m^2

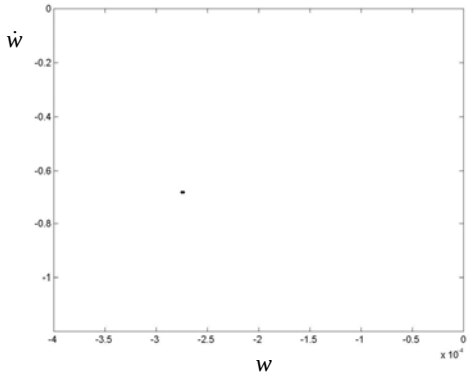

Figure 55 - Poincaré map of plate 2 $\theta = 45^{\circ}$ excited by a plane wave of 3000 N/m^2

From the Poincaré maps in Figures 50 – 55, a stable solution is found. The attractors obtained for a distributed force are presented in Table 18.

Table 18 – Attractor points for vibration of plate 2, (45,-45,45,-45,45) with different forces applied to the plate, $\alpha = 0.0001$

Force $\left(N/m^2\right)$	$\left(w, \dot{w}\right)$	
4	-0.000002221029	0.011001843
50	-0.000026992038	0.13423767
500	-0.000086438719	0.69142843
1000	-0.000086060785	0.77764522
2000	-0.00012402394	0.32740296
2500	-0.00018110176	-0.11912573
3000	-0.00027464819	-0.68290308

Considering plate 2, with $\theta = 30^{o}$ excited by a plane wave increased from 4 N/m^2 to 3000 N/m^2 the Poincaré maps are given by

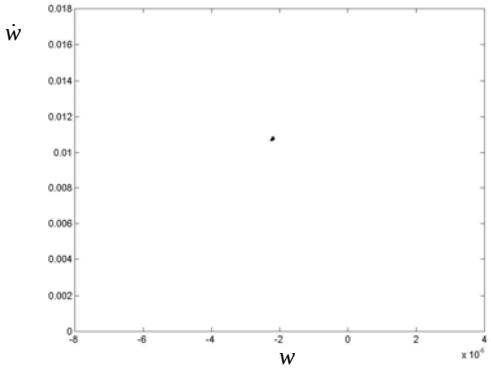

Figure 56 - Poincaré map of plate 2 $\theta = 30^{\circ}$ excited by a plane wave of 4 N/m^2

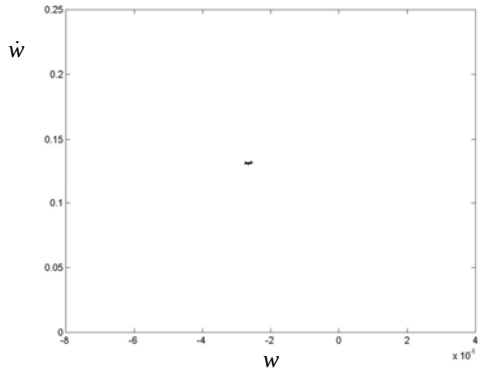

Figure 57 - Poincaré map of plate 2 $\theta = 30^{\circ}$ excited by a plane wave of 50 N/m^2

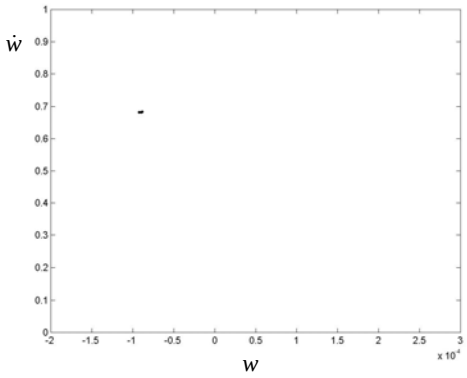

Figure 58 - Poincaré map of plate 2 $\theta = 30^{\circ}$ excited by a plane wave of 500 N/m^2

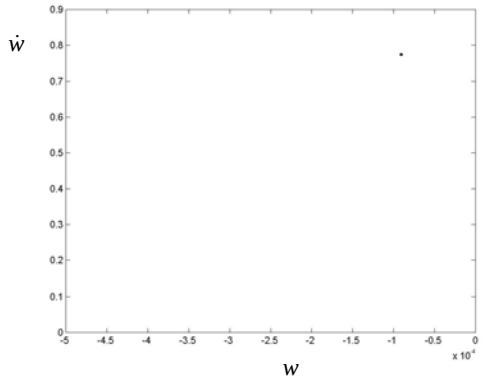

Figure 59 - Poincaré map of plate 2 $\theta = 30^{\circ}$ excited by a plane wave of 1000 N/m^2

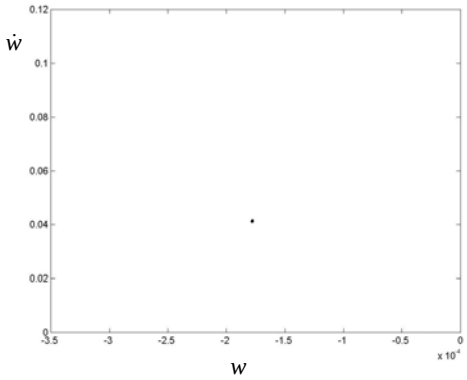

Figure 60 - Poincaré map of plate 2 $\theta = 30^{\circ}$ excited by a plane wave of 2500 N/m^2

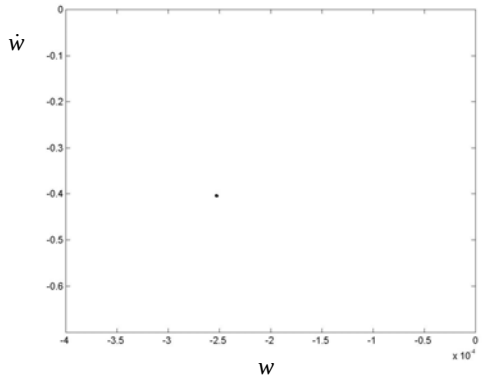

Figure 61 - Poincaré map of plate 2 $\theta = 30^{\circ}$ excited by a plane wave of 3000 N/m^2

From Figures 56 – 61, a stable fixed point is obtained, and the attractors are given in Table 19:

Table 19 - Attractor points for vibration of plate 2, (30,-30,30,-30,30) with different forces applied to the plate, α = 0.0001

Force $\left(N/m^2\right)$	$\left(w, \dot{w}\right)$	
4	-0,000002181	0,010768813
50	-0,000026514	0,131442280
500	-0,000088687	0,682919900
1000	-0,000090239	0,774106780
2500	-0,000177679	0,041165870
3000	-0,000253100	-0,404419910

For $\theta = 0^o$, a stable fixed point is also obtained for each force applied to the plate, and the attractors are given by

Table 20 - Attractor points for vibration of plate 2, (0,0,0,0,0) with different forces applied to the plate, α = 0.0001

Force $\left(N/m^2\right)$	$\left(w, \dot{w}\right)$	
4	-0,000002044	0,009946810
50	-0,000024766	0,121444390
500	-0,000085226	0,605365370
1000	-0,000118215	0,669787950
2500	-0,000105753	-0,061999104
3000	-0,000162891	-0,511205420
3300	-0,000210974	-0,800784570

For plate 1, the attractors are given in Table 21:

Table 21 - Attractor points for vibration of plate 1, with different forces applied to the plate, α = 0.0001

Force $\left(N/m^2\right)$	$\left(w, \dot{w}\right)$	
5	-0,000003785	0,019950001
1000	-0,000059534	0,121326650
1250	-0,000112039	-0,167648940

5. *CONCLUSIONS*

In this chapter, forced vibrations of composite laminated plates modelled by the HFEM are analysed. Linear and non-linear analyses are carried out. The linear frequencies were determined for plate 1, 2 and 3, and by comparison with numerical results, the model is validated and it is demonstrated that the linear natural frequencies of the first order shear deformation model for thick plates are lower than those from the thin plate theory, where the rotatory inertia and shear deformation are neglected. The influence of b/h was investigated, and as expected, for thin and moderately thick plates, the linear frequencies are lower than for thick plates. Therefore, the thicker the plate, the higher the linear natural frequencies predicted.

The influence of the fibres orientation is studied for plate 2 with $\theta = 0^o$, 30^o and 45^o and the linear natural frequency parameter is determined. As the angle increases, the value of the linear natural frequency parameter also increases, which indicates that the fibres orientations influence the linear natural parameter, therefore the value of the linear natural frequency.

In non-linear forced vibrations, plate $2\left(\theta = 0^o, 30^o \text{ and } 45^o\right)$, and plate 1 are studied. The force impinging on the plate's surface is increased.

Plate 1 is excited by a harmonic wave of 5 N/m^2 to 3000 N/m^2, at 511.112 *rad/s* and 123 DOF are considered. Plate 2 is excited by a harmonic wave of 4 N/m^2 and 123 DOF (pi=7, p_o=5, p_θ=7) are considered in the model. The fibres orientation varies from $\theta = 0^o$ to $\theta = 45^o$. The force applied to the plate is increased to 3000 N/m^2 for $\theta = 30^o$ and $\theta = 45^o$; for $\theta = 0^o$ it is increased to 3300 N/m^2. The influence of the loss parameter is investigated and is concluded that diminishing the value of α implies an increase in the amplitude of vibration. For amplitudes of vibration of the order of the thickness of the plate, the solution was always periodic and highly dominated by the harmonic with frequency equal to the excitation frequency (principal harmonic).

In both cases, as the force increases, so does the amplitude of vibration. Periodic motions are obtained for both plates and the results are confirmed with the computation of Poincaré maps and the Fourier spectrum.

Chapter5

FORCED VIBRATION OF LAMINATED PLATES - LONGITUDINAL AND TRANSVERSE FORCE

1. *INTRODUCTION*

In the previous chapter, forced vibration analysis in the transverse direction was considered. In this chapter, the force applied to the plate is changed and is applied in the transverse and longitudinal direction. Forces in the plane are constant and compressive. New types of solutions are found. The plates here analysed are given in Tables 1 and 2 of Chapter 4 and the equations of motion are solved using the Newmark method presented in Chapter 2. In order to analyse the time domain response of the plate's vibrations, the tools presented in Chapter 3 are used to determine the presence of a periodic, quasi-periodic or chaotic motion.

2. *NON-LINEAR FORCED VIBRATION ANALYSIS*

2.1 - *Distributed Applied Force*

In this section, the forced vibration of a rectangular plate is studied using the HFEM, and equation (2.71) is solved by the Newmark method. When a distributed load in the transverse and longitudinal direction is applied, the generalized forces are given by equation (2.77) in Chapter 2.

2.2 - *Numerical results*

For plate 2, and for a fibre orientation of $\theta = 45^{o}$, two cases are considered: in the first case, the plate is excited at 5000 *N*/m^2 in the *x* direction, 7000 *N*/m^2 in the *y* direction and in the *z* direction the force varies from 500 *N*/m^2 to 7000 *N*/m^2 for an excitation frequency of 762.888 *rad/s*; in the second case, the forces in the *x*, *y* and *z* directions are kept at 10000 *N*/m^2 but the frequency of excitation is changed from 762.888 *rad/s* to 900 *rad/s*; 114 DOF (pi=7, p_o=4, p_θ=7) are considered in the model, and the results are discussed. In the first case, the damping factor, α, is equal to 0.00001 and in the second is 0.000001.

For plate 3, two other cases are studied: in the first case, the forces in the *x*, *y*, *z* directions are equal and are increased from 15000 *N*/m^2 to 100000 *N*/m^2; in the second case the plate is excited at 5000 *N*/m^2 in the *x* direction, 7000 *N*/m^2 in the *y* direction and in the *z* direction the force varies from 7500 *N*/m^2 to 50000 *N*/m^2. In the first case, the damping factor, α, is equal to 0.00001 and in the second is 0.000001.

In both cases the excitation frequency is 980.592 *rad/s*. The results obtained are also discussed. For both plates, the damping factor, α, is equal to 0.00001.

In Figure 1, the time domain response and the phase plane of plate 2 are presented for a force of 5000 *N*/m^2 in the *x* direction, 7000 *N*/m^2 in the *y* direction and 500 *N*/m^2 in the *z* direction.

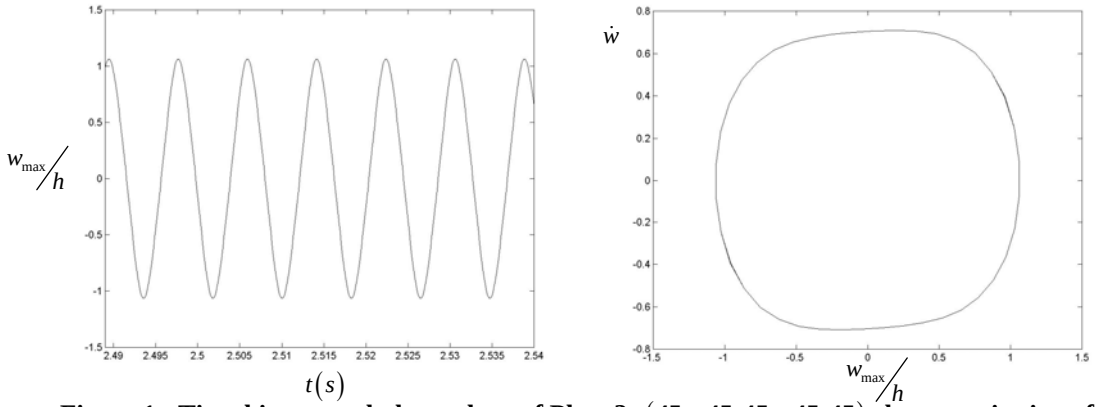

Figure 1 - Time history and phase plane of Plate 2, $(45,-45,45,-45,45)$ due to excitation of $(F_x, F_y, F_z) = (5000, 7000, 500)\ N/m^2$

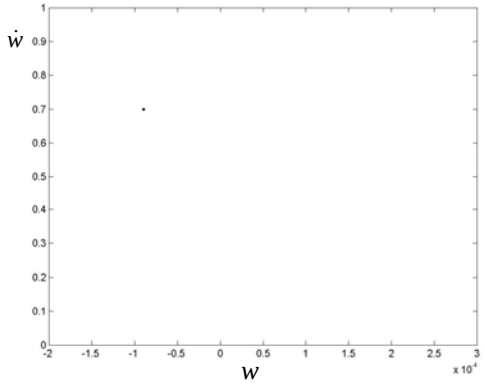

Figure 2 - Poincaré map of Plate 2, due to excitation $\left(F_x, F_y, F_z\right) = \left(5000, 7000, 500\right)$ N/m^2

From Figures 1 and 2, one sees that for $\left(F_x, F_y, F_z\right) = \left(5000, 7000, 500\right)$ *N/m*^{2}, a periodic solution is obtained. In fact, the phase portrait is closed, and the Poincaré map tends to a point.

In Figures 3 to 8, the force in the *z* direction is increased to 7000 *N/m*^{2}.

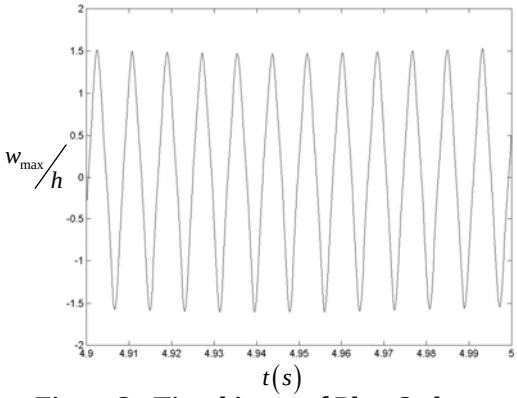

Figure 3 - Time history of Plate 2, due to excitation $\left(F_x, F_y, F_z\right) = \left(5000, 7000, 1000\right)$ N/m^2

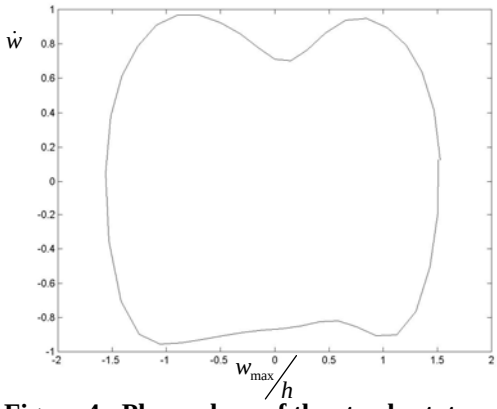

Figure 4 - Phase plane of the steady state forced vibration $\left(F_x, F_y, F_z\right) = \left(5000, 7000, 1000\right)$ N/m^2 of plate 2

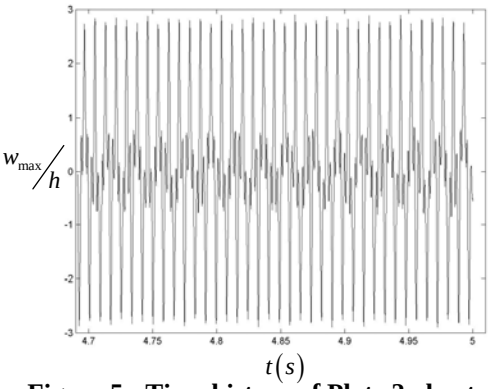

Figure 5 - Time history of Plate 2, due to excitation
$\left(F_x, F_y, F_z\right) = \left(5000, 7000, 3000\right)$ **N/m²**

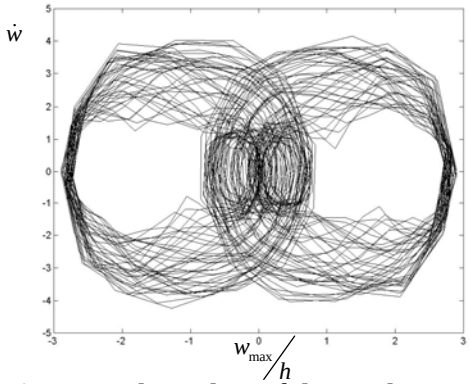

Figure 6 - Phase plane of the steady state forced vibration
$\left(F_x, F_y, F_z\right) = \left(5000, 7000, 3000\right)$ **N/m² of plate 2**

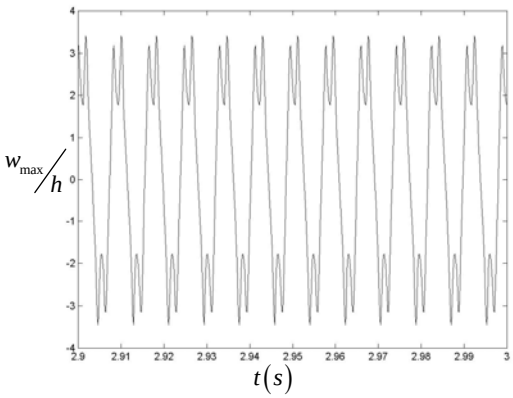

Figure 7 - Time history of Plate 2, due to excitation
$\left(F_x, F_y, F_z\right) = \left(5000, 7000, 7000\right)$ **N/m²**

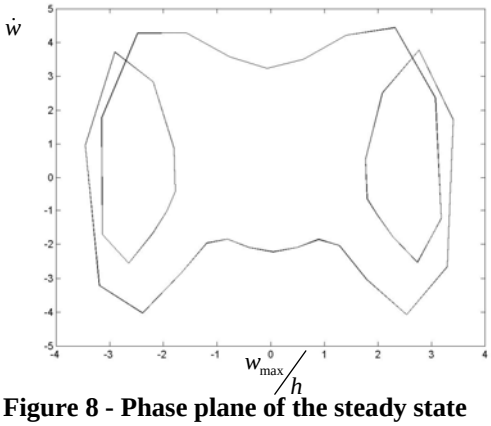

Figure 8 - Phase plane of the steady state forced vibration
$\left(F_x, F_y, F_z\right) = \left(5000, 7000, 7000\right)$ **N/m² of plate 2**

From Figures 3 to 8, different types of solutions are found. The Poincaré maps of these responses were computed and are presented in Figures 9 to 11.

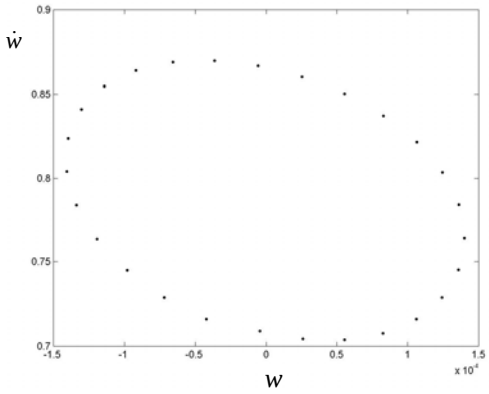

Figure 9 - Poincaré map of Plate 2, due to excitation $\left(F_x, F_y, F_z\right) = \left(5000, 7000, 1000\right)$ **N/m²**

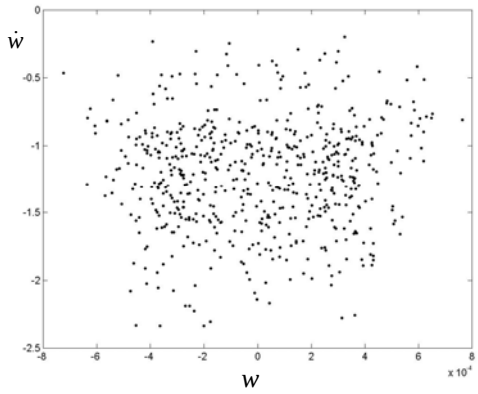

Figure 10 - Poincaré map of Plate 2, due to excitation $\left(F_x, F_y, F_z\right) = \left(5000, 7000, 3000\right)$ **N/m²**

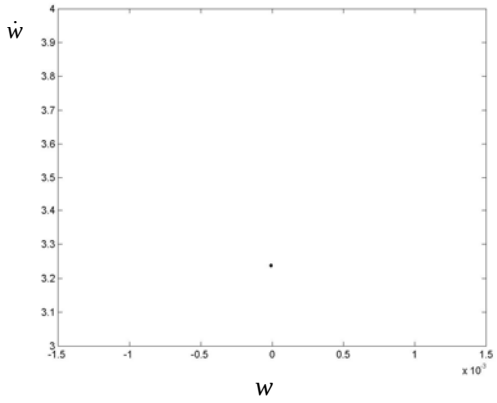

Figure 11 - Poincaré map of Plate 2, due to excitation $\left(F_x, F_y, F_z\right) = \left(5000, 7000, 7000\right)$ **N/m²**

For a force of 1000 N/m^2 in the *z* direction, once an closed path is obtained in the phase plane(Figure 4) and the Poincaré map (Figure 9) tends to a closed line, a quasi-periodic solution was found; for $F_z = 3000\ N/m^2$ (Figure 10), a cloud of points in the Poincaré map may represent a chaotic solution (to be confirmed with the computation of Lyapunov exponents); in Figure 11, once a single point is obtained in the Poincaré map, a periodic solution is obtained. In Figure 12 the Fourier spectrum for the excitation $\left(F_x, F_y, F_z\right) = \left(5000, 7000, 7000\right)$ is presented.

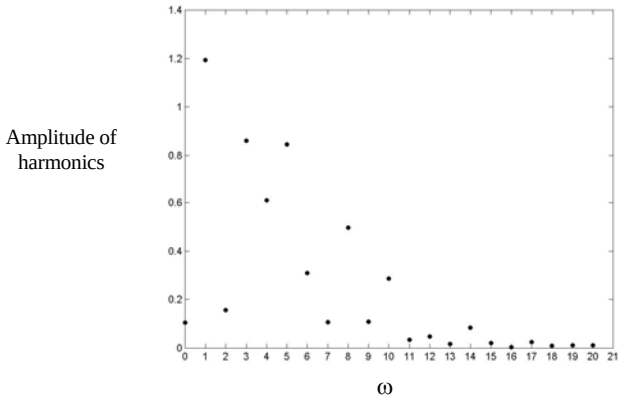

Figure 12 - Fourier spectrum of forced of Plate 2, due to excitation $\left(F_x, F_y, F_z\right) = \left(\mathbf{5000}, \mathbf{7000}, \mathbf{7000}\right)\ \mathbf{N/m^2}$

Figure 12 confirms the results obtained in the Poincaré map. For $F_z = 7000\ N/m^2$ a periodic solution is found, where harmonics of the excitation frequency are involved. In Figure 13, a positive Lyapunov exponent is obtained therefore a chaotic motion is achieved for $F_z = 3000\ N/m^2$.

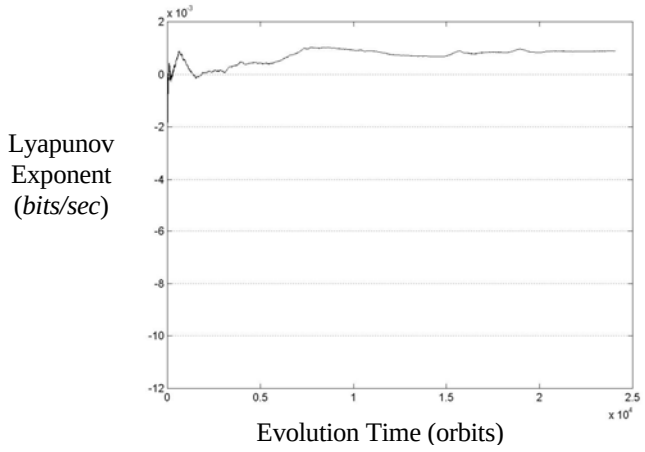

Figure 13 – Highest Lyapunov exponent for Plate 2, due to excitation $\left(F_x, F_y, F_z\right) = \left(\mathbf{5000}, \mathbf{7000}, \mathbf{3000}\right)\ \mathbf{N/m^2}$

The following case study is plate 2, where the forces in the *x*, *y* and *z* directions are kept at 10000 *N*/m^2 but the frequency of excitation is changed from 762.888 *rad/s* to 900 *rad/s*.

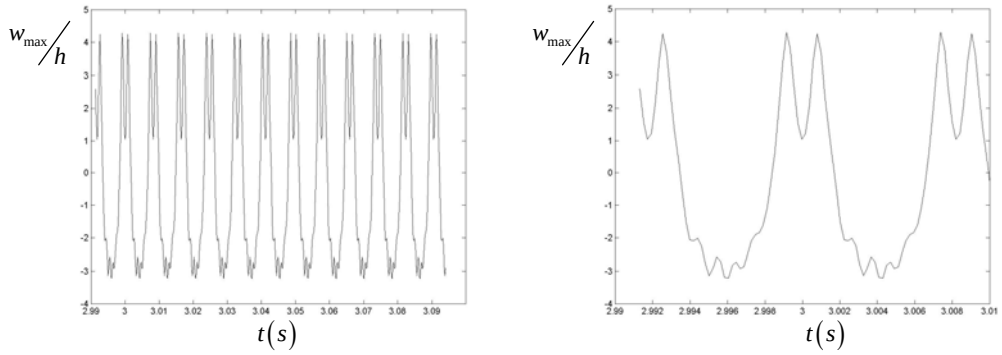

Figure 14 - Time history of Plate 2, due to excitation $(F_x, F_y, F_z) = (10000, 10000, 10000)$ N/m^2, $\omega = 762.888$ *rad/s*

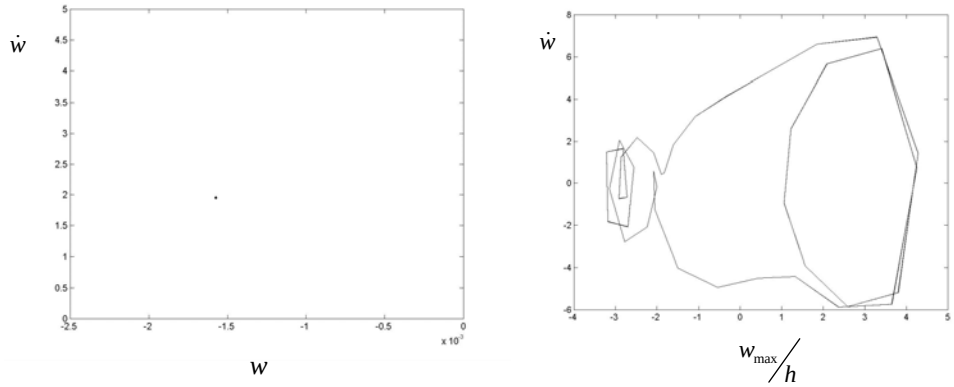

Figure 15 - Poincaré map and phase plane of the steady state forced vibration $(F_x, F_y, F_z) = (10000, 10000, 10000)$ N/m^2 of plate 2, $\omega = 762.888$ *rad/s*

In Figures 14 and 15, a closed path is obtained in the phase plane and the Poincaré map consists of a single point, therefore a periodic solution is found.

Considering $\omega = 800$ *rad/s* and $\omega = 900$ *rad/s*, the time domain responses and the phase plane are given in Figures 16 to 19:

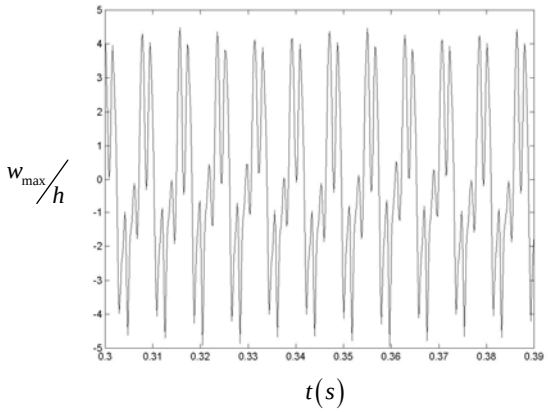

Figure 16 – Time history of Plate 2, due to excitation
$(F_x, F_y, F_z) = (10000, 10000, 10000)$ **N/m²,**
$\omega = 800$ ***rad/s***

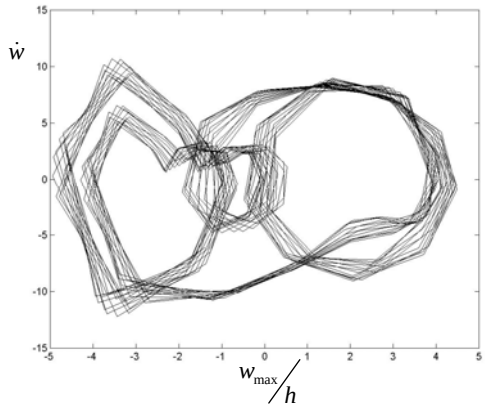

Figure 17 – Phase Plane of Plate 2, due to excitation
$(F_x, F_y, F_z) = (10000, 10000, 10000)$ **N/m²,**
$\omega = 800$ ***rad/s***

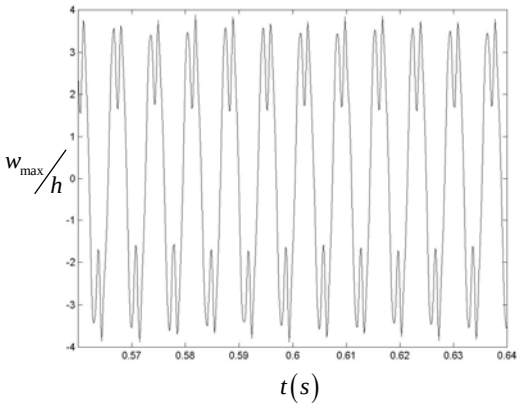

Figure 18 - Time domain response of Plate 2, due to excitation
$(F_x, F_y, F_z) = (10000, 10000, 10000)$ **N/m²,**
$\omega = 900$ ***rad/s***

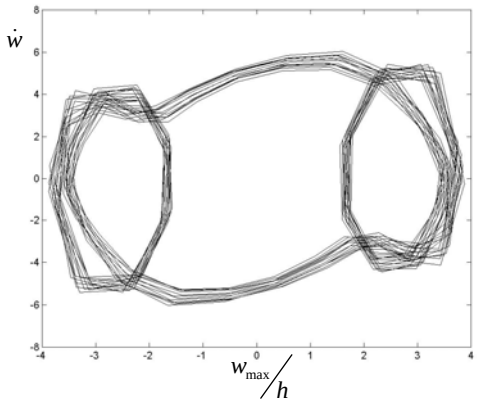

Figure 19 - Phase Plane of Plate 2, due to excitation
$(F_x, F_y, F_z) = (10000, 10000, 10000)$ **N/m²,**
$\omega = 900$ ***rad/s***

It is difficult to ascertain, from the phase planes, if the path is closed or not. Apparently it is not, meaning that the solution is not periodic. This is - again apparently - confirmed by the Poincaré maps in Figures 20 and 21, although more points would be necessary to distinguish between a periodic motion with a large period or a not periodic motion.

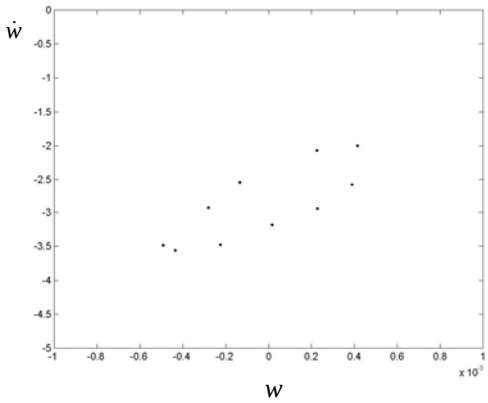

Figure 20 – Poincaré Map of Plate 2, due to excitation $\left(F_x, F_y, F_z\right) = \left(10000, 10000, 10000\right)$ **N/m²,** $\omega = 800$ ***rad/s***

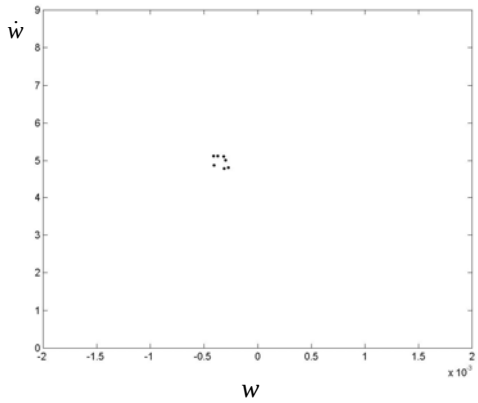

Figure 21 - Poincaré Map of Plate 2, due to excitation $\left(F_x, F_y, F_z\right) = \left(10000, 10000, 10000\right)$ **N/m²,** $\omega = 900$ ***rad/s***

In Figures 22 to 39, the time domain response, the phase plane and the Poincaré map of plate 3 are presented for a force increased from 15000 *N*/m^2 to 100000 *N*/m^2 in *x*, *y*, *z* directions and $\omega = 980.592$ *rad/s*.

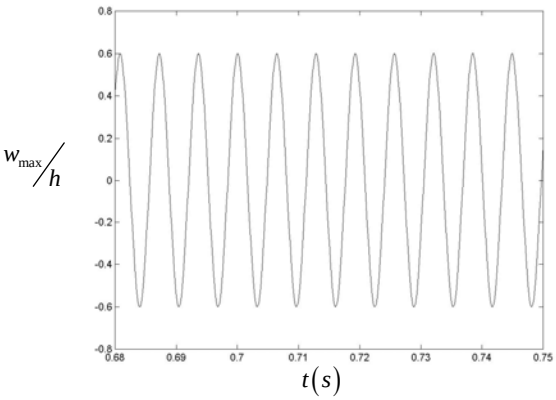

Figure 22 - Time history of Plate 3, due to excitation $\left(F_x, F_y, F_z\right) = \left(15000, 15000, 15000\right)$ **N/m²,** $\omega = 980.592$ ***rad/s***

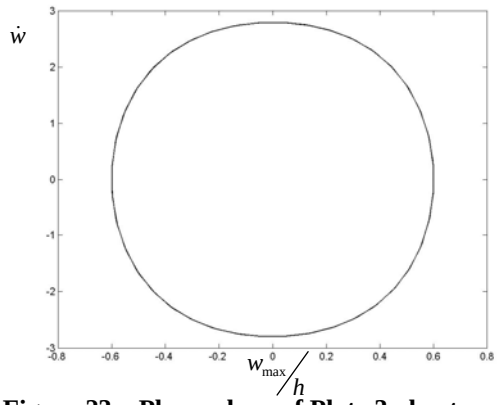

Figure 23 – Phase plane of Plate 3, due to excitation $\left(F_x, F_y, F_z\right) = (15000, 15000, 15000)$ **N/m²,** ω = **980.592** ***rad/s***

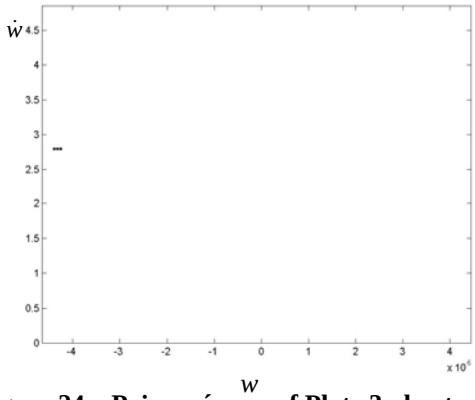

Figure 24 – Poincaré map of Plate 3, due to excitation $\left(F_x, F_y, F_z\right) = (15000, 15000, 15000)$ **N/m²,** ω = **980.592** ***rad/s***

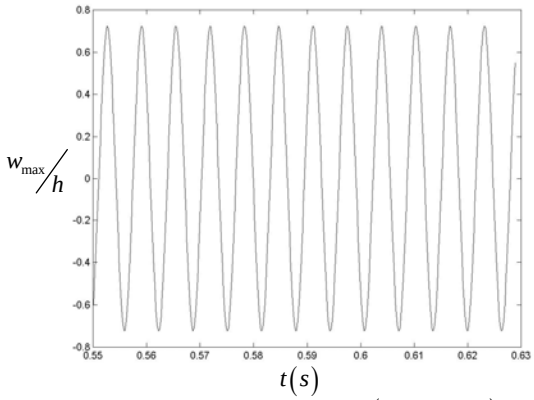

Figure 25 - Time history of Plate 3, due to excitation $\left(F_x, F_y, F_z\right) = (20000, 20000, 20000)$ **N/m²,** ω = **980.592** ***rad/s***

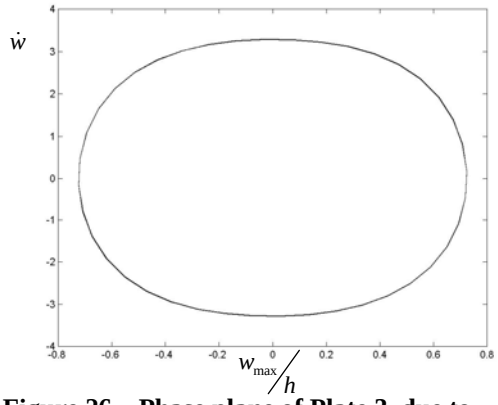

Figure 26 – Phase plane of Plate 3, due to excitation $\left(F_x, F_y, F_z\right) = (20000, 20000, 20000)$ **N/m²,** ω = **980.592** ***rad/s***

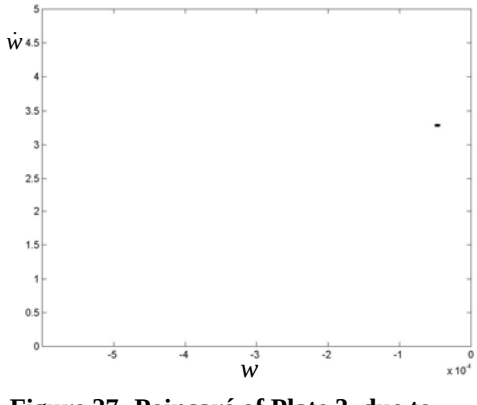

Figure 27 -Poincaré of Plate 3, due to excitation $\left(F_x, F_y, F_z\right) = (20000, 20000, 20000)$ **N/m²,** ω = **980.592** ***rad/s***

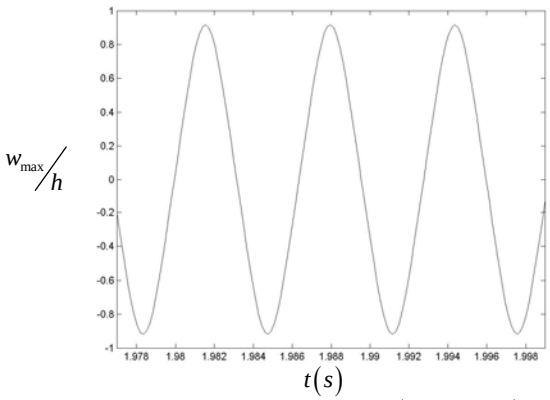

Figure 28 - Time history of Plate 3, due to excitation $(F_x, F_y, F_z) = (30000, 30000, 30000)$ N/m², ω = 980.592 *rad/s*

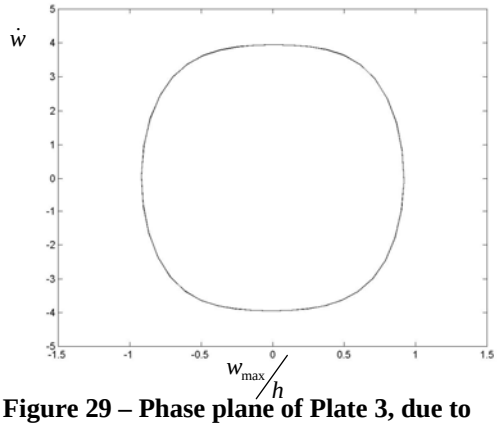

Figure 29 – Phase plane of Plate 3, due to excitation $(F_x, F_y, F_z) = (30000, 30000, 30000)$ N/m², ω = 980.592 *rad/s*

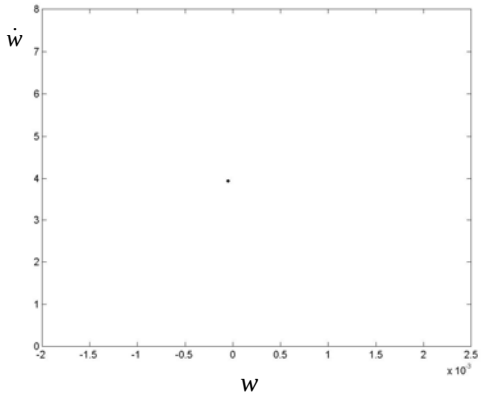

Figure 30 –Poincaré map of Plate 3, due to excitation $(F_x, F_y, F_z) = (30000, 30000, 30000)$ N/m², ω = 980.592 *rad/s*

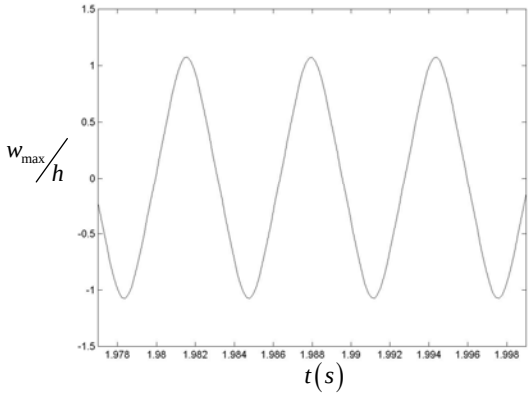

Figure 31 - Time history of Plate 3, due to excitation $(F_x, F_y, F_z) = (40000, 40000, 40000)$ N/m², ω = 980.592 *rad/s*

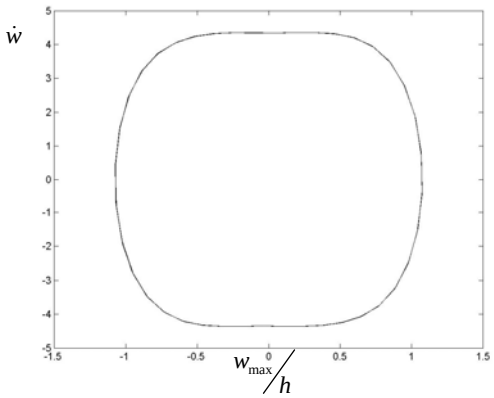

Figure 32 – Phase plane of Plate 3, due to excitation $\left(F_x, F_y, F_z\right) = \left(40000, 40000, 40000\right)$ N/m², ω = 980.592 *rad/s*

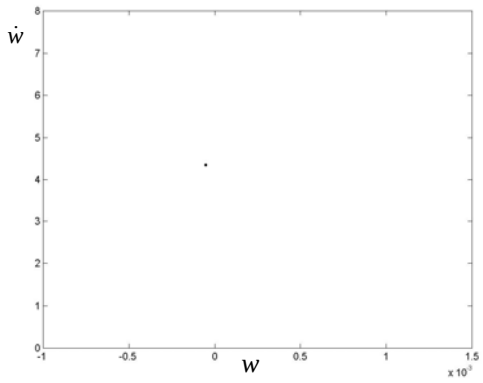

Figure 33 – Poincaré map of Plate 3, due to excitation $\left(F_x, F_y, F_z\right) = \left(40000, 40000, 40000\right)$ N/m², ω = 980.592 *rad/s*

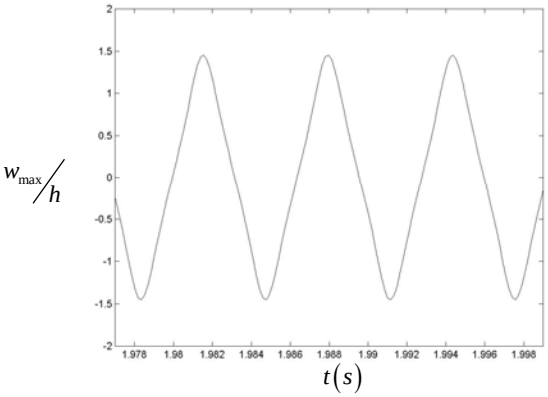

Figure 34 - Time history of Plate 3, due to excitation $\left(F_x, F_y, F_z\right) = \left(70000, 70000, 70000\right)$ N/m², ω = 980.592 *rad/s*

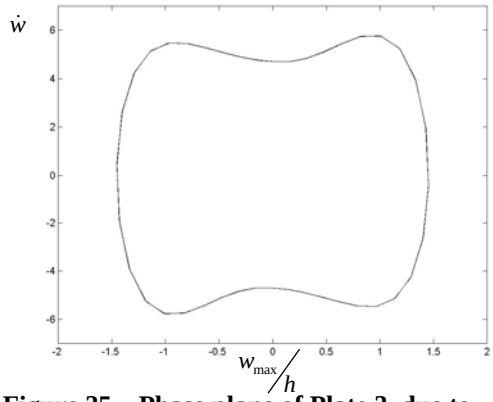

Figure 35 – Phase plane of Plate 3, due to excitation $\left(F_x, F_y, F_z\right) = \left(70000, 70000, 70000\right)$ N/m², ω = 980.592 *rad/s*

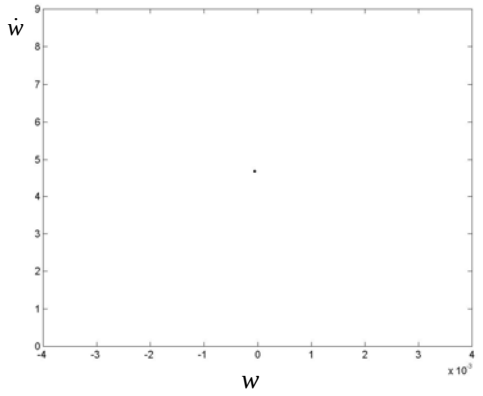

Figure 36 – Poincaré map of Plate 3, due to excitation $\left(F_x, F_y, F_z\right) = \left(70000, 70000, 70000\right)$ N/m², ω = 980.592 *rad/s*

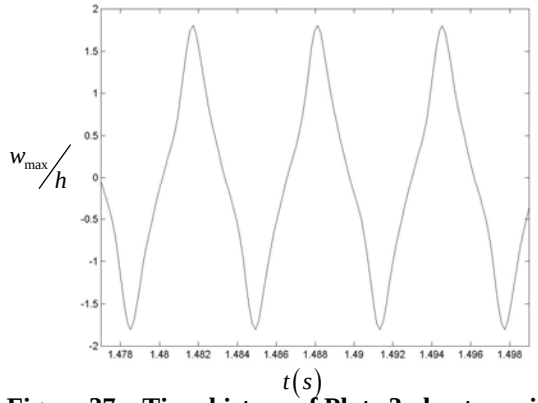

Figure 37 – Time history of Plate 3, due to excitation
$(F_x, F_y, F_z) = (100000, 100000, 100000)$ **N/m²,** $\omega = 980.592$ ***rad/s***

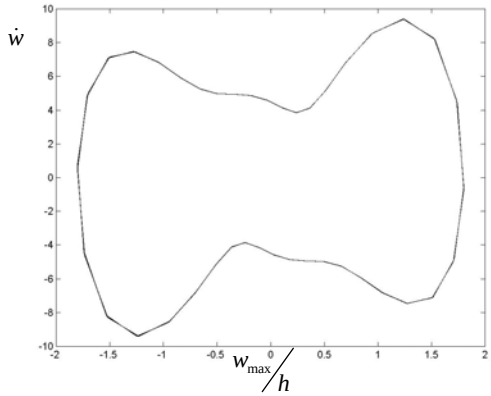

Figure 38 – Phase plane of Plate 3, due to excitation
$(F_x, F_y, F_z) = (100000, 100000, 100000)$
N/m², $\omega = 980.592$ ***rad/s***

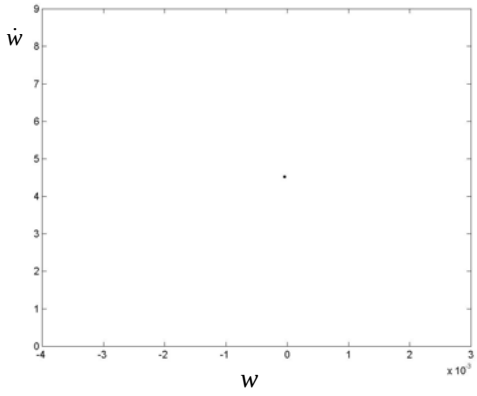

Figure 39 – Poincaré map of Plate 3, due to excitation
$(F_x, F_y, F_z) = (100000, 100000, 100000)$
N/m², $\omega = 980.592$ ***rad/s***

In all the cases presented above, the time domain response represents a periodic solution. As the force increases, so does the amplitude of vibration, as expected.

For the second case of plate 3, in Figures 40 to 60, the force is increased from 7500 N/m^2 to 50000 N/m^2 in the *z* direction and $(F_x, F_y) = (5000, 7000)$ N/m^2.

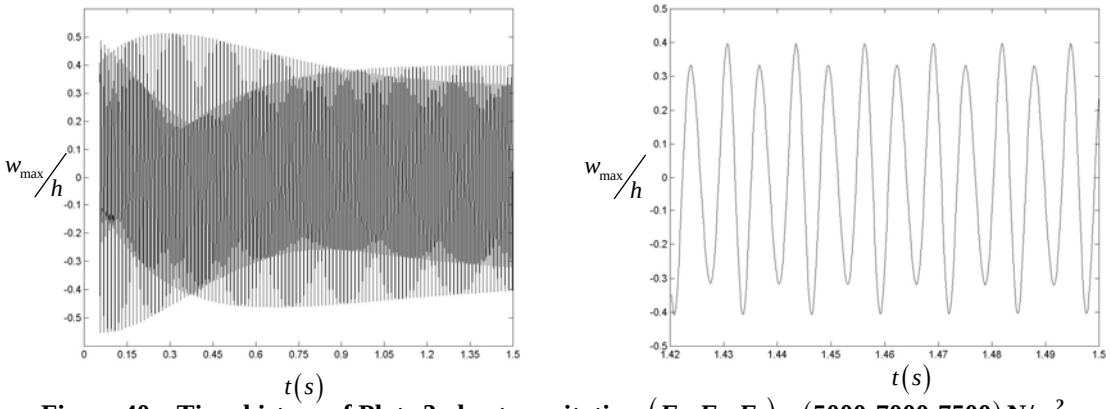

Figure 40 – Time history of Plate 3, due to excitation $(F_x, F_y, F_z) = (5000, 7000, 7500)$ N/m², ω = 980.592 *rad/s*

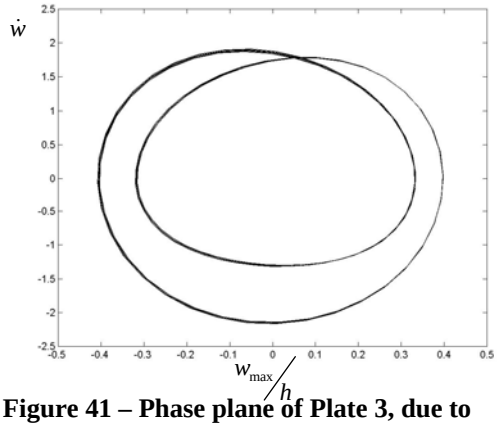

Figure 41 – Phase plane of Plate 3, due to excitation $(F_x, F_y, F_z) = (5000, 7000, 7500)$ N/m², ω = 980.592 *rad/s*

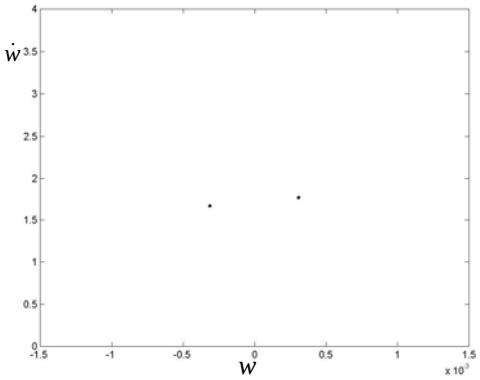

Figure 42 – Poincaré map of Plate 3, due to excitation $(F_x, F_y, F_z) = (5000, 7000, 7500)$ N/m², ω = 980.592 *rad/s*

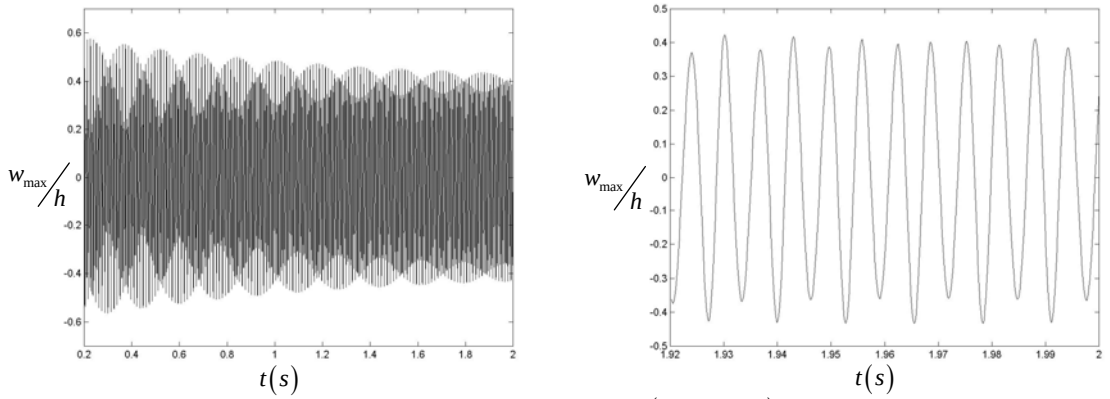

Figure 43 – Time history of Plate 3, due to excitation $(F_x, F_y, F_z) = (5000, 7000, 8500)$ N/m², ω = 980.592 *rad/s*

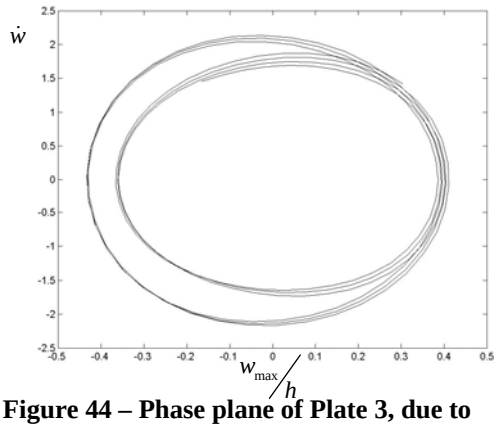

Figure 44 – Phase plane of Plate 3, due to excitation $\left(F_x, F_y, F_z\right) = \left(5000, 7000, 8500\right)$ N/m^2, ω = 980.592 *rad/s*

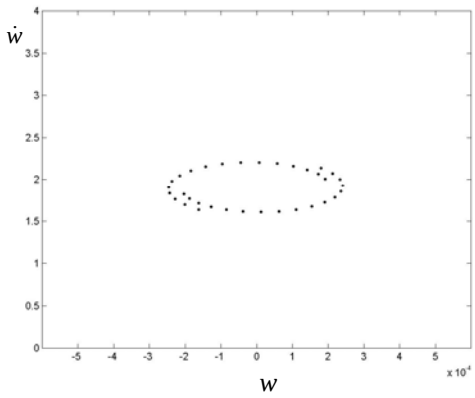

Figure 45 – Poincaré map of Plate 3, due to excitation $\left(F_x, F_y, F_z\right) = \left(5000, 7000, 8500\right)$ N/m^2, ω = 980.592 *rad/s*

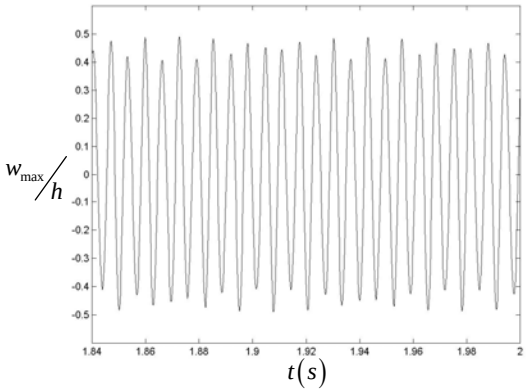

Figure 46 – Time history of Plate 3, due to excitation $\left(F_x, F_y, F_z\right) = \left(5000, 7000, 10000\right)$ N/m^2, ω = 980.592 *rad/s*

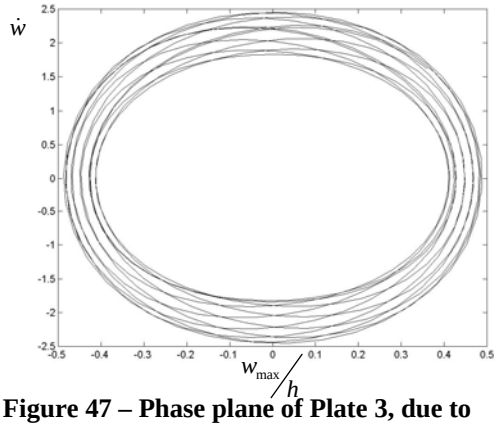

Figure 47 – Phase plane of Plate 3, due to excitation $\left(F_x, F_y, F_z\right) = \left(5000, 7000, 10000\right)$ N/m^2, ω = 980.592 *rad/s*

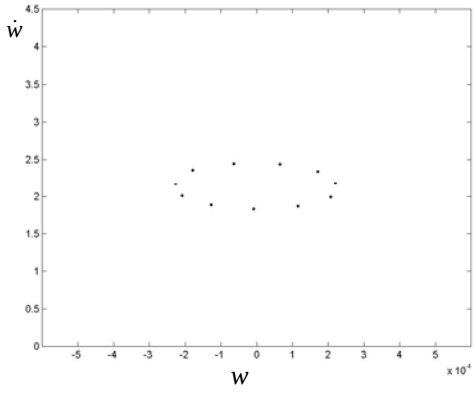

Figure 48 – Poincaré map of Plate 3, due to excitation $\left(F_x, F_y, F_z\right) = \left(5000, 7000, 10000\right)$ N/m^2, ω = 980.592 *rad/s*

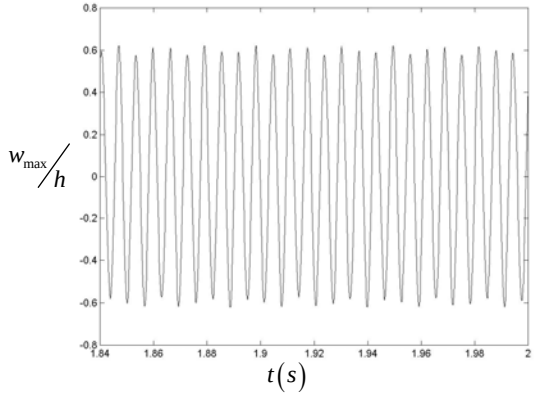

Figure 49 – Time history of Plate 3, due to excitation $(F_x, F_y, F_z) = (5000, 7000, 15000)$ N/m², ω = 980.592 *rad/s*

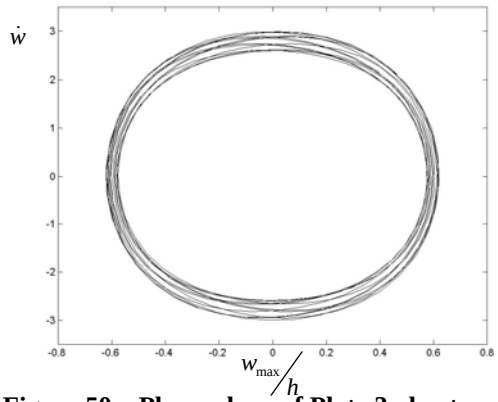

Figure 50 – Phase plane of Plate 3, due to excitation $(F_x, F_y, F_z) = (5000, 7000, 15000)$ N/m², ω = 980.592 *rad/s*

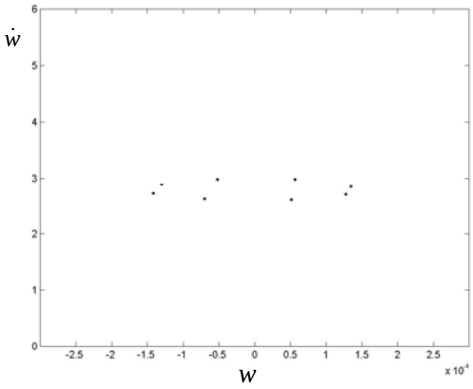

Figure 51 – Poincaré map of Plate 3, due to excitation $(F_x, F_y, F_z) = (5000, 7000, 15000)$ N/m², ω = 980.592 *rad/s*

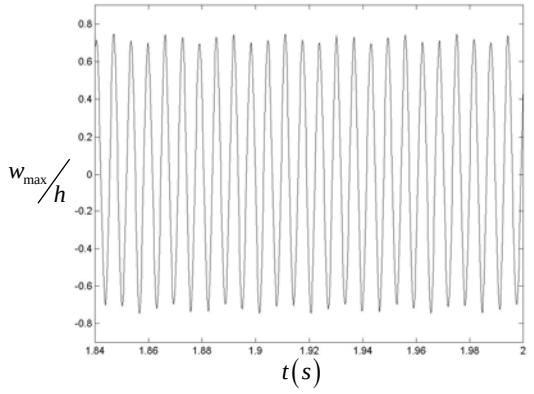

Figure 52 – Time history of Plate 3, due to excitation $(F_x, F_y, F_z) = (5000, 7000, 20000)$ N/m², ω = 980.592 *rad/s*

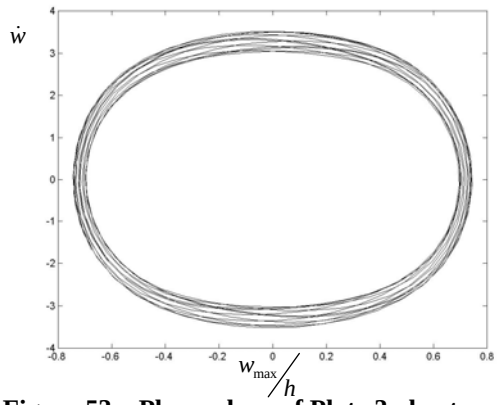

Figure 53 – Phase plane of Plate 3, due to excitation $(F_x, F_y, F_z) = (5000, 7000, 20000)$ N/m², ω = 980.592 *rad/s*

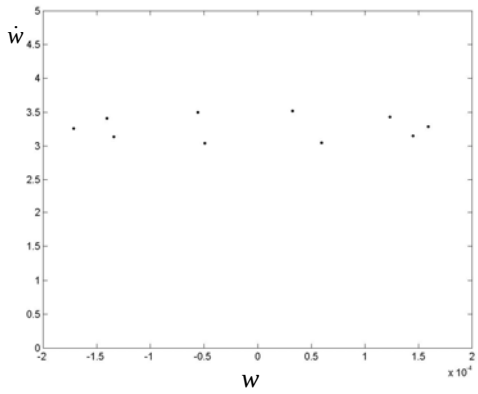

Figure 54 – Poincaré map of Plate 3, due to excitation $(F_x, F_y, F_z) = (5000, 7000, 20000)$ N/m², ω = 980.592 *rad/s*

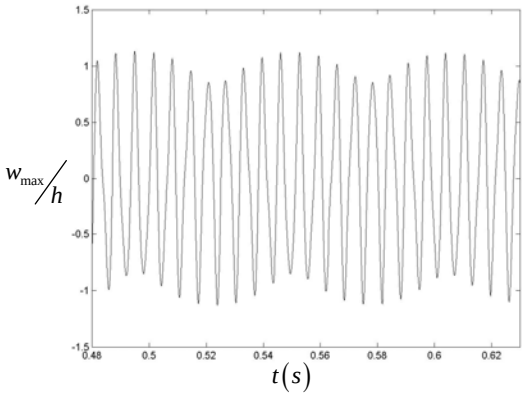

Figure 55 – Time history of Plate 3, due to excitation $(F_x, F_y, F_z) = (5000, 7000, 35000)$ N/m², ω = 980.592 *rad/s*

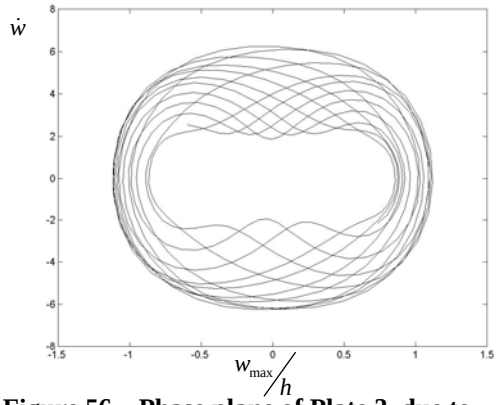

Figure 56 – Phase plane of Plate 3, due to excitation $(F_x, F_y, F_z) = (5000, 7000, 35000)$ N/m², ω = 980.592 *rad/s*

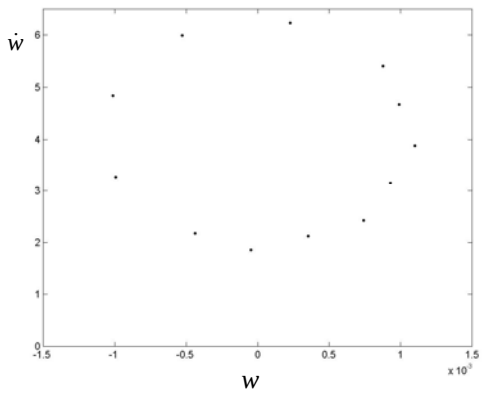

Figure 57 – Poincaré map of Plate 3, due to excitation $(F_x, F_y, F_z) = (5000, 7000, 35000)$ N/m², ω = 980.592 *rad/s*

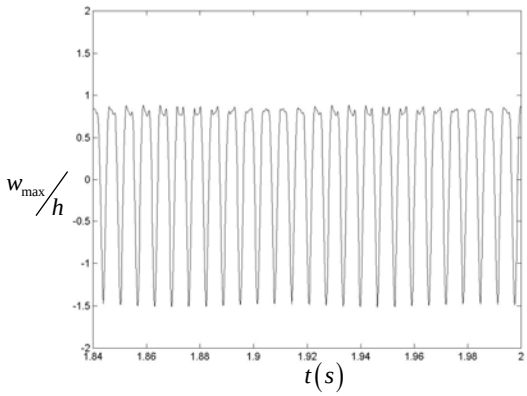

Figure 58 – Time history of Plate 3, due to excitation $(F_x, F_y, F_z) = (5000, 7000, 50000)$ N/m², ω = 980.592 *rad/s*

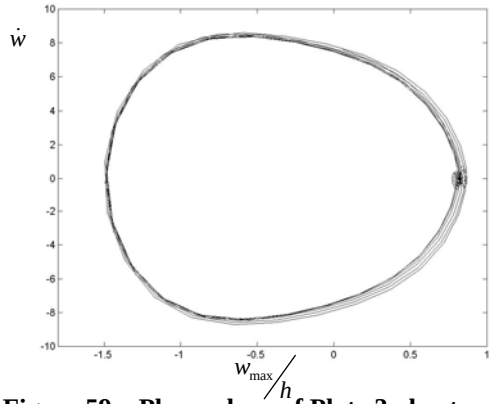

Figure 59 – Phase plane of Plate 3, due to excitation $(F_x, F_y, F_z) = (5000, 7000, 50000)$ N/m², ω = 980.592 *rad/s*

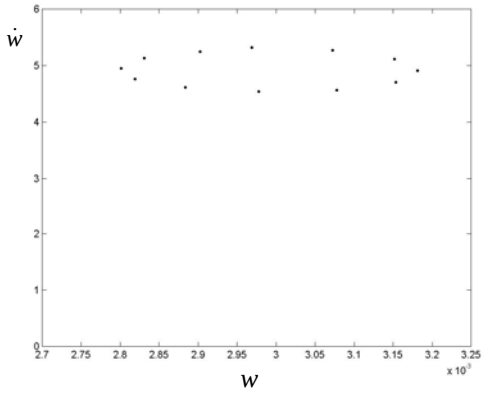

Figure 60 – Poincaré map of Plate 3, due to excitation $(F_x, F_y, F_z) = (5000, 7000, 50000)$ N/m², ω = 980.592 *rad/s*

From the figures above, one sees that the response to harmonic, transverse excitations, in the presence of in-plane constant forces, can be of several types: periodic, but almost harmonic; periodic, with strong influence of harmonics of the excitation frequency; quasi-periodic and chaotic. To remove all doubts about the possibly quasi-periodic motions it would be necessary to compute the two largest Lyapunov exponents [5.1]

3. *CONCLUSIONS*

In this chapter, forced vibrations of composite laminated plates modelled by the HFEM are analysed. The main difference from Chapter 4 is the change of the force applied to the plate.

For plate 2, two cases are considered: in the first case, the plate is excited at 5000 N/m^2 in the x direction, 7000 N/m^2 in the y direction and in the z direction the force varies from 500 N/m^2 to 7000 N/m^2 for an excitation frequency of 762.888 *rad/s*; in the second case, the forces in the x, y and z directions are kept at 10000 N/m^2 but the frequency of excitation is changed from 762.888 *rad/s* to 900 *rad/s*. For the first case as the force in the z direction increases, so does the amplitude of vibration. Periodic, quasi-periodic and chaotic motions are obtained and the results are confirmed with the computation of Poincaré maps, Fourier spectrum and Lyapunov exponents. In the second case, increasing the excitation frequency, quasi-periodic solutions are obtained and the amplitude of vibration diminishes as the excitation frequency increases.

For plate 3, two other cases are considered: in the first case, the forces in the x, y, z directions are equal and are increased from 15000 N/m^2 to 100000 N/m^2; in the second case the plate is excited at 5000 N/m^2 in the x direction, 7000 N/m^2 in the y direction and in the z direction the force varies from 7500 N/m^2 to 50000 N/m^2. In both cases the excitation frequency is 980.592 *rad/s*. In the first case, as the force in all the directions increase, so does the amplitude of vibration. Once a closed line is obtained in the phase plane and the Poincaré map consists of a single point, a periodic solution is obtained. For the second case, only when the plate is excited with a force of 7500 N/m^2, a periodic solution is obtained. In all the other responses, possible quasi-periodic solutions are obtained. To remove all doubts it would be necessary to compute the two largest Lyapunov exponents.

It must be mentioned, that it was assumed that the plate always vibrate in the linear elastic regime. Naturally, for engineering applications it ought to be confirmed if the elastic limit is not passed. The same is true in what delamination is concerned.

Chapter 6

CONCLUSIONS AND SUGGESTIONS FOR FUTURE STUDY

1. *CONCLUSIONS*

Composite laminated structures are used in many areas of engineering such as aeronautics, space engineering and naval industry. They are often subjected to large dynamic excitation levels. As a result, they can undergo large amplitude, which cause large tensions and the diminution of life due to fatigue.

In this thesis, the geometrically non-linear forced vibration of fully clamped composite laminated plates was studied. The hierarchical finite element method (HFEM) was used to create the spatial model. The equations of motion for asymmetrically composite laminated plates were derived in the time domain and Newmark direct integration scheme was used to solve them. The implementation was carried out in *FORTRAN*. In the HFEM, particularly in non-linear analysis, high order shape functions must be integrated. The symbolic manipulator *MAPLE* was used to carry out this task, thus defining very accurately the mass and stiffness matrices that constitute the model.

Employing the flexibility of choosing different shape functions to construct the HFEM model, the convergence as a function of the number of shape functions was studied. The number of in-plane shape functions required for accuracy increases as the amplitude of vibration displacement and the non-linearity increase. The use of less in-plane shape functions than the necessary increases the stiffness of the model. For larger amplitudes of vibration, more in-plane than out-of-plane shape functions become necessary. The HFEM gives accurate solutions with far fewer DOF than the *h*-version of the FEM. The influence of b/h was investigated, and as expected, for thin and moderately thick plates, the linear frequencies are lower than for thick

plates. Therefore, the thicker the plate, the higher the linear natural frequencies predicted.

The influence of the fibres orientation is studied for a particular plate, considering $\theta = 0^o$, 30^o and 45^o and determining a linear natural frequency parameter. Comparing with other numerical results, the FSDT for thick plates the parameters are lower than those obtained in the classical plate theory (CPT). As the angle increases, the value of the linear natural parameter also increases, which indicates that the fibres orientations influence the linear natural frequency.

In the non-linear analysis, the time domain response for symmetrically laminated composite rectangular plates was obtained for three plates. The force was changed in all the directions and periodic, quasi-periodic and chaotic motions were obtained. In order to analyse solutions, tools such as phase plane, Poincaré maps, Fourier spectra and Lyapunov exponents were used. Periodic, quasi-periodic and chaotic solutions were obtained and the results were discussed. On the other hand, regarding the amplitude of vibration, for all the plates studied, as the force increased, so did the amplitude of vibration.

2. *SUGGESTIONS FOR FUTURE WORK*

Based on the work discussed in the thesis, the following suggestions for future investigation can be made:

i). Once a general model valid for symmetric and asymmetric laminates was derived, work needs to be carried out in asymmetrical plates;

ii). Because of the persistent increasing demands on the performance of mechanical structures and the rising importance of lightweight construction, the mathematical models to describe mechanical systems have to meet increasingly high accuracy. Therefore work can be carried out in the experimental analysis of the plates presented in this thesis;

iii). To obtain the frequency spectrum of quasi-periodic and chaotic oscillations, other tools of signal processing, like the power spectral density function should be implemented;

iv). The algorithm used from Wolf computes the largest non-negative Lyapunov exponent from a time series. The computation of the complete spectrum from the equations of motion, and from its linearization, instead of using the time series needs to be made;

v). The study carried out intended to find non-periodic motion in plates excited harmonically. Thus, academically, some of the amplitudes considered for the forces were very large. As referred before, it will be necessary to validate the linear elastic relationship and the integrity of the plates for very large displacements.

REFERENCES

CHAPTER 1

[1.1] – Reddy, J.N. *Mechanics of Laminated Composite Plates, Theory and Analysis*, CRC Press, Boca Raton, FL, 1997.

[1.2] – Reddy, J.N. *Energy and Variational Methods in Applied Mechanics*, John Whiley, New York, 1984.

[1.3]– Reddy, J.N., *An Introduction to the Finite Element Method*, Second Edition, McGraw-Hill, New York, 1993.

[1.4] - Benamar, R. *Nonlinear Dynamic Behaviour of Fully Clamped Beams and Rectangular Isotropic and Laminated Plates*. Ph.D. Thesis, University of Southampton, 1990.

[1.5] - Nayfeh, A. H. and Mook, D. T. *Nonlinear Oscillations*. New York: John Wiley and Sons, 1995.

[1.6] - Moon, F. C. *Chaotic Vibrations. An Introduction for Applied Scientists and Engineers.* New York: John Wiley and Sons, 1987

[1.7] - Han, W. *The Analysis of Isotropic and Laminated Rectangular Plates Including Geometrical Non-linearity Using the p-version Finite Element Method*. Ph.D. Thesis, University of Southampton, 1993.

[1.8] - Han, W. and Petyt, M., *Geometrically nonlinear vibration analysis of thin, rectangular plates using the hierarchical finite element method - I: The fundamental mode of isotropic plates.* Computers and Structures, 63(2), 295-308, 1997.

[1.9] - Han, W. and Petyt, M., *Geometrically nonlinear vibration analysis of thin, rectangular plates using the hierarchical finite element method - II: 1st mode of*

laminated plates and higher modes of isotropic and laminated plates. Computers and Structures, 63(2), 309-318, 1997.

[1.10] – Vinson, J.R. and Sierakowski, R.L.. *The Behaviour of Structures Composed of Composite Materials,* Martinus Nijhoff Publishers, I: Introduction to Composite Materials. 2-4, 1987.

[1.11] – Soares, C.A.M., Soares, C.M.M. and Freitas M.J.M., *Mechanics of Composite Materials and Structures,Vol. 1 – Main Lectures,* Tróia, Portugal, I: Mechanics of composite materials, Nato Advanced Studies, 1-88, 1998.

[1.12] – Chu, H.N. and Herrmann, G., *Influence of large amplitudes on free flexural vibrations of rectangular elastic plates,* Journal of Applied Mechanics 23(4), 523-540, 1956.

[1.13] – Bert, C.W., *Dynamics of composite and sandwich panels-Part I. Shock and Vibration Digest* 8(10), 37-48, 1976.

[1.14] – Bert, C.W., *Dynamics of composite and sandwich panels-Part II,* Shock and Vibration Digest 8(11), 15-24, 1976.

[1.15] – Reddy, J.N., *Finite element modelling of structural vibrations: A review of recent advances,* Shock and Vibration Digest 11(1), 25-39, 1979.

[1.16] - Reddy, J.N., *Finite element modelling of structural layered aninsotropic composite plates and shells: A review of recent research,* Shock and Vibration Digest 13(2), 3-12, 1981.

[1.17] – Reddy, J.N., *Recent research in the analysis of composite plates,* Composite Rev. 4, 101-104, 1982.

[1.18] – Reddy, J.N., *A review of the literature on finite-element modelling of laminated composite plates,* Shock and Vibration Digest 17(4), 3-8,1985.

[1.19] – Chia, C.Y., *Nonlinear analysis of Plates,* Mc Graw-Hill, New York,1980.

[1.20]- Chia, C.Y., *Geometrically nonlinear behaviour of composite plates: a review*. Applied mechanics review 41(12), 439-451, 1988.

[1.21] – Kapania, R.K., and Raciti, S., *Recent advances of laminated beams and plates, Part II: Vibration and wave propagation*, AIAA journal 27(7), 935-946, 1989.

[1.22] – Mei, C., *Finite element displacements methods for large amplitude free flexural vibrations of beams and plates*, Computers and Structures, Vol. 3, 163-174, 1973.

[1.23] – Chiang, C.K., Gray Jr, C.E., and Mei, C., *Finite element large amplitude free and forced vibrations of rectangular thin composite plates*, Vibration and behaviour of composite structures, the winter annual meeting of the ASME, San Francisco, CA, USA., 1989.

[1.24] – Ribeiro, P. and Petyt, M., *Multi-Modal Geometrical Non-Linear Free Vibration of Fully Clamped Composite Laminated Plates*. Journal of Sound and Vibration, 225(1), 127-152, 1999.

[1.25] – Ribeiro, P. and Petyt, M., *Geometrical Non-Linear, Steady State, Forced, Periodic Vibration of Plates, Part I: Model and Convergence Studies*, Journal of Sound and Vibration, 226(5), 955-983, 1999.

[1.26] – Ribeiro, P. and Petyt M., *Geometrical Non-Linear, Steady State, Forced, Periodic Vibration of Plates, Part II: Stability Study and Analysis of Multi-Modal Response*. Journal of Sound and Vibration, 226(5), 985-1010, 1999.

[1.27] – Ribeiro, P., *Geometrical nonlinear vibration of beams and plates by the Hierarquical finite element method*, Ph.D. Thesis, University of Southampton, 1998.

[1.28] – Ribeiro, P., *A p-version finite element for non-linear vibration of moderately thick laminated plates*, 44th AIAA/ASME/ASCE/AHS/ASC

Structures, Structural Dynamics, and Materials Conference and Exhibit, paper nº AIAA-2003-1711,2003

[1.29] - Harras, B., Benamar, R. and White, R. G., *Geometrically Non-Linear Free Vibration of Fully Clamped Symmetrically Laminated Rectangular Composite Plates.* Journal of Sound and Vibration, Volume 251, Issue 4, Pages 579-619, 4 April 2002

[1.30] - Meirovitch, L., Silverberg, L.M., *Two bracketing theorems characterizing the eigensolution for the h-version of the finite element method*. International Journal for Numerical Methods in Engineering, 19, 1691-1704, 1983.

[1.31] - Meirovitch, L., Baruh, H. *On the inclusion principle for the hierarchical finite element method,* International Journal for Numerical Methods in Engineering, 19, 281-291, 1983.

[1.32] - Zienkiewicz, O.C. and Taylor, R.L. *The Finite Element Method*. 4th Edition. London: McGraw-Hill, 1988.

[1.33] - Meirovitch, L., *Elements of Vibration Analysis*. Singapore: McGraw-Hill, 1986.

[1.34] – Smith, P., *Aerospace Engineering. Acoustic fatigue of aircraft structures,* Institute of Sound and Vibration Research., 1999.

CHAPTER 2

[2.1] - Han, W., The Analysis of isotropic and laminated rectangular plates including geometrical non-linearity using the p-version finite element method. Ph.D. Thesis. University of Southampton, UK, 1993.

[2.2] - Mei, C. and Prasad, C. B. Effects of large deflection and transverse shear on responses of symmetrical composite laminates subjected to acoustic excitation. *Journal of Composite Materials*, 1989, 23(6), 606-639.

[2.3] – Zienkiwicz, O.C. and Taylor, R.L., *The Finite Element Method*. 4th Edition. McGraw-Hill, London, 1988.

[2.4] –Vinson, J.R .and Sierakowski, R.L., *The Behaviour of Structures Composed of Composite Materials*, 1987, 45.

[2.5] - Chia, C.Y. *Nonlinear Analysis of Plates*. New York: McGraw-Hill, 1980.

[2.6] - Petyt, M. *Introduction to Finite Element Vibration Analysis*. Cambridge: Cambridge University Press, 1990.

[2.7]- Leung, A. Y. T. and Chan, J. K. W. Fourier p-element for the analysis of beams and plates. *Journal of Sound and Vibration*, 1998, 212(1), 179-185.

CHAPTER 3

[3.1] - Moon, F.C. *Chaotic Vibrations. An introduction for Applied Scientists and Engineers*. New York: John Wiley and Sons, 1987.

[3.2] - Nayfeh, A. H. and Balachandran, B., *Applied Nonlinear Dynamics. Analytical, Computational and Experimental Methods*, John Wiley and Sons, 1995.

[3.3] –Seidel, R., Practical Bifurcation and Stability Analysis, From Equilibrium to Chaos, Interdisciplinary Applied Mathematics, 2nd Edition, Springer Verlag, 1994.

[3.4] – Arrowsmith, D.K., Place, C.M., *Ordinary Differential Equations – A qualitative approach with applications,* Chapman and Hall Mathematics Series, London, 1982.

[3.5] – Thomsen, Jon J., *Vibrations and Stability: Advanced Theory, Analysis and Tools,* 2nd Edition, Springer Verlag, 2003.

[3.6] – Wolf, A., Swift, J., Swinney, H., Vastano, J., *Determinig Lyapunov Exponents from a Time Series,* Physica 16D, p. 285-317, 1985.

[3.7] – Parker, T.S., Chua, L.O., *Practical Numerical Algorithms for Chaotic Systems*. Springer-Verlag, New York, 1989.

CHAPTER 4

[4.1] – Leissa, W., Vibration of plates, NASA sp-160, 1969.

[4.2] – Lin, C-C. and Kin, W.W., Free transverse vibration of rectangular unsymmetrically laminated plates, *Journal of Sound and Vibration*, 1974, 36(1), 91-103

[4.3] – Reddy, J.N., Free vibration of antisymmetric, angle-ply laminated plate including transverse shear deformation by finite element method, *Journal of Sound and Vibration*, 1979, 66(4), 565-576

[4.4] – Bert, C.W. and Mayberry, B.L., Free vibration of unsymmetric laminated anisotropic plate with clamped edges, *Journal of Composite Materials*, April 1969, 3, 282-293

[4.5] – Chow, S.T., Liew, K.M. and Lam, K. Y., Trnsverse vibration of symmetrically laminated rectangular composite plates, *Composite Structures*, 1992, 20, 213-226

[4.6] – Harras, B., *Theoretical and Experimental Investigation of the Geometrically Non-Linear Behaviour of Fully Clamped Rectangular Laminated Pannels made of Various Types of Composites.* PHD-Thesis, University Mohammed V – AGDAL, 2001.

[4.7] – Harras, B., Benamar, R. and White, R. G., *Geometrically Non-Linear Free Vibration of Fully Clamped Symmetrically Laminated Rectangular Composite Plates.* Journal of Sound and Vibration, Volume 251, Issue 4, Pages 579-619, 4 April 2002

[4.8] – Ribeiro, P. and Petyt, M. Multi-Modal Geometrical Non-Linear Free Vibration of Fully Clamped Composite Laminated Plates. *Journal of Sound and Vibration*, 1999, 225(1), 127-152.

[4.9] – Ribeiro, P. and Petyt. Geometrical Non-Linear, Steady State, Forced, Periodic Vibration of Plates, Part I: Model and Convergence Studies. *Journal of Sound and Vibration,* 1999, 226(5), 955-983.

[4.10] – Ribeiro, P., Geometrical nonlinear vibration of beams and plates by the Hierarquical finite element method. 1998, Ph.D. Thesis, University of Southampton, 1995.

[4.11] – Ribeiro, P., Petyt, M. Non-Linear vibration of composite laminated plates by the hierarchical finite element method. *Composite Structures*, 1999, 197-208.

[4.12] – Moon, F.C. *Chaotic Vibrations. An introduction for Applied Scientists and Engineers*. New York: John Wiley and Sons, 1987.

[4.13] – Press, W. H., Teukolsky, S. A., Vetterling, W.T., Flannery, B.P., *Numerical Recipes in Fortran 77 the art os Scientific Computing,* Vol 1, Cambridge University Press, 1986.

[4.14] – Han, W. *The Analysis of Isotropic and Laminated Rectangular Plates Including Geometrical Non-Linearity Using The P-Version Finite Element Method.* Ph.D. Thesis, University of Southampton, 1993.

[4.15] – R. Benamar, *Nonlinear Dynamic Behaviour of Fully Clamped Beams and Rectangular Isotropic and Laminated Plates.* Ph.D. Thesis, University of Southampton, 1990.

CHAPTER 5

[5.1] - Nayfeh, A. H. and Balachandran, B., *Applied Nonlinear Dynamics. Analytical, Computational and Experimental Methods*, John Wiley and Sons, 1995.

APPENDIX A

The first out-of-plane shape functions after the cubic polynomials are given by

$f_5 = (1/8) - (1/4)\xi^2 + (1/8)\xi^4$

$f_6 = (1/8)\xi - (1/4)\xi^3 + (1/8)\xi^5$

$f_7 = -(1/48) + (3/16)\xi^2 - (5/16)\xi^4 + (7/48)\xi^6$

$f_8 = -(1/16)\xi + (5/16)\xi^3 - (7/16)\xi^5 + (3/16)\xi^7$

$f_9 = (3/384) - (15/96)\xi^2 + (35/64)\xi^4 - (63/96)\xi^6 + (99/384)\xi^8$

$f_{10} = (5/128)\xi - (35/96)\xi^3 + (63/64)\xi^5 - (33/32)\xi^7 + (143/384)\xi^9$

$f_{11} = -(1/256) + (35/256)\xi^2 - (105/128)\xi^4 + (231/128)\xi^6 - (429/256)\xi^8 + (143/256)\xi^{10}$

$f_{12} = -(7/256)\xi + (105/256)\xi^3 - (231/128)\xi^5 + (429/128)\xi^7 - (715/256)\xi^9 + (221/256)\xi^{11}$

$f_{13} = (7/3072) - (63/512)\xi^2 + (1155/1024)\xi^4 - (1001/256)\xi^6 + (6435/1024)\xi^8 - (2431/512)\xi^{10} + (4199/3072)\xi^{12}$

$f_{14} = (21/1024)\xi - (231/512)\xi^3 + (3003/1024)\xi^5 - (2145/256)\xi^7 + (12155/1024)\xi^9 - (4199/512)\xi^{11} + (2261/1024)\xi^{13}$

$f_{15} = -(3/2048) + (231/2048)\xi^2 - (3003/2048)\xi^4 + (15015/2048)\xi^6 - (36465/2048)\xi^8 + (46189/2048)\xi^{10} - (29393/2048)\xi^{12} + (7429/2048)\xi^{14}$

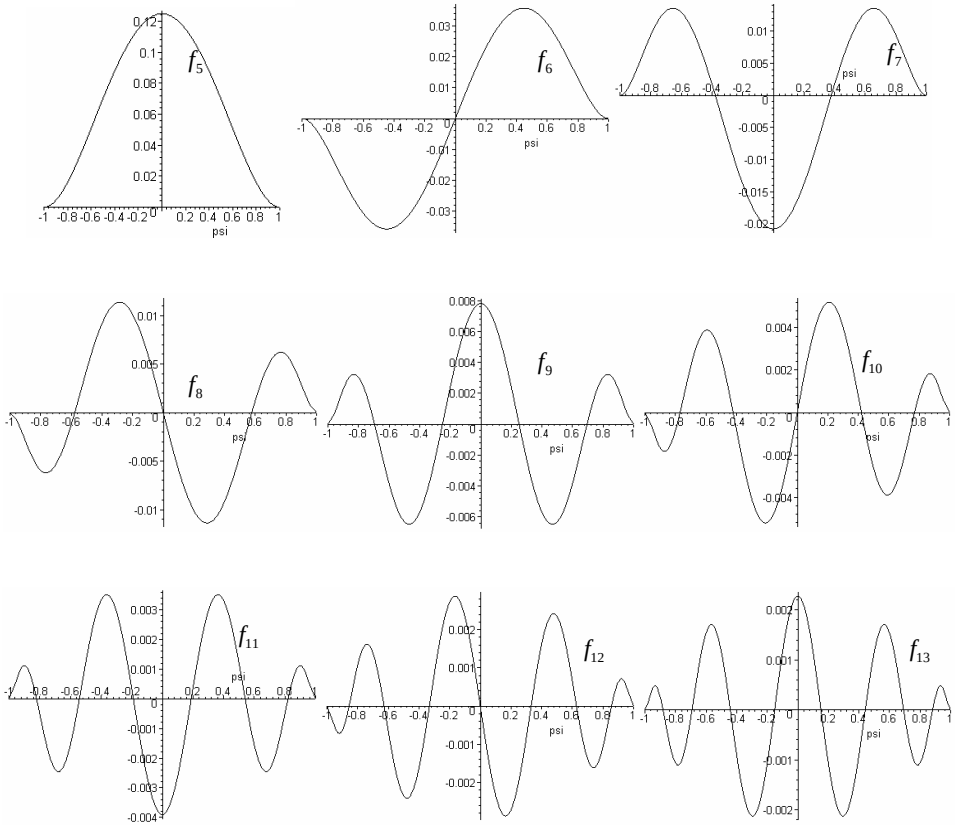

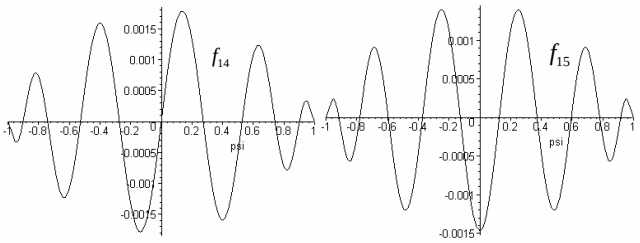

In-plane shape functions

$$g_2 = -(1/2) + (1/2)\xi^2$$
$$g_3 = -(1/2)\xi + (1/2)\xi^3$$
$$g_4 = (1/8) - (3/4)\xi^2 + (5/8)\xi^4$$
$$g_5 = (3/8)\xi - (5/4)\xi^3 + (7/8)\xi^5$$
$$g_6 = -(1/16) + (15/16)\xi^2 - (35/16)\xi^4 + (63/48)\xi^6$$
$$g_7 = -(5/16)\xi + (35/16)\xi^3 - (63/16)\xi^5 + (99/48)\xi^7$$
$$g_8 = (5/128) - (105/96)\xi^2 + (315/64)\xi^4 - (693/96)\xi^6 + (1287/384)\xi^8$$
$$g_9 = (35/128)\xi - (105/32)\xi^3 + (693/64)\xi^5 - (429/32)\xi^7 + (715/128)\xi^9$$
$$g_{10} = -(7/256) + (315/256)\xi^2 - (1155/128)\xi^4 + (3003/128)\xi^6 - (6435/256)\xi^8 + (2431/256)\xi^{10}$$
$$g_{11} = -(63/256)\xi + (1155/256)\xi^3 - (3003/128)\xi^5 + (6435/128)\xi^7 - (12155/256)\xi^9 + (4199/256)\xi^{11}$$
$$g_{12} = (21/1024) - (693/512)\xi^2 + (15015/1024)\xi^4 - (15015/256)\xi^6 + (109395/1024)\xi^8 - (46189/512)\xi^{10} + (29393/1024)\xi^{12}$$

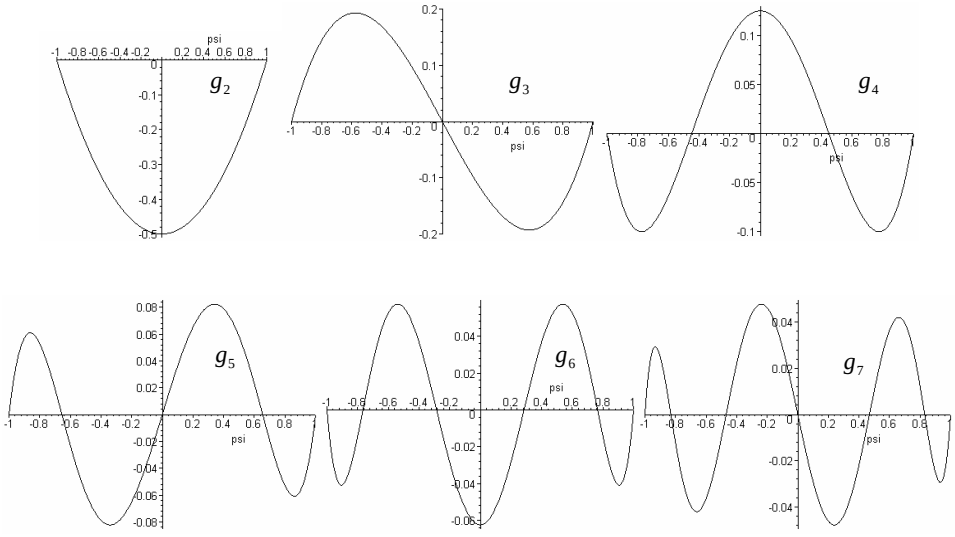

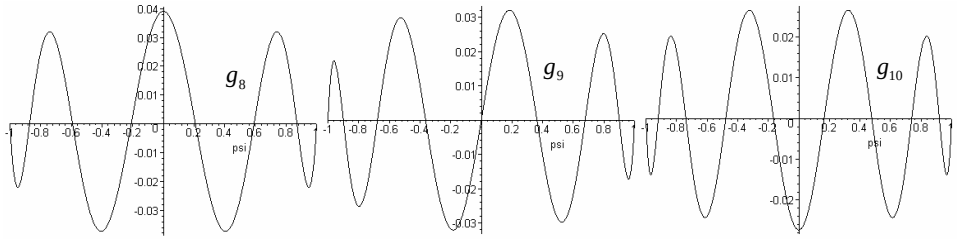
g_8
g_9
g_{10}
psi

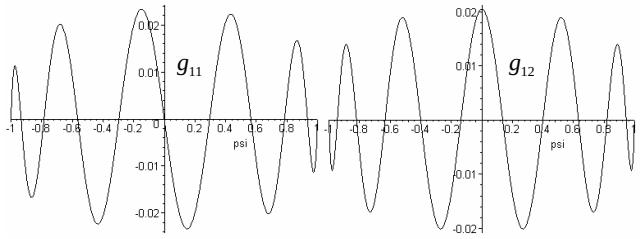
g_{11}
g_{12}
psi